GRACEFUL TRANSITIONS BETWEEN PERIODIC MOTIONS FOR NONLINEAR AND HYBRID SYSTEMS

A Dissertation
Presented to
The Academic Faculty

By

Vishal Murali

In Partial Fulfillment
of the Requirements for the Degree
Doctor of Philosophy in the
Electrical and Computer Engineering
Systems and Controls

Georgia Institute of Technology

May 2021

GRACEFUL TRANSITIONS BETWEEN PERIODIC MOTIONS FOR NONLINEAR AND HYBRID SYSTEMS

Thesis committee:

Dr. Erik I. Verriest, , Advisor
Electrical and Computer Engineering
Georgia Institute of Technology

Dr. Fumin Zhang
Electrical and Computer Engineering
Georgia Institute of Technology

Dr. Patricio Vela
Electrical and Computer Engineering
Georgia Institute of Technology

Dr. Yorai Wardi
Electrical and Computer Engineering
Georgia Institute of Technology

Dr. Ye Zhao
Mechanical Engineering
Georgia Institute of Technology

Date approved: March 25, 2021

To My Family,

ACKNOWLEDGMENTS

I would like to thank my advisor, Dr. Erik Verriest for accepting me as his student and guiding me through the PhD program. I have benefited greatly from his advice and perspective on dynamics and control, and it is sure to shape my future career. I would like to thank all of the faculty members for serving on the committee and providing valuable feedback. I will miss the interesting discussions with Nak-Seung Patrick Hyun, who has been a second mentor to me. Finally, many thanks to my family without whose constant support, this thesis would not be possible.

TABLE OF CONTENTS

LIST OF TABLES

LIST OF FIGURES

SUMMARY

The objective of this dissertation is to provide a set of methods by which a graceful transition is synthesised for a large class of nonlinear and hybrid systems. A special focus of this thesis is on transitioning between periodic orbits. The primary motivation for this is in the application to legged locomotion. The Gluskabi Raccordation provides a general framework to accomplish this. In this thesis, we utilize the Gluskabi raccordation as a general framework for encapsulating the abstract notion of gracefulness. We extend the kernel method to a certain class of hybrid systems. We show how to construct a carefully formulated optimization problem, the solution of which yields graceful transitions. This is illustrated on hopping systems on elastic and granular terrain. The image method, which is dual to the kernel method, is also used as an alternative method to realize graceful transitions. This involves the careful formulation of a parameterized optimal control problem, the solution of which yields parameterized periodic orbits. A dynamically feasible trajectory is then constructed staying close to this orbit family, which yields a different notion of gracefulness. The method is illustrated on fully actuated and underactuated planar bipedal robots. Finally, energy efficient locomotion is also considered in the context of bipedal robots. The partial hybrid zero dynamics framework is employed to generate stable energy efficient periodic walking gaits. An optimal control problem is solved which generates energy efficient transitions between these stable periodic walking gaits.

CHAPTER 1
INTRODUCTION

The objective of this thesis is to present new methods for transitioning gracefully between different periodic orbits of dynamical systems. The primary motivation for this work is transitioning between different gaits for legged robotic systems.

Animals have a wide variety of agile, dynamic and efficient gaits for locomotion. These gaits vary based on the traveling speed, environment terrain type, etc. However, it may not be possible to switch between these different gaits instantaneously due to the inertia of the system, mechanical constraints and actuator limitations. Thus, one of the goals of this thesis is to present methods that achieve transitions between different gaits in an *elegant* and *graceful* manner for legged robotic systems such as hoppers and bipedal robots. Intuitively, transiting gracefully between different gaits may be connected to more efficient locomotion, and may also be used as a measure of safety for the system. There may be other compelling reasons for not wanting to transit instantaneously: aesthetics in dance is one, perhaps also to hide intentions (e.g. when stalking prey) [1]. The problem of transitioning between different gaits has received attention by the research community. However, owing to the high dimensionality of these systems and highly nonlinear dynamics, the problem of *graceful transitions* have largely been left unaddressed. Our goal in this thesis is to take the first steps to tackle this problem.

As noted in [2, 3], the problem of transitioning between different gaits can be viewed as part of a larger set of problems, namely connecting distinct trajectories but of a similar type of a dynamical system in a smooth and graceful manner. The trajectories being connected could be stationary (constant) solutions, periodic (non constant) solutions, or non-periodic solutions. A related problem in thermodynamics is a quasi-static transition between equilibrium points, where a transition occurs very slowly, in such a way that the system could

be assumed to be in equilibrium at each time. The Gluskabi Raccordation problem was introduced in [4, 5] and sets up the basic framework to mathematically define the abstract notion of gracefulness. A fundamental question related to transitions is that of reachability or controllability. If the system is not completely reachable, then transiting between distinct trajectories could be infeasible. On the other hand, there could be a set of ways to transit between trajectories. The Gluskabi raccordation problem seeks to define and select from this set, a graceful transition in a systematic and principled manner.

As introduced in [4, 5] there are two basic approaches to define gracefulness as per the gluskabi raccordation framework. They are the *kernel method* and the *image method* respectively. These two methods can be seen as dual to each other. In the *kernel method* the trajectories to be connected are nulled by an operator. The kernel of this operator defines the type of the trajectories. During transition, this type condition could be violated, but we would like to find a transition in which this condition *maximally persists*. This involves constructing a cost functional to measure this type violation condition and minimizing this subject to the necessary boundary conditions and dynamics constraints. Solution of this optimal control problem yields a transition that is *graceful*. In the *image method*, the desired trajectories are in the image of a parameter set under a (possibly nonlinear) operator. In other words, we have a parameterized family of trajectories. In order to transit between distinct trajectories in this family, a reference trajectory is constructed from this parameterized family by formulating suitable dynamics for the parameter variation. The goal then is to stay as close to this reference as possible, which provides an alternative notion of gracefulness.

The work in [2] initially focused on transitioning between signals in a graceful manner while ignoring any dynamical constraints. Subsequently, it focused on transitioning between periodic orbits of linear systems and uniformly convergent nonlinear systems. The work in [3] focused on applying the kernel method to transit between trajectories of continuous time Linear Time Invariant (LTI) Systems, LTI systems with Commensurate Delays

and discrete time LTI systems. The work in [3] culminated in obtaining graceful transitions between different gaits for the biomimetic worm which was modeled as a switched linear system. A special focus of this thesis is on synthesis of graceful transitions between periodic orbits of hybrid systems.

This thesis is organized as follows. Chapter 2 introduces the relavent background material necessary. The behavioral theory [6] is introduced as it is helpful to define types of trajectories. The kernel and the image methods are also introduced. Hybrid systems are also defined as they serve as very useful models for legged locomotion. Pre-existing gait transition methods are briefly explained. Chapter 3 uses the kernel method to synthesize raccordations for controllable linear systems. Chapter 4 introduces the image method for smooth nonlinear systems. Chapter 5 takes the first steps towards synthesizing transitions for simple low order hybrid systems. Chapter 6 synthesizes transitions for hopping robots on deformable terrain using the kernel method. Chapter 7 focuses on transitions between walking gaits of bipeds using the image method. Chapter 8 examines transitions between walking gaits of fully actuated bipedal robots in the context of energy efficiency.

CHAPTER 2

BACKGROUND MATERIAL

This chapter first introduces the behavioral theory developed by Jan Willems [6]. It is a general framework for modeling of systems and interconnections between them, and is more general than state space models. The kernel method is introduced which makes use of the behavioral theory. The image method is also introduced as part of the raccordation framework. Subsequently, a hybrid system and its solutions are defined. Finally, a brief overview is provided of related pre-existing gait transitions methods.

2.1 Behavioral Theory

The behavioral approach is a broad framework encompassing state space models and transfer function models. The basic idea is to construct a *universum* that contains all possible events. The *behavior* then constrains these to only those events that respect the physical laws of the system under consideration. Precise definitions follow.

Definition 2.1.1. *A dynamical system is a tuple* $\Sigma = (\mathbb{T}, \mathbb{W}, \mathcal{B})$. *Here* $\mathbb{T}$ *represents the time set which is either a subset of* $\mathbb{R}$ *or* $\mathbb{Z}$. $\mathbb{W}$ *is a set in which the signals of interest take their values and* $\mathcal{B}$ *is a subset of* $\mathbb{W}^{\mathbb{T}} = \left\{ w \middle| w : \mathbb{T} \to \mathbb{W} \right\}$ *the set of functions from* $\mathbb{T}$ *to* $\mathbb{W}$. *The set* $\mathcal{B}$ *is called a behavior.*

Usually the set $\mathbb{W}$ is a vector space i.e. $\mathbb{R}^n$. The dynamical system is said to be linear if $\mathcal{B}$ is a subspace of $\mathbb{W}^{\mathbb{T}}$. It is said to time invariant if $S_\tau w \in \mathcal{B} \iff w \in \mathcal{B}$ where S_τ is the shift operator by τ seconds. The dynamical system as defined above in the sense of behavioral theory encompasses state space models of the form

$$\dot{x} = f(x, u),\ y = h(x, u) \tag{2.1}$$

where $x \in \mathbb{R}^n$, $u \in \mathbb{R}^m$ and $y \in \mathbb{R}^k$. The full behavior $\mathcal{B}_f \subset \mathbb{W}_f^{\mathbb{T}}$ where $\mathbb{W}_f = \mathbb{R}^m \times \mathbb{R}^k \times \mathbb{R}^n$ consisting of tuples (u, y, x) and $\mathcal{B}_f$ is the subset of signals $(u(t), y(t), x(t))$ satisfying (Equation 2.1). Here x is typically called the *latent* variable while the variables (u, y) are called the *manifest* variables. The manifest behavior $\mathcal{B}_m$ is then $\left\{ (u(t), y(t)) \middle| \exists x(t) : (u(t), y(t), x(t)) \in \mathcal{B}_f \right\}$. The manifest variables are variables that are of interest to the modeller while latent variables are auxiliary variables used for the modelling process [6].

2.2 Kernel Method

At a very high level, the kernel method involves setting up an optimal control problem, the solution of which will be defined as a *graceful transition*. We define the *type* of the trajectories that we wish to transit between as follows.

Definition 2.2.1. *A type $\mathcal{T} \subset \mathcal{B}$ is the kernel of an operator $\mathbf{O_p} : \mathcal{A} \to \mathcal{V}$, i.e. $\mathcal{T} = \{w(t) \in \mathcal{A} : \mathbf{O_p} w(t) = 0\}$ where $\mathcal{A} \subset \mathcal{B}$ is the domain of definition of this operator. The set $\mathcal{V}$ is a function space. In other words, $\mathbf{O_p}$ maps functions in the set $\mathcal{A}$ to functions in the set $\mathcal{V}$.*

Essentially, the type $\mathcal{T}$ restricts the behavior to a certain set of trajectories that we wish to transit between. For example, the type of constant functions could be described as a kernel of the operator $\mathbf{O_p} = \mathbf{D}$, where $\mathbf{D}$ is the differentiation operator. As another example, the type $\mathcal{T}$ of periodic signals with period T can be described as the kernel of the linear operator $\mathbf{O_p} = I - S_T$. Equivalently (for smooth functions) it can be described as the kernel of $\mathbf{O_p} = \mathbf{D} \cdot \Pi_{i=0}^{\infty}(\mathbf{D^2} + i^2\omega^2\mathbf{I})$ where $\omega = \frac{2\pi}{T}$. Our focus in this thesis is on the type of periodic functions.

For the definition below, we adopt the following notation. Given a function f defined on a time set $\mathbb{T} \subset \mathbb{R}$ we define f restricted to an interval $\mathcal{I}$ denoted $f|_{\mathcal{I}}$ as f defined on $\mathbb{T} \cap \mathcal{I}$. In this way, given a function space $\mathcal{V}$ we can define $\mathcal{V}|_{\mathcal{I}}$ as functions in $\mathcal{V}$ restricted to $\mathcal{I}$.

Definition 2.2.2. *Given a type $\mathcal{T}$ described by an operator $\mathbf{O_p}$ and two signals $w_1 \in \mathcal{T}$ and $w_2 \in \mathcal{T}$ i.e. they satisfy $\mathbf{O_p} w_1 = 0$ and $\mathbf{O_p} w_2 = 0$ and a raccordation interval $\mathcal{I} = [t_0, t_1]$. The* **gluskabi raccordation** *is a function $\bar{w} \in \mathcal{B}$ such that $\bar{w}(t) = w_1(t)$ for $t \leq t_0$ and $\bar{w}(t) = w_2(t)$ for $t \geq t_1$ and further, in the interval $\mathcal{I} = [t_0, t_1]$ it minimizes $\|\mathbf{O_p} w\big|_{\mathcal{I}}\|$ where $\|\cdot\|$ is an appropriate norm on $\mathcal{V}|_{\mathcal{I}}$.*

From the definition above we see that the gluskabi raccordation $\bar{w}$ connects two given functions w_1 and w_2 of the same type over an interval $\mathcal{I} = [t_0, t_1]$ and moreover does this in a *maximally persistent* way during the transition, i.e. by minimizing $\|\mathbf{O_p} w\big|_{\mathcal{I}}\|$. Thus the transition is such that the given type persists during the transition which encapsulates a notion of gracefulness. In essence, the kernel method is a formalism to set up an optimal control problem. Solving this optimal control problem produces maximally persistent or graceful transfer. The optimal control problem formed from the kernel method depends on the choice of $\mathbf{O_p}$, the choice of $\|\cdot\|$ and even the choice of $\mathcal{B}$.

Definition 2.2.3. *A trait ($\mathcal{T}_\theta \subset \mathcal{T}$) is a subtype of the type, i.e. it described by an operator $\mathbf{O}^\theta_{\mathbf{p}}$ and*

$$\mathcal{T}_\theta = \{w \in \mathcal{T} \big| \mathbf{O}^\theta_{\mathbf{p}} w = 0\} \tag{2.2}$$

The trait is useful when we want to enforce greater restrictions (e.g. smoothness conditions on state and input) on the type of signals to transit between. The kernel method has been applied to obtain graceful transitions for signals of the same type for a variety of different types (not necessarily periodic) [7, 8]. It has also been used to obtain graceful transitions for systems with dynamics such as linear time invariant systems [3, 2, 9]. It has also been used to obtain graceful transition for the biomimetic worm, which is a switched linear system (i.e a system where the different modes are linear and the state is continuous) in [10]. The kernel method is also used for a simple two dimensional nonlinear systems in [11] where the operator $O_p = I - S_T$ and the norm is chosen as $\|\cdot\|_Q$ for some positive definite matrix Q.

2.3 Image Method

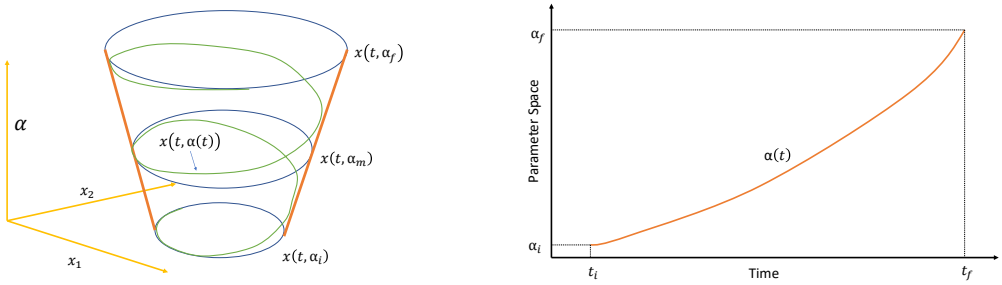

(a) Image Method (b) Parameter Law

Figure 2.1: Schematic of the image method. (b) represents the parameter law variation. In (a) the green line represents the image of the the parameter law variation under the map ϕ which represents the desired reference.

In the image method, we assume that we have a (smooth) map $\phi : \mathcal{A} \to \mathcal{X}$ where $\mathcal{A}$ is a manifold that represents the parameter space and $\mathcal{X}$ is an infinite dimensional function space. Thus for each parameter $\alpha \in \mathcal{A}$, $\phi(\alpha) \in \mathcal{X}$ is a function $\phi(\alpha) : \mathbb{T} \to \mathbb{R}^n$. We can represent this equivalently as a (smooth) function with two arguments $x(t, \alpha)$ where for each α we have $x(\cdot, \alpha) = \phi(\alpha)$ as functions.

Let α_i and α_f be two distinct parameters and $x(t, \alpha_i)$ represent the initial function and $x(t, \alpha_f)$ represents the final function. Let a raccordation interval $\mathcal{I} = [t_i, t_f]$ be given. Then we choose a path $\alpha(t)$ connecting α_i and α_f in the interval $\mathcal{I}$ and also set $\alpha(t) = \alpha_i$ for $t \leq t_i$ and $\alpha(t) = \alpha_f$ for $t \geq t_f$. Then $x_{tr}(t) = x(t, \alpha(t))$ is a graceful transition from $x(t, \alpha_i)$ to $x(t, \alpha_f)$.

There are several different choices of paths $\alpha(t)$ connecting α_i and α_f. In [4] the authors, first construct a Riemannian metric on Θ as follows: assume $\mathcal{X}$ is the space of square integrable functions, then we have the inner product $\langle x, y \rangle = \int_{\mathbb{T}} x^\top(t) y(t) dt$. Since $\mathcal{X}$ is a vector space, this same inner product can be considered for tangent spaces $T_x\mathcal{X}$. Now given tangent vectors v and w in $T_\alpha\mathcal{A}$. We can define $\langle v, w \rangle_{\mathcal{A}} = \langle \frac{\partial \phi}{\partial \theta} v, \frac{\partial \phi}{\partial \theta} w \rangle_{\mathcal{X}}$. This induces a Riemannian metric on $\mathcal{A}$.

More concretely, if $\phi(\alpha)(t) = x(t, \alpha)$ then $\frac{\partial \phi}{\partial \alpha}(\alpha)(t) = \frac{\partial x}{\partial \alpha}(t, \alpha)$. Therefore

$$\langle v, w \rangle_{\mathcal{A}} = v^\top G(\alpha) w = v^\top \cdot \int_{\mathbb{T}} \frac{\partial x}{\partial \alpha}(t, \alpha)^\top \frac{\partial x}{\partial \alpha}(t, \alpha) dt \cdot w \tag{2.3}$$

which defines the metric $G(\alpha)$ for $\alpha \in \mathcal{A}$. With the Riemannian metric defined on $\mathcal{A}$, the path $\alpha(t)$ can be chosen as a geodesic connecting α_i and α_f, i.e. by minimizing the integral given by $\int \dot{\alpha}^\top(t) G(\alpha(t)) \dot{\alpha}(t) dt$. The image method has been applied in [5] to connect signals ignoring dynamics and also to connect periodic orbits of linear systems $\dot{x} = Ax + Bu$. It is also applied in [12] where periodic signals are parameterized by their Fourier coefficients. Here, the authors also discuss an extension of the image method to uniformly convergent nonlinear systems.

Remark : Note that the kernel and image methods only give open loop signals $u(t)$ when applied to systems with dynamics.

2.4 Hybrid Systems

Our definition of a hybrid system is related to [13]. Hybrid systems encompass continuous time dynamical systems and have been used as models for a wide variety of applications including Automated Highway Systems, Air Traffic Management, Thermal Systems, Gear Shifters for Automobiles, and for Legged Locomotion [13].

Definition 2.4.1. *A hybrid system is a tuple* $\mathcal{H} = (\mathcal{I}, \{\mathcal{X}_i\}, \{\mathcal{U}_i\}, \{f_i\}, \mathcal{E}, \mathcal{G}, \mathcal{R})$ *where :*

- $\mathcal{I}$ *is a discrete indexing set.*
- $\mathcal{X}_i$ *are manifolds (also called domains) for* $i \in \mathcal{I}$.
- $\mathcal{U}_i$ *is an input set for* $i \in \mathcal{I}$.
- $f_i(\,\cdot\,,\,\cdot\,) : \mathcal{X}_i \times \mathcal{U}_i \to \mathcal{T}\mathcal{X}_i$ *are controlled smooth vector fields.*
- $\mathcal{E} \subseteq \mathcal{I} \times \mathcal{I}$ *is a set of edges.*

- *With $e = (i_1, i_2) \in \mathcal{E}$, $\mathcal{G}(e) \in \mathcal{P}(X_i \times U_i)$ is collection of guard conditions for each edge. Here $\mathcal{P}(X_i \times U_i)$ denotes power set of $X_i \times U_i$.*

- *$\mathcal{R}(e) : \mathcal{X}_{i_1} \to \mathcal{X}_{i_2}$ is collection of reset maps where $e = (i_1, i_2) \in \mathcal{E}$.*

Broadly speaking, a hybrid system is a combination of a continuous time ordinary differential equation to describe continuous evolution and a state machine to describe discrete transitions. The idea of a solution of a continuous time differential equation can be readily extended to hybrid systems as follows [13].

Definition 2.4.2. *A hybrid time set is a sequence of intervals $\tau = \{I_0, I_1, ..., I_N\} = \{I_i\}_{i=0}^{N}$, finite or infinite (i.e. $N < \infty$ or $N = \infty$) such that*

- *$I_i = [\tau_i, \tau_i']$ for each i.*

- *if $N < \infty$, then either $I_n = [\tau_n, \tau_n']$ or $[\tau_n, \tau_n')$ possibly with $\tau_n' = \infty$.*

- *$\tau_i \leq \tau_i' = \tau_{i+1}$ for all i.*

With the definition of a hybrid time set, we now define the *trajectory* of a hybrid system as follows.

Definition 2.4.3. *A trajectory of a hybrid system consists of $(\tau, \{\mathcal{X}_i\}, \{\mathcal{U}_i\})$ where τ is a hybrid time set, and the following are satisfied :*

- *Continuous evolution, for each $i \in \tau$:*

$$\frac{dx_i}{dt} = f_{q_i}(x_i(t), u_i(t)) \tag{2.4}$$

  where $x_i : I_i \to \mathcal{X}_{q_i}$ and $u_i : I_i \to \mathcal{U}_{q_i}$.

- *Discrete transitions, for $\tau_i' \in I_i$ and $\tau_{i+1} \in I_{i+1}$ we have $(q_i, q_{i+1}) \in \mathcal{E}$, $(x(\tau_i'), u_i(\tau_i')) \in \mathcal{G}(q_i, q_{i+1})$ and $x(\tau_{i+1}) = \mathcal{R}(q_i, q_{i+1})x(\tau_i')$.*

Essentially, this means that the system follows the vector field specified by the given domain until a guard condition is met. Once the guard is reached, the discrete transition occurs to transfer the state to a new domain with it's corresponding vector field.

Remark 2.4.1. *The manifolds $\mathcal{X}_i$ could be of different dimensions in the hybrid system. This results in multi mode multi-dimensional (M3D) systems. One example is running gaits for bipedal robots where the ground phase has a smaller dimension because of holonomic constraints on the foot, while the entire robot body is unconstrained in the flight phase.*

Existence and Uniqueness of Solutions : From our definition of hybrid systems, local existence and uniqueness of the solution is guaranteed. To see this, we know from standard results on Ordinary Differential Equations [14], local existence and uniqueness of the solution is guaranteed on each domain because of our assumption of smooth vector fields. The discrete transitions serve only to reset the state to a (possibly) different domain. However similar to ODEs, global existence of the solution is not guaranteed, as finite escape time may occur in any particular domain. This will not occur if all of the domains of the hybrid system are compact, or if all vector fields in all domains are affine (i.e. a piecewise affine system). This is the case, for example, for the hopper on a trampoline discussed later.

Hybrid Systems may also exhibit *Zeno behavior*. This means that there are infinitely many transitions in a finite amount of time. A classic example of a hybrid system exhibiting zeno phenomenon is the bouncing ball system [13].

2.5 Related Work on Gait Transitions

2.5.1 Raibert Hoppers and Related Models

The most famous examples of robots exhibiting dynamic and graceful locomotion are Marc Raibert's hopping robots developed in the 1980's [15]. We briefly describe his approach here for planar hoppers. The hopper in Figure 2.2 consists of a radial actuator for the leg length and an angular actuator to control the relative angle of the leg with respect to the

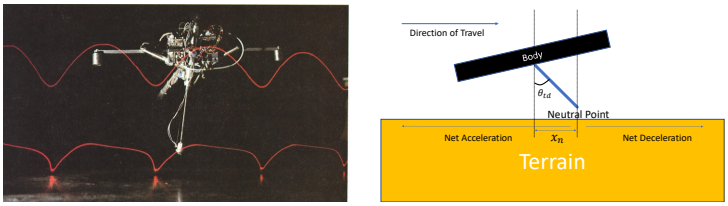

(a) Raibert's Hopper (b) Neutral Point Illustration

Figure 2.2: Figure (a) represents Raibert's Hopper taken from [15]. (b) illustrates the neutral point. Placing the foot at the neutral point leads to zero net velocity change during the subsequent ground phase.

body. In their approach, they used a fixed duration thrust in stance to regulate vertical jump height. The larger the duration of thrust, the larger the jump height and vice versa. The second ingredient was control of body posture during stance via PD control. These two subtasks completely determine the control in stance. We move to the flight phase where forward velocity is constant.

To regulate forward velocity, they observed that there is a point on the ground (during flight phase) where, if the swing leg were placed there, the robot would have *zero net acceleration* in the subsequent stance phase. This point was called the neutral point. Placing the swing leg *before* the neutral point results in a net *positive* acceleration in the next stance phase while placing it ahead of the neutral point results in negative acceleration. Thus, in the flight phase, the swing leg is controlled to the desired location by the angular torque PD controller. This is the essence of their approach and it is also called a "foot placement strategy" to regulate forward velocity. To transition between gaits from a lower to a higher speed, an appropriate foot placement strategy can be used, and to increase/decrease the vertical jump height, the duration of thrust can be changed to achieve transitions in height.

A limitation of this approach is that the control strategy is somewhat ad-hoc. This strategy relied on the fact that the mass of the body is much larger than the mass of leg and so coupling effects between body posture and swing leg movement is minimal. A proof that approximately explains stability of this approach can be found in [16].

Spring Loaded Inverted Pendulum

The Spring Loaded Inverted Pendulum (SLIP) is related to Raibert's hopper if we ignore body pitch angle and consider the closed loop feedback dynamics of the system [16]. It is also commonly observed as the center of mass dynamics of many biological organisms for walking and running [17]. In the formalism of anchors and templates proposed in [18], the SLIP model serves as a *template* for walking/running that can be *anchored* onto robots with complex joints and many degrees of freedom. This has precisely been done in [19, 20, 21, 22]. Owing to the simplicity of the model, it is suitable for analyzing the periodic gaits and their regions of attraction and this is done in [23]. Transition between different gaits for a SLIP model was achieved in [24]. Here the apex-to-apex Poincare map was numerically calculated and a two step deadbeat touchdown angle control was used to transition between different fixed points of the Poincare map. [25] switches between limit cycles of a SLIP model through funnel based switching. The limit cycles were stabilized by a discrete control lyapunov function.

2.5.2 ZMP based locomotion and related methods

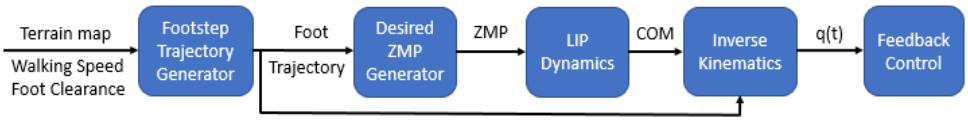

Figure 2.3: Architecture of the ZMP Method.

Figure 2.3 shows the basic architecture of the ZMP method. Based on the environment and other user defined parameters, one first has a footstep planner that generates the future desired trajectories of the footsteps. Given the footstep trajectories, Linear Inverted Pendulum (LIP) models are used to generate desired Center of Mass (COM) trajectories. With the future COM positions and foot positions defined, inverse kinematics can be used to find joint configurations $q(t)$ that satisfy these requirements. A feedback controller is then

used to track this reference $q(t)$. This is the method followed in [26, 27]. More generally, one can use centroidal linear and angular momentum dynamics along with footstep plans or full kinematics to generate whole body plans $q(t)$ as is done in [28, 29, 30]. In [28] this involves solving a trajectory optimization but does not involve the full dynamics (Mass Matrices, Coriolis etc) of the robot.

2.5.3 Full Body Dynamics Optimization

In these methods the full dynamics of the robot is used to formulate a trajectory optimization to yield optimal feasible trajectories $(q(t), \dot{q}(t), u(t))$ that satisfy all dynamics and physical constraints and yield walking/running gaits. Feedback control is then used to track these trajectories. This is the approach used in [31] wherein a full body dynamics optimization is performed as a motion planner to generate references, ans subsequently LQR is used around this trajectory to construct a value function. Finally, an online Quadratic Program is formulated to descend this value function in presence of ground forcing constraints to achieve trajectory tracking. Alternatively an optimal trajectory and a feedback stabilizing controller can be achieved in one shot by solving a *single* trajectory optimization by the Hybrid Zero Dynamics (HZD) Framework [32, 33, 34]. These methods as presented can be easily extended to achieve transitions between different gaits by formulating suitable full dynamics optimization problems.

Remark 2.5.1. *The methods based on full dynamics optimization are slower but are applicable (with suitable tracking controllers) to underactuated robots because the references satisfy the dynamics. In contrast, motion planners based on ZMP and related methods might not produce feasible joint references if the system is underactuated, although they are faster.*

2.5.4 Funnel Based Approaches to Transitions

A popular approach to motion planning and transitioning uses the concept of funnels. For a robot executing a maneuver with feedback control, there is an associated funnel or an invariant set that the closed loop system is constrained to lie in. If the outlet of one funnel, pours into the next one at the end, then one can switch between controllers to execute different maneuvers. This idea is first proposed in [35], but the funnels were obtained through tedious experiments. More recently, [36] uses Sums of Squares (SOS) methods for computing funnels for fixed wing aircraft and used it for online obstacle avoidance. This has also been done in the context of bipedal walkers for motion planning in [37]. Similarly [38] generates a continuum of walking gaits based on forward velocity but switches between them to achieve transitions.

CHAPTER 3

KERNEL METHOD FOR LINEAR SYSTEMS

3.1 Introduction

In this chapter we apply the kernel method for linear systems. We seek to obtain graceful transitions between periodic orbits. Thus the type (see § 2.2) that we focus on is the type of *periodic signals*. A novel operator describing all periodic signals with *fixed* period is given. The kernel method (see § 2.2) is applied with this operator to formulate the optimal control problem. First order necessary conditions for optimality are derived. This is extended to cover the case where we want to transit the input in a graceful manner in addition to the state. To transit between periodic orbits of *different periods* a time warping function is constructed [9], to reduce this to the equal period raccordation case. Finally, we discuss how these methods can be extended to certain classes of nonlinear systems. Throughout this chapter, we assume that the linear system is completely controllable to ensure that a transition exists. Much of the work presented in this chapter is based on [3]. The main novelty in this chapter is the consideration of a different operator describing the type of periodic signals, namely the operator given by (Equation 3.2). In contrast, previous works [3] considered the operator given in (Equation 3.3) to describe the type of periodic signals of a given period.

3.1.1 System Model

In the sense of behavioral theory, we have the system $\Sigma = (\mathbb{T}, \mathbb{W}, \mathcal{B})$, where $\mathbb{T} = \mathbb{R}$, $\mathbb{W} = \mathbb{R}^{m+n}$, and the behavior $\mathcal{B} \subset \mathbb{W}^{\mathbb{T}}$ is given by

$$[\mathbf{D}\mathbf{I} - A\ ,\ -B] \begin{bmatrix} x \\ u \end{bmatrix} = 0 \tag{3.1}$$

where $x(t) \in \mathbb{R}^n$ and $u(t) \in \mathbb{R}^m$. We assume that $\mathcal{V} = \mathcal{L}^2_{loc}(R, R^k)$ in Definition 2.2.2. Hence, $\mathcal{V}|_{\mathcal{I}}$ is a hilbert space for compact connected intervals $\mathcal{I}$ when endowed with the inner product $\langle f, g \rangle = \int_{\mathcal{I}} f^\top g \, \mathrm{dt}$.

3.2 Raccordation of Periodic Signals.

3.2.1 Case of equal periods

We consider the behavioral system representation of $\dot{x} = Ax + Bu$. Suppose we want to connect two periodic signals $x_0(t)$ and $x_1(t)$ of a common frequency ω_0 on the interval $[t_0, t_1]$. It is clear that $x_i(t)$ where $i = 0, 1$ satisfy the equation

$$\mathbf{D} \prod_{k=1}^{\infty} \left((\mathbf{D}^2 + k^2 \omega_0^2) \mathbf{I} \right) x_i = 0 \tag{3.2}$$

The authors in [3] considered the operator describing the type as

$$(\mathbf{I} - \mathbf{S_T}) x_i = 0 \tag{3.3}$$

where $\mathbf{S_T}$ is the shift operator. The main novelty in this chapter is to consider the operator describing the type as given by (Equation 3.2) instead of (Equation 3.3). We assume that the signals to be connected only have n harmonic components. We make this assumption as it simplifies analysis and further the Fourier coefficients of $x_i(t)$ go to zero as $n \to \infty$ by the Riemann-Lebesgue lemma [39]. We also assume that the signals have the same DC Fourier component, that is the average value of both signals across one period is the same. Hence the operator that defines the trait is $\widehat{\mathbf{O}}_p(x, u) = (\prod_{k=1}^{n} (\mathbf{D}^2 + k^2 \omega_0^2) \mathbf{I}) \, x$. Let us define the differential operator

$$a(\mathbf{D}) = \prod_{k=1}^{n} (\mathbf{D}^2 + k^2 \omega_0^2) \mathbf{I} \tag{3.4}$$

That is, the type $\mathcal{T}$ in Definition 2.2.2 is given by

$$\mathcal{T} = \left\{ (x,u) \middle| a(\mathbf{D})x = 0 \right\}$$

We emphasize that the $x_i(t)$ $(i = 1, 2)$ are solutions of the dynamical system,

$$\begin{bmatrix} \mathbf{DI} - A(t) & B(t) \end{bmatrix} \begin{bmatrix} x_i(t) \\ u_i(t) \end{bmatrix} = 0$$

To find a raccordation, we are thus led by Definition 2.2.2 and (Equation 3.4) to the following optimization problem:

$$\min_{w(t)} J(w) = \min_{w(t)} \int_{t_0}^{t_1} (a(\mathbf{D})x)^\top (a(\mathbf{D})x) dt \tag{3.5}$$

where $w = [x^\top, u^\top]^\top$ and subject to the constraints

$$[\mathbf{DI} - A(t), -B(t)]\, w = 0. \tag{3.6}$$

and the boundary conditions

$$\sigma_{t_0}(\mathbf{D}^j x) = \sigma_{t_0}(\mathbf{D}^j x_0). \tag{3.7}$$

$$\sigma_{t_1}(\mathbf{D}^j x) = \sigma_{t_1}(\mathbf{D}^j x_1). \tag{3.8}$$

for $j = 1, 2, \cdots, 2n-1$.

The conditions (Equation 3.7) and (Equation 3.8) above are needed to ensure the required smoothness of the raccordation. In the definition of the behavior given in the previous section, we required our functions $w(t)$ in the behavior to be C^{2n-2}.

Proposition 3.2.1. *Consider the optimal control problem given by equations* (Equation 3.5)-(Equation 3.8). *The first order necessary conditions for optimality can be obtained by solv-*

ing the system of differential equations

$$\begin{bmatrix} (\mathbf{DI} - A(t)) & -B(t) & 0 \\ a(\mathbf{D})^2 & 0 & -(\mathbf{DI} + A(t))^\top \\ 0 & 0 & -B(t)^\top \end{bmatrix} \begin{bmatrix} x \\ u \\ \lambda \end{bmatrix} = \begin{bmatrix} 0 \\ 0 \\ 0 \end{bmatrix} \tag{3.9}$$

Proof. We recall that $\langle f, g \rangle = \int_{t0}^{t1} f^\top g dt$.We can rewrite the cost as

$$J(w) = \frac{1}{2}\langle a(\mathbf{D})x, a(\mathbf{D})x\rangle + \langle \lambda, (\mathbf{DI} - A)x - Bu\rangle. \tag{3.10}$$

Now we use standard methods of optimal control theory [40]. We denote the variation in u by $u + \epsilon v + o(\epsilon^2)$ and the corresponding variation in x as $x + \epsilon\eta + o(\epsilon^2)$. We obtain,

$$\begin{aligned} J(u + \epsilon v) = \frac{1}{2}\langle a(\mathbf{D})x, a(\mathbf{D})x\rangle &+ \epsilon\langle a(\mathbf{D})x, a(\mathbf{D})\eta\rangle \\ &+ \langle \lambda, (\mathbf{DI} - A)x - Bu\rangle + \epsilon\langle \lambda, (\mathbf{DI} - A)\eta - Bv\rangle \\ &+ o(\epsilon^2). \\ &= J(u) + \epsilon(\langle a(\mathbf{D})x, a(\mathbf{D})\eta\rangle) \\ &+ \epsilon(\langle \lambda, (\mathbf{DI} - A)\eta - Bv\rangle) + o(\epsilon^2). \end{aligned}$$

We obtain

$$\begin{aligned} \lim_{\epsilon \to 0} \frac{J(u + \epsilon v) - J(u)}{\epsilon} &= \langle a(\mathbf{D})x, a(\mathbf{D})\eta\rangle \\ &+ \langle \lambda, (\mathbf{DI} - A)\eta - Bv\rangle. \end{aligned} \tag{3.11}$$

We also see from equations (Equation 3.7) and (Equation 3.8) that the variation η satisfies

$$\sigma_{t_0}(\mathbf{D}^j\eta) = 0. \tag{3.12}$$

$$\sigma_{t_1}(\mathbf{D}^j\eta) = 0. \tag{3.13}$$

for $j = 1, 2, \cdots, 2n-1$. Equations (Equation 3.12) and (Equation 3.13) combined with repeated integration by parts yields

$$\delta J(v) = \langle a(-\mathbf{D})a(\mathbf{D})x - (\mathbf{DI} + A^\top)\lambda, \eta\rangle - \langle B^\top\lambda, v\rangle. \tag{3.14}$$

The Euler-Lagrange equations and optimality conditions yield

$$a(-\mathbf{D})a(\mathbf{D})x - (\mathbf{DI} + A^\top)\lambda = 0 \tag{3.15}$$

$$-B^\top\lambda = 0 \tag{3.16}$$

(Equation 3.15), (Equation 3.16) and (Equation 3.1) combined with the fact that $a(\mathbf{D})^* = a(-\mathbf{D}) = a(\mathbf{D})$ yield (Equation 3.9). □

We are left with a system of higher order differential equations, which in principle can be solved for instance by a generalization of the gaussian elimination.

3.2.2 Case of different periods

Suppose that the two periodic functions $x_0(t)$ and $x_1(t)$ to be connected are of different frequencies ω_0 and ω_1 respectively. Let us define now,

$$a(\mathbf{D}, \omega(t)) = \left(\prod_{k=1}^{n}(\mathbf{D}^2 + k^2\omega^2(t))I\right). \tag{3.17}$$

We want the solution of the raccordation problem $x(t)$ such that $a(\mathbf{D}, \omega(t))x(t)$ is close to zero, but we also want to ensure that $\omega(t)$ changes slowly. Since $\omega(t)$ is a function of time, we have to augment the behavior by defining $\hat{w} = [w^\top\omega]^\top$. The operator $\overline{\mathbf{O}}_p$ that defines the trait is now given by

$$\overline{\mathbf{O}}_p(\hat{w}) = \begin{bmatrix} a(\mathbf{D}, \omega)x \\ \mathbf{D}\omega \end{bmatrix} \tag{3.18}$$

where we recall also that $w = [x^\top, u^\top]^\top$. The trajectories to be connected in the extended behavior are $\hat{w}_0(t) = [x_0^\top(t), \omega_0]^\top$ and $\hat{w}_1(t) = [x_1^\top(t), \omega_1]^T$ where ω_0 and ω_1 are the respective frequencies of x_1 and x_2. Looking back at Definition 2.2.2 of the raccordation problem, we arrive at the following optimal control problem,

$$\min_{w,\omega} J(w,\omega) = \frac{1}{2}\left(\langle a(\mathbf{D},\omega)x, a(\mathbf{D},\omega)x\rangle + \langle \mathbf{D}\omega, \mathbf{D}\omega\rangle\right) \tag{3.19}$$

subject to the constraints given in (Equation 3.1), (Equation 3.7) and (Equation 3.8) and the additional constraints for ω given by

$$\sigma_{t_0}(\omega) = \omega_0. \tag{3.20}$$

$$\sigma_{t_0}(\mathbf{D}^j\omega) = 0. \tag{3.21}$$

and the boundary conditions,

$$\sigma_{t_1}(\omega) = \omega_1. \tag{3.22}$$

$$\sigma_{t_1}(\mathbf{D}^j\omega) = 0. \tag{3.23}$$

for $j = 1, 2, \cdots, 2n-1$. Proceeding as earlier, we introduce the augmented cost

$$\hat{\mathcal{J}}(\hat{w}) = \frac{1}{2}\left(\langle a(\mathbf{D},\omega)x, a(\mathbf{D},\omega)x\rangle + \langle \mathbf{D}\omega, \mathbf{D}\omega\rangle\right) \tag{3.24}$$

$$+ \langle \lambda, (\mathbf{DI} - A)x - Bu\rangle. \tag{3.25}$$

Computing the Gateaux variation in the same way as detailed previously yields the following necessary conditions which we state as a proposition :

Proposition 3.2.2.

$$\begin{bmatrix} (\mathbf{DI} - A(t)) & -B(t) & 0 \\ a(\mathbf{D},\omega)^* a(\mathbf{D},\omega) & 0 & -(\mathbf{DI} + A(t))^\top \\ 0 & 0 & -B(t)^\top \end{bmatrix} \begin{bmatrix} x \\ u \\ \lambda \end{bmatrix} = \begin{bmatrix} 0 \\ 0 \\ 0 \end{bmatrix} \tag{3.26}$$

where ω satisfies an ODE

$$\mathbf{D}^2\omega = f(x, \mathbf{D}x, ..., \mathbf{D}^{2n-1}x, \omega, \mathbf{D}\omega, ..., \mathbf{D}^{2n-1}\omega) \tag{3.27}$$

Once again $a(\mathbf{D},\omega)^*$ is the adjoint operator given by

$$a(\mathbf{D},\omega)^* = (\mathbf{D}^2 + n^2\omega^2(t))(\mathbf{D}^2 + (n-1)^2\omega^2(t))...(\mathbf{D}^2 + \omega^2(t)) \tag{3.28}$$

Compare (Equation 3.26) with (Equation 3.9). Note that $a(\mathbf{D},\omega)^*$ is not the same as $a(\mathbf{D},\omega)$ as ω now is a function of time and the operators $(\mathbf{D}^2 + m^2\omega^2)$ and $(\mathbf{D}^2 + n^2\omega^2)$ no longer commute. (Equation 3.26) and (Equation 3.27) coupled with the boundary conditions given by equations (Equation 3.7) -(Equation 3.8) and (Equation 3.20)-(Equation 3.23) correspond to the optimality conditions given by the first variation.

3.2.3 Raccordation of State and Input

So far, we only considered, a raccordation of the state and not the input. If the signals $x_i(t)$ ($i = 1, 2$) to be connected are periodic then so are the associated inputs $u_i(t)$ ($i = 1, 2$) if the system is linear and time invariant. We once again make the assumption that all signals have the same period. In this case, we define the operator that yields the trait as,

$$\widehat{\mathbf{O}}_p(w) = \begin{bmatrix} a(\mathbf{D})x \\ c(\mathbf{D})u \end{bmatrix} \tag{3.29}$$

where $a(\mathbf{D})$ is as in (Equation 3.4) and $c(\mathbf{D})$ divides $a(\mathbf{D})$. We make this assumption because $x(t)$ is smoother that $u(t)$. Denote the degree of the polynomial $c(x)$ by m. The raccordation problem in Definition 2.2.2 yield :

$$\min_{x,u} J(x,u) = \frac{1}{2}\left(\langle a(\mathbf{D})x, a(\mathbf{D})x\rangle + \langle c(\mathbf{D})u, c(\mathbf{D})u\rangle\right) \tag{3.30}$$

subject to the constraints (Equation 3.1), (Equation 3.7) and (Equation 3.8) and the following additional boundary constraints for u :

$$\sigma_{t_0}(\mathbf{D}^j u) = \sigma_{t_0}(\mathbf{D}^j u_0). \tag{3.31}$$

$$\sigma_{t_1}(\mathbf{D}^j u) = \sigma_{t_1}(\mathbf{D}^j u_1). \tag{3.32}$$

where $j = 1, 2, \cdots, m$. We state the necessary conditions for the optimal $x(t)$ and $u(t)$ formally as follows:

Proposition 3.2.3. *Consider the optimal control problem with cost* (Equation 3.30) *and boundary conditions* (Equation 3.31)-(Equation 3.32). *The optimal solution* $(x(t), u(t))$ *satisfies the following differential equation*

$$\begin{bmatrix} (\mathbf{DI} - A) & -B & 0 \\ a(\mathbf{D})^2 & 0 & (\mathbf{DI} + A)^\top \\ 0 & c(\mathbf{D})^2 & -B^\top \end{bmatrix} \begin{bmatrix} x \\ u \\ \lambda \end{bmatrix} = \begin{bmatrix} 0 \\ 0 \\ 0 \end{bmatrix} \tag{3.33}$$

Proof. We introduce the augmented cost

$$\hat{\mathcal{J}} = \frac{1}{2}\Big(\langle a(\mathbf{D})x, a(\mathbf{D})x\rangle + \langle c(\mathbf{D})u, c(\mathbf{D})u\rangle\Big) \tag{3.34}$$

$$+ \langle \lambda, (\mathbf{DI} - A)x - Bu\rangle. \tag{3.35}$$

Proceeding as earlier, we compute the variation

$$\delta J = \langle a(-\mathbf{D})a(\mathbf{D})x - (\mathbf{DI} + A^\top)\lambda, \eta\rangle + \langle c(-\mathbf{D})c(\mathbf{D}) - B^\top\lambda, v\rangle. \tag{3.36}$$

By equating the coefficients of η and v to zero, we arrive at the equations described. □

3.3 Multi step method to generate raccordation

Consider the case when the two periodic orbits $x_1(t)$ and $x_2(t)$ have different periods T_0 and T_1 respectively. Assume a raccordation is sought over $[t_0, t_1]$. Fix a common period $T > 0$ and any two numbers a and b such that $b > a$. Consider the functions $\hat{x}_1(z) = x_1(\frac{T_0}{T}(z-a) + t_0)$ and $\hat{x}_2(z) = x_2(\frac{T_1}{T}(z-b) + t_1)$. We can check that $\hat{x}_1$ and $\hat{x}_2$ have the same period T. Hence we can construct a raccordation $y(z)$ to connect $\hat{x}_1$ and $\hat{x}_2$ over the interval $[a, b]$ by solving the optimal control problem given by equations (Equation 3.5) - (Equation 3.8) . We want to use this function y to construct a raccordation of the original functions x_1 and x_2 (of different periods) over the interval $[t_0, t_1]$. To do this we need to generate a "time warping function" $\tau(t)$. The function $\tau(t)$ must satisfy the following properties :

1. $\tau(t) = \frac{T}{T_0}(t - t_0) + a$ for $t \leq t_0$. This ensures that $\hat{x}_1(\tau(t)) = x_1(t)$.
2. $\tau(t) = \frac{T}{T_1}(t - t_1) + b$ for $t \geq t_1$. This ensures that $\hat{x}_2(\tau(t)) = x_2(t)$.
3. τ needs to be a C^∞ function on R and also be a bijection between $[t_0, t_1]$ and $[a, b]$.
4. $\dot{\tau}(t_0) = \frac{T}{T_0}$ and $\dot{\tau}(t_1) = \frac{T}{T_1}$ and $\dot{\tau} > 0$.

We want τ to be C^∞ because we do not want the smoothness properties of $y(z)$ to be lost under under the composition of y with $\tau(t)$. We explain property 4 as follows. Suppose we have a smooth function $y(z)$. As $y(\tau(t))$ is a reparametrization of $y(z)$, $\dot{\tau}$ represents the speed at which we run along the graph of y. Hence, $\dot{\tau}$ can be thought of as the "instantaneous frequency". Property 4 above simply requires that the "instantaneous frequency" of

$y(\tau(t))$ at t_0 and t_1 match up with the frequencies of $x_1(t)$ and $x_2(t)$ respectively. Since the function $y(\tau(t))$ would be a raccordation between the signals $x_1(t)$ and $x_2(t)$, we would like the "instantaneous frequency" to change slowly from ω_0 to ω_1 as time goes from t_0 to t_1. Hence, we are led to the following optimization problem :

$$\min_{\tau} \int_{t_0}^{t_1} \ddot{\tau}^2(t)dt. \tag{3.37}$$

subject to the constraints

$$\tau(t_0) = a \tag{3.38}$$

$$\dot{\tau}(t_0) = \frac{T}{T_0} \tag{3.39}$$

$$\dot{\tau}(t_1) = \frac{T}{T_1}. \tag{3.40}$$

$$\dot{\tau}(t) > 0. \tag{3.41}$$

$$\sigma_{t_0}(D^j\tau) = 0 \tag{3.42}$$

$$\sigma_{t_1}(D^j\tau) = 0 \tag{3.43}$$

for all $j \geq 2$. Unfortunately, the optimal control problem above does not have a C^∞ solution $\tau(t)$. However, we can find smooth functions $\tau(t)$ that are arbitrarily close to the minimum value as we now explain. We know from (Equation 3.39) and (Equation 3.40) that $\int_{t_0}^{t_1} \ddot{\tau}(t)dt = T\left(\frac{1}{T_1} - \frac{1}{T_0}\right)$. The Cauchy-Schwartz inequality applied to the functions $\ddot{\tau}(t)$ and $1(t)$ implies $\int_{t_0}^{t_1} \ddot{\tau}^2(t)dt \geq \frac{c^2}{t_1 - t_0}$ where $c = T\left(\frac{1}{T_1} - \frac{1}{T_0}\right)$. Furthermore, the bound is actually attained for a (non C^∞) function $\tau(t)$. Consider $\tau(t) = a + \int_{t_0}^{t} \frac{T}{T_0} + (s - t_0)\left(\frac{T}{T_1} - \frac{T}{T_0}\right) ds$ for t lying between t_0 and t_1 . One can check by direct calculation that $\int_{t_0}^{t_1} \ddot{\tau}^2 dt = \frac{c^2}{t_1 - t_0}$. It is also clear that τ is not smooth as $\ddot{\tau} = T\left(\frac{1}{T_1} - \frac{1}{T_0}\right)$ in the interval $[t_0, t_1]$ but $\ddot{\tau} = 0$ outside this interval. Hence τ is a unique global optimum for the problem given by (Equation 3.37) - (Equation 3.43) if we ignore the boundary constraints given by (Equation 3.42) - (Equation 3.43).

If we include the constraints (Equation 3.42) - (Equation 3.43) then there is no global optimal solution. However, given any $\epsilon > 0$ we can find a C^∞ function $\tau(t)$ that satisfies the boundary constraints (Equation 3.38)-(Equation 3.43) *and* also satisfies $\frac{c^2}{t_1-t_0} \leq \int_{t_0}^{t_1} \ddot{\tau}^2 dt < \frac{c^2}{t_1-t_0} + \epsilon$. Let $g(t)$ be a C^∞ function such that

$$g(t) = \begin{cases} 0 & \text{if } t \leq t_0 \\ T(\frac{1}{T_1} - \frac{1}{T_0}) + \gamma & \text{if } t_0 + \delta \leq t \leq t_1 - \delta \\ 0 & \text{if } t \geq t_1 \end{cases} \tag{3.44}$$

To construct such a function first consider

$$f(t) = \begin{cases} \exp\left(-\frac{1}{t^2}\right) & \text{if } t \geq 0 \\ 0 & \text{if } t \leq 0 \end{cases}$$

It can be verified that $f(t)$ is C^∞.Then define

$$\hat{f}(t) = f(t - t_0)f(t_0 + \delta - t).$$

Define

$$h(t) = \frac{\int_{-\infty}^{t} \hat{f}(s)ds}{\int_{-\infty}^{\infty} \hat{f}(s)ds}$$

It can be verified that $h(t)$ is C^∞ that $h(t) = 0$ for $t \leq t_0$ and $h(t) = 1$ for $t \geq t_0 + \delta$. Now it can be verified that

$$g(t) = \left(T\left(\frac{1}{T_1} - \frac{1}{T_2}\right) + \gamma\right) h(t)h(t_1 + t_0 - t).$$

satisfies all the properties listed and is C^∞. We can choose the constant γ in (Equation 3.3) to arrange that $\int_{t_0}^{t_1} g(t) = T(\frac{1}{T_1} - \frac{1}{T_0})$. For instance, if we define $q(\delta) = \int_{t_0}^{t_0+\delta}(T(\frac{1}{T_1} - \frac{1}{T_0}) - g(t))dt + \int_{t_1-\delta}^{t_1}(T(\frac{1}{T_1} - \frac{1}{T_0}) - g(t))dt$ then we can set $\gamma = \frac{T(\frac{1}{T_1} - \frac{1}{T_0}) - q(\delta)}{1-2\delta}$. We then

define

$$\tau(t) = a + \int_{t_0}^{t} \left(\frac{T}{T_0} + \int_{t_0}^{y} g(s)ds \right) dy \tag{3.45}$$

One can also check that we can ensure $\int_{t_0}^{t_1} \ddot{\tau}^2 dt < \frac{c^2}{t_1 - t_0} + \epsilon$ by choosing δ sufficiently small. We can also set $a = 0$ in (Equation 3.45) as we can find a raccordation $y(z)$ between $[0, b-a]$ instead of $[a, b]$.

To summarise, we have the following algorithm :

1. Given $x_0(t)$ and $x_1(t)$ with periods T_0 and T_1 select an arbitrary common period T and a desired tolerance ϵ. Construct $\tau(t)$ with (Equation 3.45) to satisfy boundary conditions and meet the optimality tolerance ϵ.

2. Construct the auxiliary signals $\hat{x}_1(z) = x_1(\frac{T_0}{T}z + t_0)$ and $\hat{x}_2(z) = x_2(\frac{T_1}{T}(z - \tau(t_1)) + t_1)$ and the auxiliary system

$$\dot{y}(z) = \frac{A}{\dot{\tau}\left(\tau^{-1}(z)\right)} y(z) + Bu(z).$$

   Solve the optimal control problem (Equation 3.5)-(Equation 3.8) to construct $y(z)$ on the interval $[0, \tau(t_1)]$ for the auxiliary signals $\hat{x}_1$ and $\hat{x}_2$ with the auxiliary $\dot{x} = \frac{A}{\dot{\tau}}x + Bu$.

3. Construct the full raccordation $y(\tau(t))$ for the original system. The input to the original system is $\dot{\tau}(t)u(\tau(t))$.

3.4 Results

3.4.1 Kernel Method for State Raccordation

Equal Periods

We consider a first order system $\dot{x} = ax + bu$ where a and b are not zero. The optimization problem being considered here is given by (Equation 3.5)-(Equation 3.8). In this case,

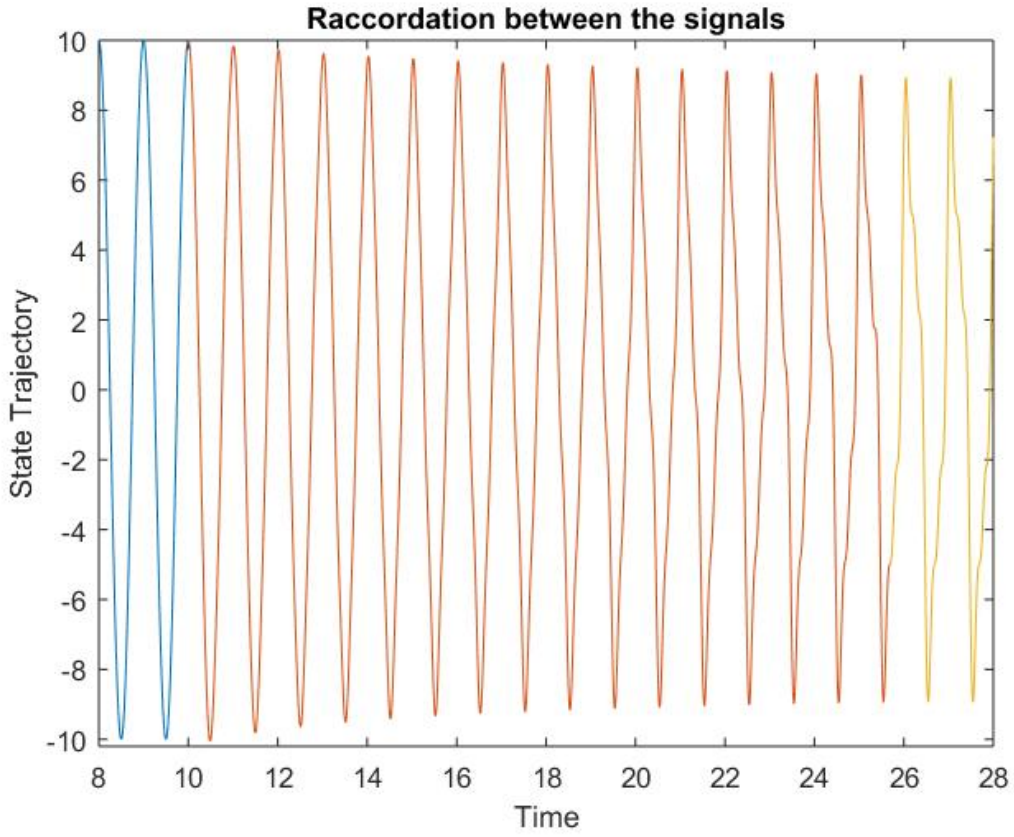

Figure 3.1: Raccordation between signals of equal period $x_1(t)$ and $x_2(t)$

(Equation 3.9) reduces to :

$$b\lambda(t) = 0. \tag{3.46}$$

$$a(\mathbf{D})^2 x(t) = (\mathbf{DI} + A^\top)\lambda(t) \tag{3.47}$$

This reduces to $\lambda(t) = 0$ and

$$(\mathbf{D}^2 + \omega_0^2)^2(\mathbf{D}^2 + 4\omega_0^2)^2 ....(\mathbf{D}^2 + n^2\omega_0^2)^2 x(t) = 0. \tag{3.48}$$

We can write the general solution

$$x(t) = \sum_{k=1}^{n} (a_k + c_k t)\cos(k\omega t) + (b_k + d_k t)\sin(k\omega t). \tag{3.49}$$

The $4n$ constants a_k, b_k,c_k and d_k can be determined from the $4n$ boundary conditions given by equations (Equation 3.7) and (Equation 3.8). We show in Figure 3.1 the raccordation between $x_1(t) = 10\cos(2\pi t)$ and $x_2(t) = 7\cos(2\pi t + \frac{\pi}{4}) + 2\cos(6\pi t + \frac{\pi}{4}) + \cos(8\pi t + \frac{\pi}{4})$.

Different Periods

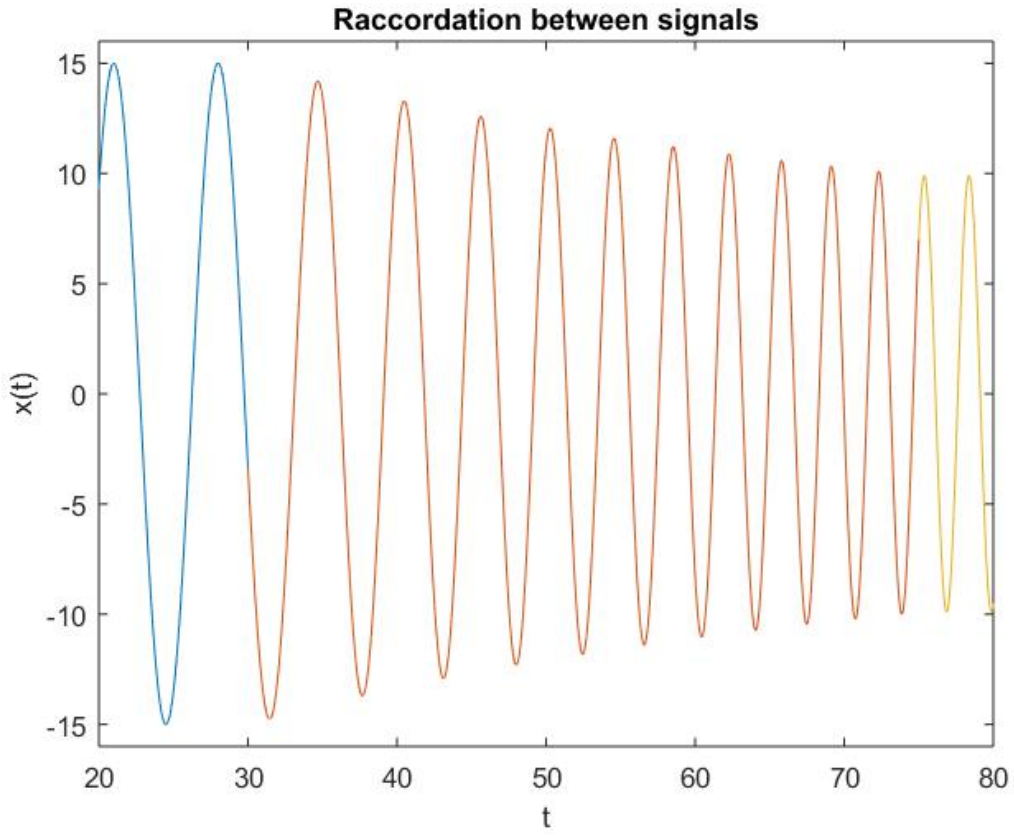

Figure 3.2: Kernel Method for generating raccordation between $x_1(t)$ and $x_2(t)$ of different periods

With the same system $\dot{x} = ax + bu$ we now try to connect signals of different periods using the cost (Equation 3.19). In this case, the system of equations (Equation 3.26)

reduces to:

$$b\lambda(t) = 0. \tag{3.50}$$

$$(\mathbf{D}^2 + \omega^2(t))(\mathbf{D}^2 + \omega^2(t))x(t) = 0 \tag{3.51}$$

and (Equation 3.27) becomes

$$\mathbf{D}^2\omega = 2\omega(t)x(t)\left((\mathbf{D}^2 + \omega^2(t))x(t)\right) \tag{3.52}$$

It can be verified that this is equivalent to the following sixth order system:

$$\begin{bmatrix} \dot{x}_1 \\ \dot{x}_2 \\ \dot{x}_3 \\ \dot{x}_4 \\ \dot{x}_5 \\ \dot{x}_6 \end{bmatrix} = \begin{bmatrix} x_2 \\ -x_1x_3^2 - x_5 \\ -x_6 \\ x_5x_3^2 \\ -x_4 \\ 2x_3x_5x_1 \end{bmatrix} \tag{3.53}$$

There are boundary conditions given by (Equation 3.7)-(Equation 3.8) and (Equation 3.20)-(Equation 3.23). These translate to initial conditions on $x_1(t_0)$, $x_2(t_0)$ and $x_3(t_0)$ and final conditions on $x_1(t_1)$, $x_2(t_1)$ and $x_3(t_1)$. We have shown here the raccordation between $x_1(t) = A_1\cos(\frac{2\pi t}{7})$ and $x_2(t) = A_2\cos(\frac{2\pi t}{3} + \frac{\pi}{4})$ in Figure 3.2. The raccordation interval is $[30, 75]$. The boundary value problem was solved numerically with MATLABs bvp4c package. A sinusoidal profile for $x(t)$ and a linear profile for $\omega(t)$ was given for the initial guess.

3.4.2 Multi Step Method

We also show in Figure 3.3, a raccordation between periodic signals of different periods using the multi step method. The raccordation interval is $[30, 75]$. The time warping function

$\tau(t)$ was generated by numerical integration of the C^∞ function $g(t)$.

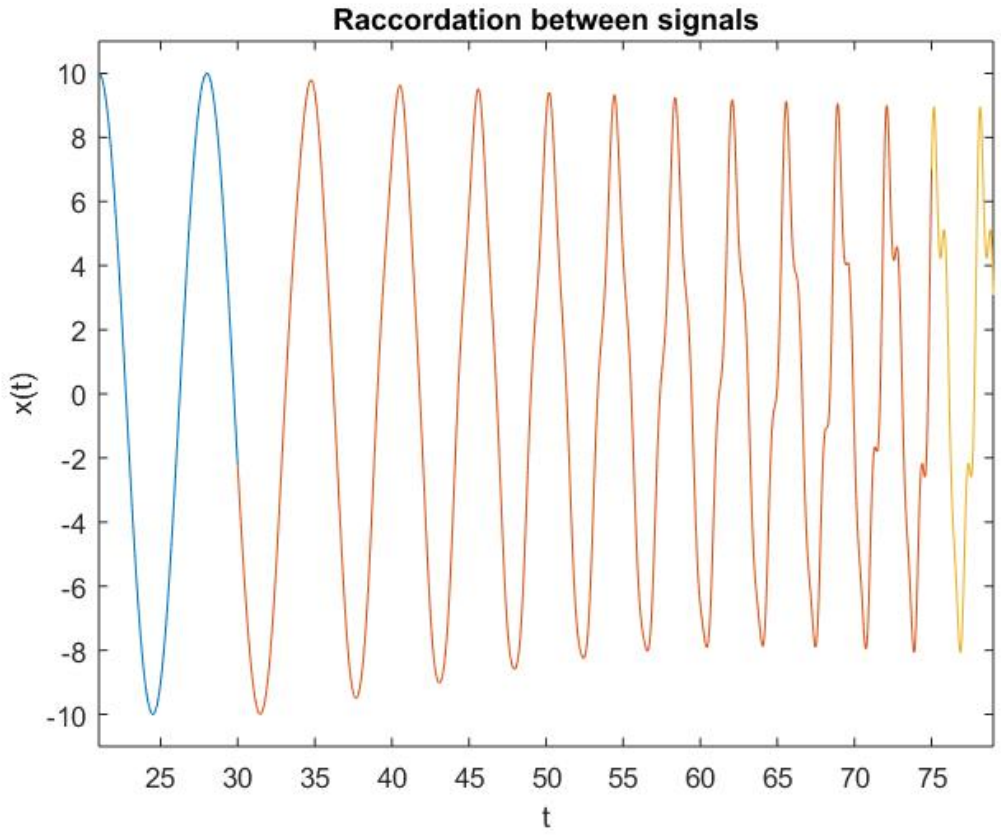

Figure 3.3: Multi Step Method for generating raccordation between $x_1(t)$ and $x_2(t)$ of different periods

3.4.3 Input and State Raccordation

We consider a scalar system $\dot{x} = ax + bu$. We solved the optimal control problem (30) by setting $\omega = 1$, $a(\mathbf{D}) = (\mathbf{D}^2 + 1)(\mathbf{D}^2 + 4)$ and $c(\mathbf{D}) = (\mathbf{D}^2 + 1)$. This was solved numerically by converting the optimal control problem to a nonlinear programming problem by parameterising $x(t)$ and $u(t)$ as splines. The differential equation was imposed as constraints on a set of collocation points in the desired interval $[t_0, t_1]$. The integral cost is approximated as a sum in terms of the spline coefficients. This process can be found in [41]. The software used to achieve this transcription was OPTRAGEN. The resulting nonlinear optimisation problem was solved by SNOPT, a nonlinear programming solver.

We show the results in Figure 3.4. We remark that this result was obtained by discretization and not by solving (Equation 3.26). Hence, we cannot guarantee that the result is globally optimal. However we clearly see the pinching effect in the amplitude during the transition. This phenomenon was explained earlier from a differential geometric viewpoint in [5].

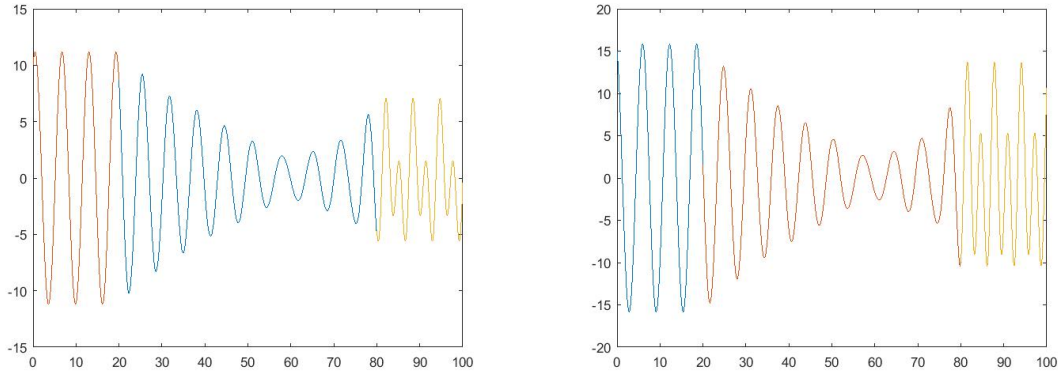

(a) Raccordation of State Part

(b) Raccordation of Input Part

Figure 3.4: Raccordation for both states and inputs.

3.4.4 Different Averages

We consider in the following two signals of different averages. We reduce it to a problem of a raccordation of signals with the same average as follows. Let us assume that the average of x_1 is less than average of x_2. If the signals to be connected are $x_1(t)$ and $x_2(t)$ then we can assume that average of $x_1(t)$ is zero by subtracting the DC component of x_1 from both signals. Now subtract the DC component of x_2 (which we denote by F_2), i.e ensure that $x_1(t)$ and $x_2(t)$ both have zero average. Now we solve the problem (Equation 3.5)-(Equation 3.8) to get a transition $\hat{x}_r(t)$ between the signals. Then define $x_r(t) = \frac{F_2}{t_1 - t_0} t + \hat{x}_r(t)$. The result is illustrated in Figure 3.5.

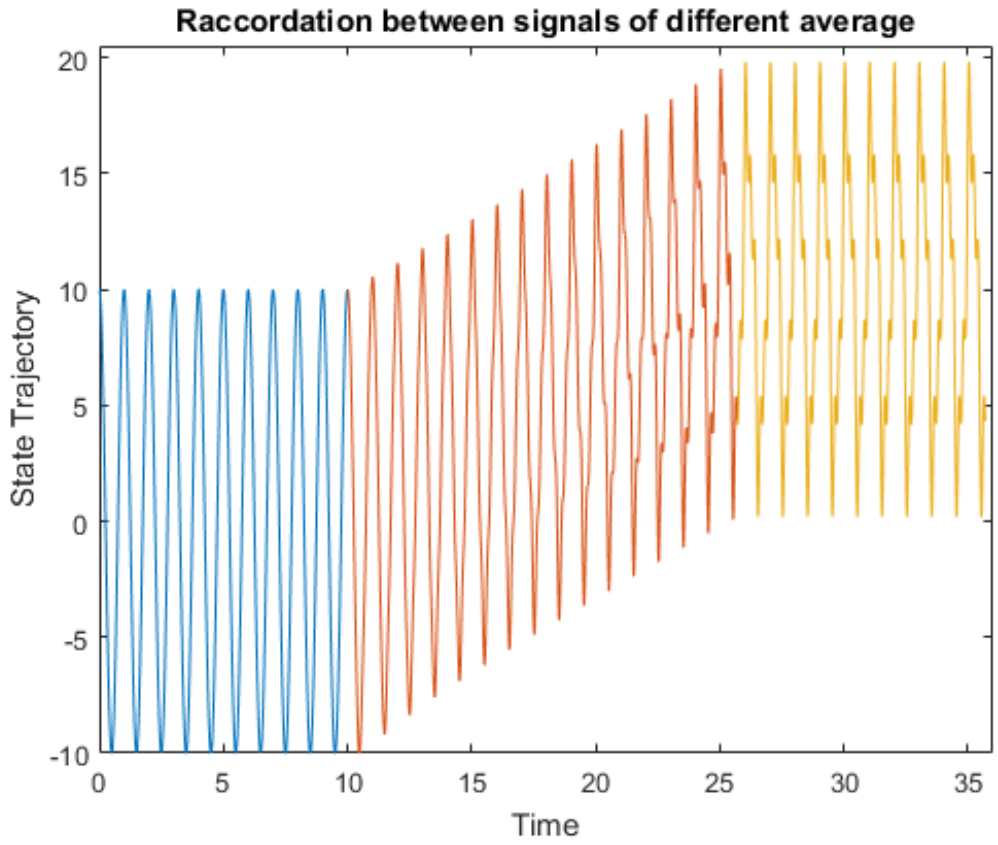

Figure 3.5: Raccordation of Signals with Different Average

3.5 Extensions to Nonlinear Systems

The method proposed above can be readily extended to feedback linearizable nonlinear systems. Consider an affine system of the form

$$\dot{x} = f(x) + g(x)u. \tag{3.54}$$

If the system is feedback linearizable, there exists an output $y = h(x)$ and a feedback controller [42]

$$u = u_{\text{nom}}(x) + v \tag{3.55}$$

that transforms the system into the form

$$\frac{d^n y}{dt^n} = v \tag{3.56}$$

which is a completely controllable linear systems. The results of this chapter can be applied to this linear system to determine v. The full control could then be recovered from (Equation 3.55). Examples of feedback linearizable system include fully actuated fixed base robot manipulators [43]. Similar extensions hold for differentially flat systems (i.e. dynamically feedback linearizable systems) such as quadrotors, wheeled mobile robots [44, 43].

CHAPTER 4

IMAGE METHOD FOR SMOOTH NONLINEAR SYSTEMS

4.1 Introduction

In this chapter we will focus on transitions between periodic orbits of smooth nonlinear underactuated systems. Thus it may not be feasible to make transitions between arbitrary regions in the state space. However, in the framework of the image method (see § 2.3) applied to periodic orbits, we assume that our nonlinear systems have a parameterized family of periodic orbits. Examples of this are certain mechanical systems such as a mass spring damper system, an inverted spherical pendulum on a cart [45] and systems undergoing super critical hopf bifurcation [46]. It can also occur in controlled (possibly hybrid) dynamical systems such as bipedal robots where there are a family of open loop or closed loop control signals to generate a family of periodic gaits [32].

We first assume that we have a parameterized family of smooth autonomous system $\dot{x} = f(x, \alpha)$ and each system has an exponentially stable periodic orbit $\mathcal{O}(\alpha)$. We first establish a stable raccordation theorem which states that a slow parameter variation keeps the state close to this family of orbits. Stability of the final orbit then guarantees that the state transits to the final orbit. We then move to the case where we have a control system $\dot{x} = f(x, u)$, which has a parameterized family of (not necessarily stable) periodic orbits $\mathcal{O}(\alpha)$. A parameterized family of controllers $u(x, \alpha)$ are derived based on existing methods in the literature, to yield the parameterized autonomous system $\dot{x} = f(x, u(x, \alpha))$. Application of the stable raccordation theorem then allows us to achieve graceful transitions. Examples are provided which illustrate the method.

4.2 Raccordation for Stable Periodic Orbits

Consider a dynamical system of the form

$$\dot{x} = f(x, \alpha) \tag{4.1}$$

where $x \in \mathbb{R}^n$ and $\alpha \in \mathcal{A} \subset \mathbb{R}^k$. Here $\mathcal{A}$ is a compact subset of $\mathbb{R}^k$. In this section, we think of $\mathcal{A}$ both as a parameter and an input to the system. We assume that f is smooth and that the partial Jacobians $\frac{\partial f}{\partial x}$ and $\frac{\partial f}{\partial \alpha}$ are locally bounded, i.e. $\forall (x, \alpha)$ there exists a neighborhood U of (x, α) with compact closure such that they are bounded on $\bar{U}$. We assume that for each fixed $\alpha \in \mathbb{R}^k$ the dynamical system has an exponentially stable periodic orbit that varies smoothly with α and with smoothly varying period $T(\alpha)$. We denote each orbit by $\mathcal{O}(\alpha)$. We denote by $\phi(t, x, \alpha)$ the flow of the differential equation at time t with initial condition x and parameter α.

We briefly indicate how this can occur. Suppose we have a nominal periodic orbit $\phi(t, x_0, \alpha)$ and we choose a Poincare Section $\mathcal{S}$ (a hyperplane transversal to the periodic orbit) and define the Poincare return map as $P_r|_{\mathcal{S}}(x, \alpha) = \phi(T_{\text{im}}(x), x, \alpha)$ where T_{im} is the Time to Impact function, then $P_r(x_0, \alpha) = x_0$ is a fixed point of the map. By the implicit function theorem [47] we have that if

$$rank \left(\left. \frac{dP_r}{dx_0} \right|_{\mathcal{S}} (x_0, \alpha) - I_{n-1} \right) = n - 1 \tag{4.2}$$

then we have a family of initial conditions $x_0(\alpha)$ on the hyperplane S such that $P_r(x_0(\alpha), \alpha) = x_0(\alpha)$. Then $x_0(\alpha)$ would be an initial condition for a periodic orbit of $f(x, \alpha)$ and $\psi(t, \alpha) = \phi(t, x_0(\alpha), \alpha)$ where $0 \leq t \leq T(x_0(\alpha))$ would be a parameterization for a two dimensional surface of orbits over $\mathcal{A}$. The matrix $\frac{dP_r}{dx_0} - I$ has full rank, for example, when the orbit is locally exponentially stable (all the eigenvalues of $\frac{dP_r}{dx_0}$ lie in the interior of the unit ball). It is clear that all such periodic orbits for nearby parameters α will also be exponentially

stable because the eigenvalues of the Poincare map are continuous functions of α.

We introduce the notation $\|x\|_{\mathcal{O}(\alpha)} = \inf_{y\in\mathcal{O}(\alpha)} \|x-y\|$. We will need the following Lemma from [48].

Lemma 4.2.1. *There exists a smooth (converse) lyapunov function $V(x,\alpha)$ and positive constants c_1,c_2,c_3 and c_4 (independent of α) such that*

$$c_1 \|x\|^2_{\mathcal{O}(\alpha)} \leq V(x,\alpha) \leq c_2 \|x\|^2_{\mathcal{O}(\alpha)} \tag{4.3}$$

$$\frac{\partial V}{\partial x} f(x,\alpha) \leq -c_3 \|x\|^2_{\mathcal{O}(\alpha)} \tag{4.4}$$

$$\left\| \frac{\partial V}{\partial x}(x,\alpha) \right\| \leq c_4 \|x\|_{\mathcal{O}(\alpha)} \tag{4.5}$$

Proof. In [48], where the lemma is proved for a single exponentially stable periodic orbit. Here we have a family of exponentially stable periodic orbits parametrized by α. Hence we need to show that all inequalities hold independent of α. From [48] we have a collection of converse lyapunov functions (for each parameter α)

$$V(x,\alpha) = \rho^\top P(\theta,\alpha)\rho \tag{4.6}$$

where ρ is a set of transverse coordinates along the orbit and $\theta \in \mathbb{S}^1$ is a variable that describes the phase of the orbit. $P(\theta,\alpha)$ is a positive definite matrix for all θ and α. We know that the maximum and minimum values $c_2 = \max_{\theta,\alpha} \lambda_{\max}(P(\theta,\alpha))$ and $c_1 = \min_{\theta,\alpha} \lambda_{\min}(P(\theta,\alpha))$ exist because of compactness of $\mathbb{S}^1 \times \mathcal{A}$ and continuity of $\lambda_{\max}(.)$ and $\lambda_{\min}(.)$. With these definitions of c_1 and c_2, (Equation 4.3) holds. Similarly because the induced norm $\|.\|$ of a matrix is continuous we have that (Equation 4.5) holds. Finally we have,

$$\frac{dV}{dx} f = -\rho^\top Q(\theta)\rho + O(\|x\|^3_{\mathcal{O}}, z) \leq \frac{-\rho^\top Q(\theta)\rho}{2} \tag{4.7}$$

in a small neighborhood surrounding each periodic orbit. Defining $c_3 = \max_\theta \lambda_{max}\left(-\frac{Q(\theta)}{2}\right)$ establishes (Equation 4.4). □

Fix a $\alpha_0 \in \mathcal{A}$. We are interested in obtaining an upper bound for $\|x(t)\|_{\mathcal{O}(\alpha_0)}$ whenever we have $\dot{x} = f(x, \alpha(t))$ where $|\alpha(t) - \alpha_0| < b$. We also want this upper bound to be independent of α_0.

Consider the system

$$\dot{x} = f(x, \alpha(t)) \tag{4.8}$$

where $|\alpha(t) - \alpha_0| < b$. This can be viewed as a perturbation of the system

$$\dot{x} = f(x, \alpha_0) + g(t, x) \tag{4.9}$$

where

$$g(t, x) = f(x, \alpha(t)) - f(x, \alpha_0) \tag{4.10}$$

Let us for clarity also denote the Lyapunov function $V(x, \alpha_0)$ for the nominal system $f(x, \alpha_0)$ by $V_{\alpha_0}(x)$. We calculate the derivative of $V_{\alpha_0}(x)$ along trajectories of the system (Equation 4.9).

$$\dot{V}_{\alpha_0}(x) = \frac{\partial V_{\alpha_0}}{\partial x}\left(f(x, \alpha_0) + g(t, x)\right). \tag{4.11}$$

Note that by the mean value theorem

$$g(t, x) = \frac{\partial f}{\partial \alpha}(x, \zeta)(\alpha(t) - \alpha_0) \tag{4.12}$$

for some $\zeta(t)$ in the line segment joining $\alpha(t)$ and α_0. We can assume that Jacobians are bounded on a fixed compact set K containing the surface of all periodic orbits. Now (Equation 4.12) yields

$$|g(t, x)| \leq L_1 b \tag{4.13}$$

while (Equation 4.11) yields

$$\begin{aligned}\dot{V}_{\alpha_0}(x) &\leq -c_3 \|x\|^2_{\mathcal{O}(\alpha_0)} + c_4 \|x\|_{\mathcal{O}(\alpha_0)} L_1 b \\ &= -(0.5)c_3 \|x\|^2_{\mathcal{O}(\alpha_0)} - (0.5)c_3 \|x\|^2_{\mathcal{O}(\alpha_0)} + c_4 \|x\|_{\mathcal{O}(\alpha_0)} L_1 b \\ &\leq -(0.5)c_3 \|x\|^2_{\mathcal{O}(\alpha_0)} \\ &\leq -(0.5)\frac{c_3}{c_2} V_{\alpha_0}(x) \end{aligned} \tag{4.14}$$

whenever

$$\|x\|_{\mathcal{O}(\alpha_0)} \geq \frac{2c_4 L_1 b}{c_3} \tag{4.15}$$

Now using (Equation 4.14) we see using the comparison theorem for ODEs that

$$V_{\alpha_0}(x(t)) \leq V_{\alpha_0}(x(t_0)) \exp\left(-(0.5)\frac{c_3}{c_2}(t - t_0)\right) \tag{4.16}$$

whenever (Equation 4.15) holds. On the set

$$\|x\|_{\mathcal{O}(\alpha_0)} = \frac{2c_4 L_1 b}{c_3} \tag{4.17}$$

we see that $\dot{V}_{\alpha_0}(x) < 0$. Hence the set defined by

$$\|x\|_{\mathcal{O}(\alpha_0)} \leq \frac{2c_4 L_1 b}{c_3} \tag{4.18}$$

is forward invariant. Combining all these facts, we finally upperbound $\|x(t)\|_{\mathcal{O}(\alpha_0)}$ by

$$\max\left\{\frac{2c_4 L_1 b}{c_3}, \sqrt{\frac{c_2}{c_1}} \|x(t_0)\|_{\mathcal{O}(\alpha_0)} \exp\left(-\frac{c_3}{4c_2}(t - t_0)\right)\right\} \tag{4.19}$$

Theorem 4.2.1. *Consider the dynamical system* (Equation 4.1) *and assume that it has a surface of smoothly varying (with respect to α) periodic orbits $O(\alpha)$ with smoothly varying periods $T(\alpha)$. Let a parameter interval $[\alpha_i, \alpha_f]$ and a tolerance $\epsilon > 0$ be given. Then there*

exists a $\delta > 0$ *such that for all monotonic functions* $\alpha_g : [0, R] \to [\alpha_i, \alpha_f]$ *with* $|\dot{\alpha}_g(t)| < \delta$ *we have that the solution* $\dot{x}_g(t) = f(x_g, \alpha_g)$ *satisfies* $\|x_g(t)\|_{\mathcal{O}(\alpha_g(t))} < \epsilon$.

Proof. First let us choose a smooth *initial condition* function $x_0(\alpha) \in \mathcal{O}(\alpha)$. For each $\alpha_0 \in [\alpha_i, \alpha_f]$ there exists an interval I_α centered at α_0 such that for all $\alpha_1 \in I_\alpha$ and $\alpha_2 \in I_\alpha$, we have $|\phi(t, x_0(\alpha_1), \alpha_1) - \phi(t, x_0(\alpha_2), \alpha_2)| < \frac{\bar{\epsilon}}{2}$ and for all $0 \leq t \leq \sup_{\alpha \in [\alpha_i, \alpha_f]} T(\alpha)$. Here $\bar{\epsilon}$ is given by

$$\sqrt{\frac{c_2}{c_1}}\bar{\epsilon} = \frac{\epsilon}{2} \tag{4.20}$$

Note that $\bar{\epsilon} < \frac{\epsilon}{2}$ as $c_2 > c_1$ by (Equation 4.3). The collection of all I_α covers $[\alpha_i, \alpha_f]$ and by compactness we can select a finite subcover. Let us denote by $\delta\alpha$ be the minimum length of all the intervals in this subcover. Let us then choose $b = \frac{\alpha_f - \alpha_i}{N}$ for some (large enough) integer N such that $b < \delta\alpha$ *and*

$$\frac{2c_4 L_1 b}{c_3} < \frac{\bar{\epsilon}}{2} \tag{4.21}$$

We now define $\alpha_k = \alpha_i + kb$ where $1 \leq k \leq N$. By our choice of $\delta\alpha$ we have for all α_1 and α_2 in $[\alpha_j, \alpha_{j+1}]$,

$$|\phi(t, x_0(\alpha_1), \alpha_1) - \phi(t, x_0(\alpha_2), \alpha_2)| < \frac{\bar{\epsilon}}{2} \tag{4.22}$$

Given any monotonic function w, the times t_k (which depend on w) are defined so that $w(t_k) = \alpha_k$. We now are going to find the required δ inductively. We now prove the following : suppose there exists a $\delta_k > 0$ such that for all monotonic functions w_k with $w_k([0, t_k]) = [\alpha_i, \alpha_k]$ and $|\dot{w}_k| < \delta_k$ we have that the solution $x_k(t)$ satisfies

- $\|x_k(t)\|_{\mathcal{O}(w_k(t))} < \epsilon$.
- $\|x_k(t_k)\|_{\mathcal{O}(\alpha_k)} < \bar{\epsilon}$.

Then there exists a $\delta_{k+1} > 0$ such that for all monotonic functions w_{k+1} with $w_{k+1}([0, t_{k+1}]) = [\alpha_i, \alpha_{k+1}]$ we have that the solution $x_{k+1}(t)$ satisfies 1) $\|x_{k+1}(t)\|_{O(w_{k+1}(t))} < \epsilon$ and 2) $\|x_{k+1}(t_{k+1})\|_{\mathcal{O}(\alpha_{k+1})} < \bar{\epsilon}$.

To do this let us choose T such that

$$\frac{\epsilon}{2}\exp\left(-\frac{c_3}{4c_2}T\right) < \frac{\bar{\epsilon}}{2} \tag{4.23}$$

and set δ_{k+1} as

$$\delta_{k+1} = \min\left\{\frac{b}{T}, \delta_k\right\} \tag{4.24}$$

We claim that δ_{k+1} is the required one. To see this, let $w_{k+1} : [0, t_{k+1}] \to [\alpha_i, \alpha_{k+1}]$ be any monotonic function with $\dot{w}_{k+1} < \delta_{k+1}$. We note that in the interval $[0, t_k]$ where $w_{k+1}([0, t_k]) = [\alpha_i, \alpha_k]$ the induction hypothesis is satisfied i.e $\|x_{k+1}\|_{\mathcal{O}(w_{k+1})(t)} \leq \epsilon$ for $0 \leq t \leq t_k$ and $\|x_{k+1}(t_k)\|_{\mathcal{O}(\alpha_k)} < \bar{\epsilon}$.

By our choice of δ_{k+1} it follows that $t_{k+1} - t_k \geq T$. In the interval $[t_k, t_{k+1}]$ we have $\|x_{k+1}(t)\|_{\mathcal{O}(\alpha_k)} < \frac{\epsilon}{2}$ from the inductive hypothesis $\|x_{k+1}(t_k)\|_{\mathcal{O}(\alpha_k)} < \bar{\epsilon}$ and (Equation 4.19). Combining this with (Equation 4.22) we get $\|x_{k+1}(t)\|_{\mathcal{O}(w_{k+1}(t))} < \epsilon$.

From (Equation 4.23) and (Equation 4.19) we also get $\|x_{k+1}(t_{k+1})\|_{\mathcal{O}(\alpha_k)} < \frac{\bar{\epsilon}}{2}$. Combining this with (Equation 4.22)) we get $\|x_{k+1}(t_{k+1})\|_{\mathcal{O}(\alpha_{k+1})} < \bar{\epsilon}$. This completes the induction hypothesis. Finally we see the required $\delta = \min_k \delta_k$ which is positive since the minimum is over a finite set. □

Remark 4.2.1. *For a general parameter space $\mathcal{A}$ one can choose a smooth path $\gamma : [p_i, p_f] \to \mathcal{A}$ such that $\gamma(p_i) = \alpha_i$ and $\gamma(p_f) = \alpha_f$. Then apply the Theorem 4.2.1 to $f(x, \gamma(p))$ which depends smoothly on x and p.*

Example : We consider the simplified Selkov Model for glycolysis [49] :

$$\dot{x}_1 = -x_1 + ax_2 + x_1^2 x_2 \tag{4.25}$$

$$\dot{x}_2 = b - ax_2 - x_1^2 x_2 \tag{4.26}$$

This has a stable limit cycle for $a = 0.1$ and $0.4 \leq b \leq 0.9$. We show the raccordation from $b = 0.43$ to $b = 0.85$ and a fixed to 0.1. The function b was a ramp from 0.43 to 0.85.

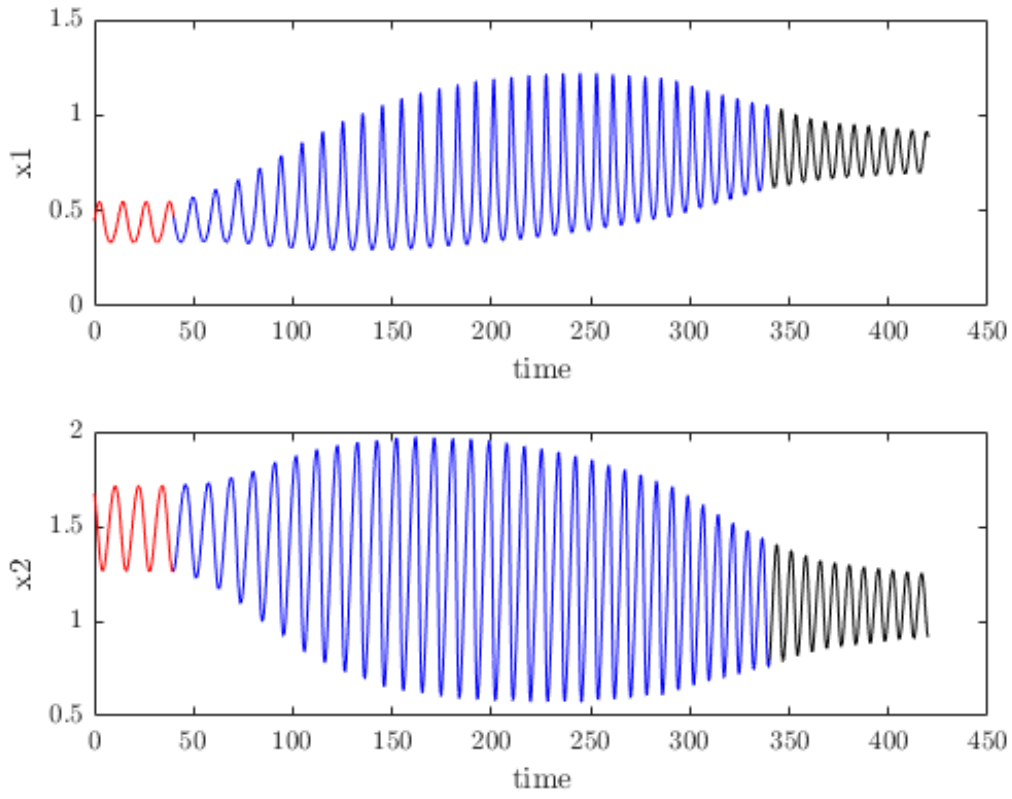

Figure 4.1: Plot of Raccordation for Selkov System

4.3 Raccordation for Unstable Periodic Orbits

Consider the nonlinear system

$$\dot{x} = f(x, u) \tag{4.27}$$

and suppose it has an unstable periodic orbit $\mathcal{O}(\alpha)$ generated by a nominal controller $u_\alpha^n(t)$ for each parameter α. We also denote the resulting nominal periodic solution generated by the nominal controller $u_\alpha^n(t)$ as $x_\alpha^n(t)$. If for each α we can find a stabilizing state feedback controller $u(x, \alpha)$ such that the autonomous system

$$\dot{x} = f(x, u(x, \alpha)) \tag{4.28}$$

has $\mathcal{O}(\alpha)$ as a locally exponentially stable periodic orbit for each fixed α, then we can use Theorem 4.2.1 to move from the initial orbit α_i to the final orbit α_f in a graceful manner. Note that such a stabilizing state feedback controller must of necessity satisfy

$$f(x_\alpha^n(t), u(x_\alpha^n(t), \alpha)) = f(x_\alpha^n(t), u_\alpha^n(t)) \tag{4.29}$$

i.e. the vector fields obtained by substituting $u(x, \alpha)$ and $u_\alpha^n(t)$ in $f(\cdot\ ,\ \cdot)$ must coincide on the orbit $\mathcal{O}(\alpha)$ but can differ away from the orbit.

Remark 4.3.1. *A special case where we have a family of parameterized (unstable) periodic orbits $\mathcal{O}(\alpha)$ generated by nominal controllers $u_\alpha^n(t)$ is for the parameterized system $\dot{x} = f(x, \alpha)$. This can be viewed as a system $\dot{x} = f(x, u)$ where the nominal controller $u_\alpha^n(t) = \alpha$ generates the (unstable) periodic orbit $\mathcal{O}(\alpha)$.*

There are several methods to stabilize an unstable periodic orbit, two of which we explain in this chapter. One is Transverse Feedback Linearization [50] and the other is Transverse Linearization [51].

4.3.1 Transverse Feedback Linearization

We reproduce the definition from [50].

Definition 4.3.1. *Consider the nonlinear affine system*

$$\dot{x} = f(x) + g(x)u \tag{4.30}$$

The system is said to be Transverse Feedback Linearizable *(TFL) at the Orbit $\mathcal{O}$ if there exists a (local) coordinate transformation in a neighborhood of $\mathcal{O}$ given by $T(x) = [\theta, \rho]^\top$ where $\theta \in R$ and $\rho = [\rho_1, \rho_2, ..., \rho_{n-1}] \in R^{n-1}$ such that*

$$\dot{\theta} = 1 + f_1(\theta, \rho) + g_0(\theta, \rho)v \tag{4.31}$$

where $f_1(\theta, 0) = 0$ *and for* $j = 1, 2, \cdots, n-2$ *we have*

$$\dot{\rho}_j = \rho_{j+1} \tag{4.32}$$

$$\dot{\rho}_{n-1} = v \tag{4.33}$$

The orbit $\mathcal{O}$ in the transformed coordinates is $[\theta, 0_{n-1}]$. The orbit $\mathcal{O}$ for a Transverse Feedback Linearizable system can be easily stabilized. Indeed choose a gain vector K_g so that $v = -K_g\rho$ yields an exponentially stable closed loop system for the transverse dynamics $\dot{\rho} = A_{cl}\rho$. It is clear that this stabilizes the whole system because $f_1(\theta, 0) = 0$ and $v = -K_g\rho = 0$ when $\rho = 0$. Necessary and Sufficient Conditions for Transverse Feedback Linearization can be found in [50]. In our application, we assume that (Equation 4.30) has a family of periodic orbits $\mathcal{O}(\alpha)$ generated by nominal controllers $u_\alpha(t)$. For each α and each orbit $\mathcal{O}(\alpha)$ we find a coordinate transformation $T_\alpha(x) = [\theta_\alpha, \rho_\alpha]$ where $\theta_\alpha \in \mathbb{R}$ and $\rho_\alpha \in \mathbb{R}^{n-1}$ such that θ_α and ρ_α satisfy (Equation 4.31) - (Equation 4.33)). Then $v = -k\rho_\alpha$ stabilizes *each orbit* $\mathcal{O}(\alpha)$ for the system (Equation 4.30). We see that such a stabilizing controller depends on ρ_α and hence depends on both x and α.

Example : Consider the nonlinear affine system in R^2 given by

$$\dot{x}_1 = -ux_2 + \left(\frac{1}{x_1^2 + x_2^2} - u\right) x_1 \tag{4.34}$$

$$\dot{x}_2 = ux_1 + \left(\frac{1}{x_1^2 + x_2^2} - u\right) x_2 \tag{4.35}$$

This system has an unstable periodic orbit at $\|x\|^2 = \frac{1}{\alpha}$ generated by a (constant) nominal controller $u_\alpha^n(t) = \alpha$. This system is transverse feedback linearizable with coordinate transformation

$$T_\alpha(x) = \begin{bmatrix} \frac{1}{\alpha} \tan^{-1}\left(\frac{x_2}{x_1}\right) \\ \frac{1}{2}(x_1^2 + x_2^2 - \frac{1}{\alpha}) \end{bmatrix} \tag{4.36}$$

In the new coordinates the equations are

$$\dot{\theta}_\alpha = \frac{u}{\alpha} \tag{4.37}$$

$$\dot{\rho}_\alpha = 1 - \|x\|^2 u \tag{4.38}$$

This is not quite in the form (Equation 4.31) - (Equation 4.33), however the feedback

$$u(x,\alpha) = \frac{1}{\|x\|^2}(1-v) \tag{4.39}$$

puts it in the required form. Then choosing $v = -k\rho_\alpha$ for any $k > 0$ exponentially stabilizes the orbit. Note that each of the controllers $u(x,\alpha)$ in (Equation 4.39) are different since $v = -k\rho_\alpha$ and ρ_α clearly depends on α. Thus, we have the parameterized autonomous system $\dot{x} = f(x, u(x,\alpha))$ that has an exponentially stable periodic orbit $\mathcal{O}(\alpha)$ given by $\|x\|^2 = \frac{1}{\alpha}$ for each α. We then use Theorem 4.2.1 to obtain the raccordation from α_i to α_f. Note also here that the necessary condition (Equation 4.29) is satisfied i.e $u(x,\alpha) = \alpha = u^n_\alpha(t)$ on the set $\|x\|^2 = \frac{1}{\alpha}$.

We show in Figure 4.2 the raccordation from $\alpha_i = 1$ to $\alpha_f = 0.2$. The raccordation interval is $R = 100$. The initial orbit is shown in red. The final orbit is shown in black. The raccordation is shown in blue.

4.3.2 Transverse Linearization

Transverse Linearization is a general method to stabilize unstable periodic orbits for underactuated mechanical systems [51],[52]. Roughly speaking, Tranverse Feedback Linearzation can be compared to Feedback Linearization while Transverse Linearization can be compared to the Jacobian Linearization (discarding the phase). The key part is identifying a set of transverse coordinates to the periodic orbit where analytical computation of the linearization is feasible. Our main reference was [51]. We summarize the method as follows. We recall that any underactuated mechanical system has the following equations

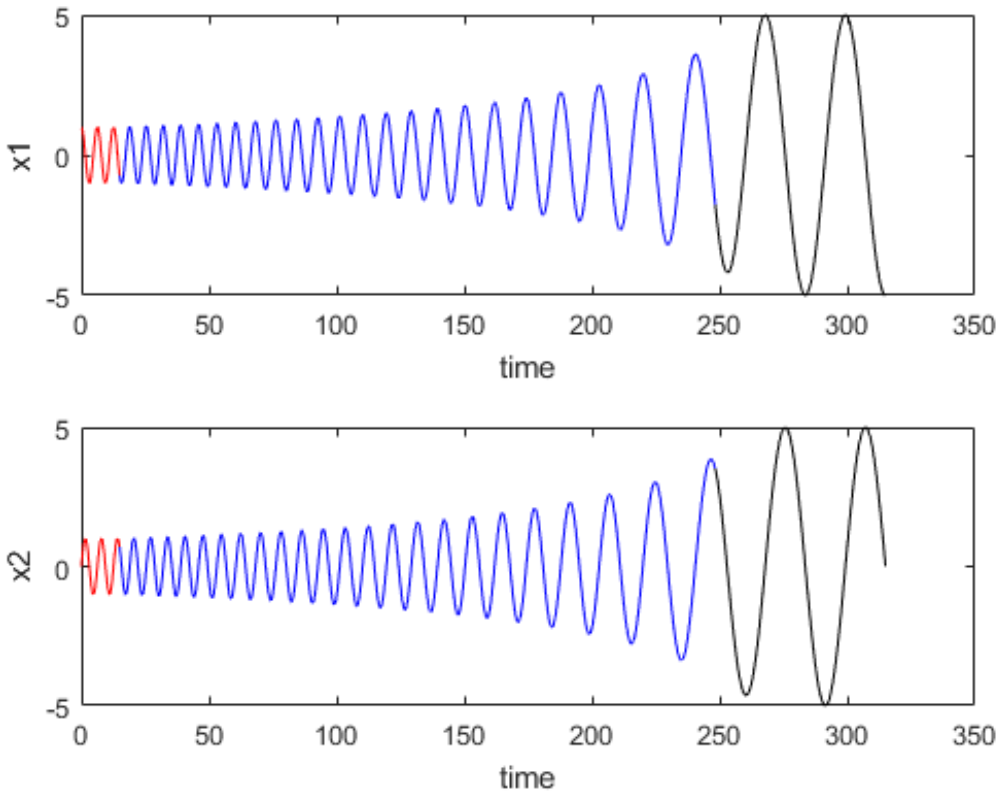

Figure 4.2: Plot of Raccordation Using TFL

of motion :

$$M(q)\ddot{q} + C(q,\dot{q})\dot{q} + G(q) = Bu \tag{4.40}$$

We recall that this is a system of dimension $2n$ since that states are the generalized co-ordinates q and their derivatives $\dot{q}$. We assume here that (Equation 4.40) has a family of periodic orbits denoted by $\mathcal{O}(\alpha)$ and generated by $u_\alpha(t)$.

Step 1 For each fixed α we compute the *Transverse Linearization* of (Equation 4.40) about the orbit $\mathcal{O}(\alpha)$ which is a Linear Time Varying System (LTV) of dimension $2n-1$

$$\dot{x}_{\text{lin}} = A(t,\alpha)x_{\text{lin}} + B(t,\alpha)v_{\text{lin}} \tag{4.41}$$

The matrices $A(.)$ and $B(.)$ can be *explicitly computed*. The $A(.)$ and $B(.)$ are smooth with respect to α because the orbits $\mathcal{O}(\alpha)$ smoothly vary with respect to α.

Step 2: Construct a stabilizing state feedback controller for the LTV system above (Equation 4.41)

$$v_{\text{lin}}(x, \alpha) = H(t, \alpha)x \tag{4.42}$$

For example, $H(t, \alpha)$ can be obtained by solving the Periodic Riccati Differential Equation (PRDE) for each orbit $\mathcal{O}(\alpha)$. We solved it by the method outlined in [53]. This method involves solving a Semidefinite Program (SDP). We used the MATLAB software CVX to solve the SDP [54]. The number of Fourier Coefficients we use is 20.

Step 3: Use the $H(t, \alpha)$ obtained in Step 2 to construct a stabilizing nonlinear controller by *parameterizing time in terms of state* i.e.

$$v = H(\tau(q, \dot{q}), \alpha)x_{\perp} \tag{4.43}$$

Here $\tau(q, \dot{q})$ can be found by solving the equation (for τ)

$$[q - q_*(\tau), \dot{q} - \dot{q}_*(\tau)] \begin{bmatrix} \dot{q}_*(\tau) \\ \ddot{q}_*(\tau) \end{bmatrix} = 0 \tag{4.44}$$

$\tau(q, \dot{q})$ always exists locally. It is clear that the v in Step 3 is a state feedback controller that depends on α because for each α we want to stabilize the particular orbit $O(\alpha)$. In other words $v = v(q, \dot{q}, \alpha)$.

The steps detailed above yield an autonomous parameterized system

$$M(q)\ddot{q} + C(q, \dot{q})\dot{q} + G(q) = Bv(q, \dot{q}, \alpha) \tag{4.45}$$

with stable family of periodic orbits $\mathcal{O}(\alpha)$ for each α. We can then use Theorem 4.2.1 to move across the orbits.

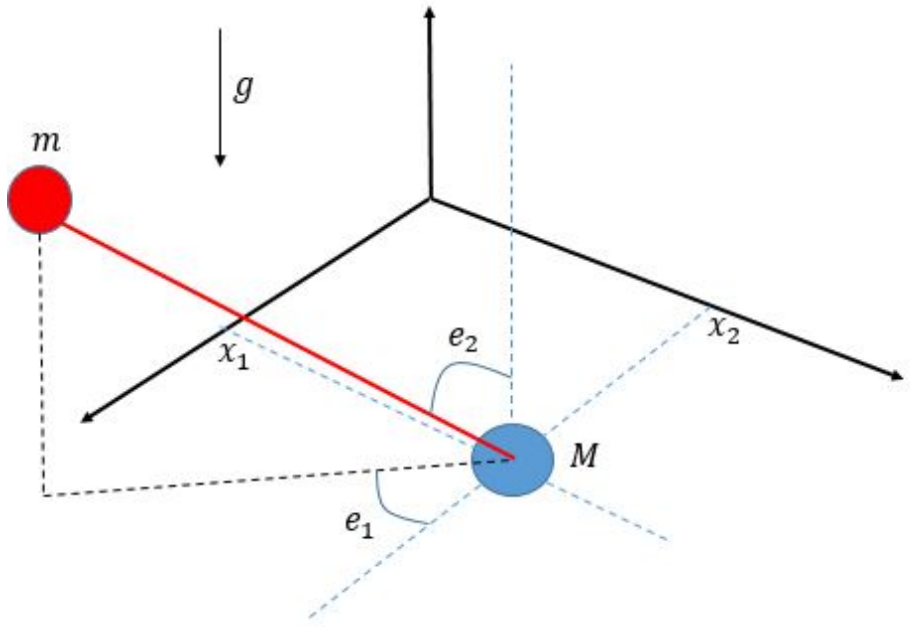

Figure 4.3: Schematic for Spherical Pendulum

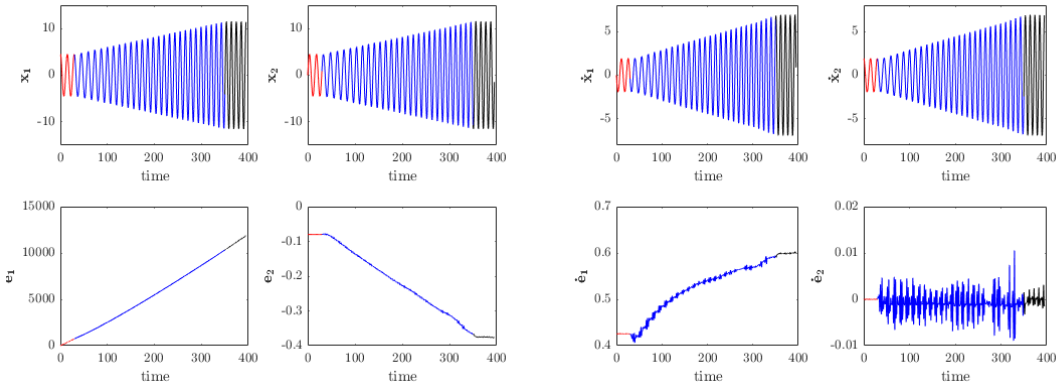

(a) $q(t)$ (b) $\dot{q}(t)$

Figure 4.4: Plot of raccordations for the inverted pendulum

Spherical Pendulum on a Cart

Here, we use the method of Transverse Linearization to obtain graceful transitions between distinct (unstable) periodic orbits of the Pendulum on the Cart studied in [51]. The generalized coordinates are

$$q = \begin{bmatrix} x_1 \\ x_2 \\ e_1 \\ e_2 \end{bmatrix} \tag{4.46}$$

where x_1 and x_2 denote the positions and e_1 and e_2 denotes the angles (see Figure 4.3). The cart has two thrusters u_1 and u_2 to control the x_1 and x_2 positions of the cart respectively.

The Lagrangian of the system is

$$L(.) = K_{\text{puck}}(.) + K_{\text{pend}} - \text{Pot}_{\text{pend}}(.) \tag{4.47}$$

where $\text{Pot}_{\text{pend}} = mgL\cos e_2$ and

$$K_{\text{puck}} = \frac{1}{2}M\left[\left(\frac{dx_1}{dt}\right)^2 + \left(\frac{dx_2}{dt}\right)^2\right] \tag{4.48}$$

$$\begin{aligned} K_{\text{pend}} =& \frac{1}{2}m\left[\frac{d}{dt}\{x_1 + L\cos(e_1)\sin(e_2)\}\right]^2 \\ &+ \frac{1}{2}m\left[\frac{d}{dt}\{x_2 + L\sin(e_1)\sin(e_2)\}\right]^2 \\ &+ \frac{1}{2}m\left[\frac{d}{dt}\{L\cos(e_2)\}\right]^2 \end{aligned}$$

From [51] we know that this system has a family of Periodic Orbits (parameterized by R and c_e given by

$$x_1 = R\cos(e_1(t)), x_2 = R\sin(e_2(t)) \tag{4.49}$$

where

$$e_1 = \sqrt{\frac{g\sin(-e_2)}{(R + L\sin(e_2))\cos(e_2)}}t \tag{4.50}$$

$$e_2(t) = c_e \tag{4.51}$$

In this example the parameter space $\mathcal{A}$ is two dimensional i.e $\mathcal{A} = \{R, c_e | R, c_e > 0\}$. Note here that the nominal controller $u^n(t, R, c_e)$ that generates the periodic orbit $\mathcal{O}(R, c_e)$ is *not constant*. It can be explicitly computed to be a sinusoidal function of time. For each R and c_e we construct a stabilizing controller $u(q, \dot{q}, R, c_e)$ so that the resulting autonomous system (Equation 4.40) has an exponentially stable orbit $\mathcal{O}(R, c_e)$ given by (Equation 4.49) - (Equation 4.50) using Transverse Linearization. We then apply Theorem 4.2.1 to the autonomous system to get our required transition. We show below in Figure 4.4a and Figure 4.4b a transition from $R = 4.5$ and $c_e = -0.08$ radians to $R = 11.5$ and $c_e = -0.38$ radians. The initial orbit is shown in red. The final orbit is shown in black. The raccordation is shown in blue.

CHAPTER 5
KERNEL METHOD FOR SIMPLE HYBRID SYSTEMS

5.1 Introduction

The previous chapters focused on smooth linear and nonlinear systems respectively. In this chapter, we will take the first steps to synthesize graceful transitions to some simple low order hybrid systems.

The first system we consider in this chapter is a simple one dimensional system on spring like terrain (see Figure 5.1). The motivation for considering this system is to understand the most critical aspects of dynamics and locomotion on deformable terrain. We strip away any longitudinal motion and consider only vertical motion. We first characterize the periodic orbits of this system by giving necessary and sufficient conditions for periodicity. We then illustrate different *types* of periodic orbits along with their *timing diagrams*. Finally an optimization problem is posed based on the kernel method, that synthesizes a graceful transition between the different periodic orbits of the system.

The second system we consider is a rimless wheel with impulsive inputs (see Figure 5.10). This system exhibits periodic orbits with only a ground phase where one spoke is in contact with the ground, and periodic orbits that contain both a ground phase and a flight phase where all spokes are above the ground. The motivation for considering this system is to better understand how to transit between different types of gaits for legged robots, such as walking gaits to running gaits, or trotting gaits to bounding gaits in the case of quadrupeds. For example, in the case of transitions from walking to running, there is an appearance of a flight phase for the running gait, which is not present in a walking gait. In this chapter, we first describe completely the system model of this rimless wheel which locomotes on hard, flat ground. An impulsive input is described to inject the requisite en-

ergy into the system that is lost in impacts. An algorithm for generating different periodic orbits is given based on the choice of angular velocity. Finally, an algorithm is presented which transits the system between different periodic orbits of the system. In this chapter and the subsequent one, we assume complete knowledge of the terrain forces. In presence of unknown (or partly unmodeled) terrain forces learning based approaches for estimating substrate forces exist [55, 56].

5.2 System Model for Simple Vertical Hopper

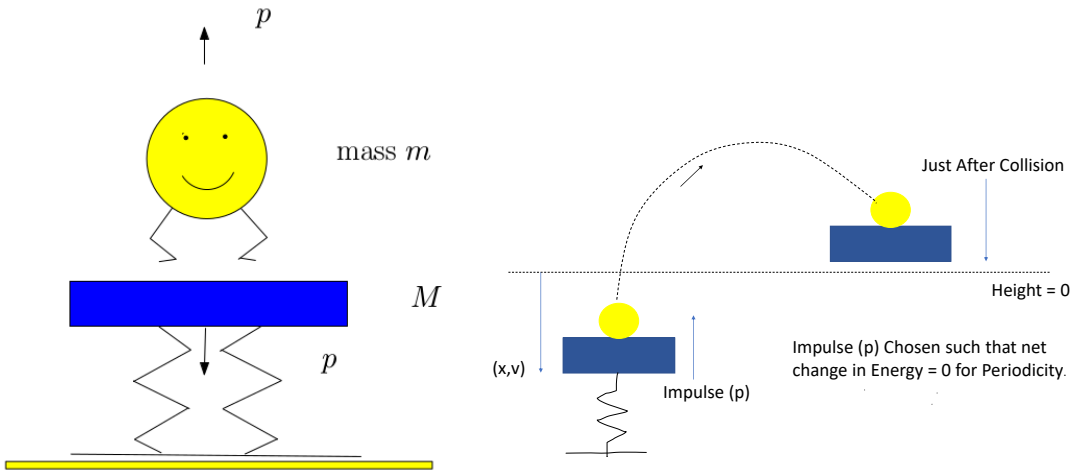

Figure 5.1: Vertical Jumper on Spring Like Terrain.

Our model is a controlled extension of an autonomous system analyzed in [57]. It was shown that the autonomous model has a discrete set of initial conditions for which the energy in the system is conserved, thus exhibiting periodic behavior. These energy states are akin to Bohr's quantum model of the atom, and defines quantum-like behavior in this macroscopic system. The focus here is to consider transitions between such energy states, and more generally, any induced periodic behavior. In Figure 5.1a, the yellow mass represents the jumper, while the blue mass and the spring represent the trampoline. The mass of the platform is M, while the mass of the jumper is m. The spring constant is denoted by k_g. Two distinct modes (ground phase and ballistic phase) exist if the system

has sufficient energy, as shown below.

5.2.1 Ground Phase

In this mode, the jumper remains on the platform, and the two masses coalesce into a single mass. The dynamics is obtained from Newton's laws.

$$(M+m)\ddot{x} = -k_g x - (M+m)g \tag{5.1}$$

x represents the position of the combined mass. The normal force is $N = m(\ddot{x}+g) = -\frac{k_g m}{M+m}x$. The masses remain together as long as $N \geq 0$, i.e., $x \leq 0$. Thus transition to the ballistic flight phase occurs if $x \geq 0$ and $\dot{x} > 0$.

5.2.2 Flight Phase

In this mode, the two masses separate, and the yellow mass in Figure 5.1 is in flight. We denote by x_p the position of the trampoline (blue mass) and by x_j the position of the jumper (yellow mass). The equations of motion are given by Newton's laws

$$M\ddot{x}_p = -k_g x_p - Mg\,, \quad m\ddot{x}_j = -mg \tag{5.2}$$

Transition to the ground phase occurs whenever, $x_p = x_j$ and $\dot{x}_j - \dot{x}_p \leq 0$. The combined post-impact velocity of the jumper-trampoline is obtained from the law of conservation of momentum, and is given by

$$v = \frac{M\dot{x}_p + m\dot{x}_j}{M+m}. \tag{5.3}$$

5.2.3 Control Input

The control input is an impulsive kick that can be applied by the jumper at any point of time in the ground phase. The strength of the impulse is denoted by p (see Figure 5.1). Once the impulsive kick is applied, the transition from ground phase to flight phase occurs,

where $x_j = x_p = x$ and the corresponding velocities are given as

$$m(v_j - v) = p\,, \quad M(v_p - v) = -p \tag{5.4}$$

where v is the velocity of the combined jumper-trampoline just before application of the impulse, and v_j and v_p are the velocities of the jumper and trampoline respectively post application of the impulse.

5.3 Obtaining Periodic Orbits

In this section, we set up the conditions for the periodicity of the behavior of the alternating two-mode system from energetic considerations.

5.3.1 Conditions for Periodicity

Change in Energy due to Application of Impulse

We denote by (x, v) the combined position and velocity of the jumper-trampoline just before the application of the impulse (see Figure 5.1b). The change in energy is given by

$$\begin{aligned}\Delta E_{g\to f} &= \Delta \text{ Kinetic Energy} \\ &= \frac{1}{2}M\left(v - \frac{p}{M}\right)^2 + \frac{1}{2}m\left(v + \frac{p}{m}\right)^2 \\ &\quad - \frac{1}{2}(M+m)v^2\end{aligned} \tag{5.5}$$

On simplifying, this is

$$\Delta E_{g\to f}(p) = \left(\frac{p^2}{2}\right)\frac{M+m}{Mm} \tag{5.6}$$

Change in Energy due to impact of jumper and trampoline

If we denote by v the combined velocity of the jumper-trampoline post-impact, and denote the velocity of the jumper and trampoline pre-impact by v_j and v_p, then the change in energy is given by,

$$\Delta E_{f\to g} = \frac{1}{2}(M+m)v^2 - \frac{1}{2}Mv_p^2 - \frac{1}{2}mv_j^2 \tag{5.7}$$

which, since v is given by (Equation 5.3) allows us to express

$$\Delta E_{f\to g}(v_p, v_j) = -\frac{1}{2}\frac{Mm}{M+m}\left(v_p - v_j\right)^2 \tag{5.8}$$

Necessary and Sufficient Condition for periodicity are given in the proposition below.

Proposition 5.3.1. *A necessary and sufficient condition for the periodic behavior of the jumper system in Figure 5.1 is that*

$$\Delta E_{\text{net}} = \Delta E_{g\to f} + \Delta E_{f\to g} = 0 \tag{5.9}$$

Proof. Necessity follows from the fact that energy injected into the system due to the impulse is exactly lost during impact to maintain periodicity. This condition is also seen to be sufficient. Applying an impulse p to make $\Delta E_{\text{net}} = 0$ during a jump (say at position x), the ground phase energy of the jumper-trampoline does not change. Thus, when the jumper-trampoline reaches position x, the velocity remains unchanged and the application of p reproduces the same trajectories in the flight phase for the jumper and the trampoline respectively. □

5.3.2 Numerical Computation of a Periodic Orbit

We fix the ground phase energy E_g of the periodic orbit we wish to find. Note that this is given by

$$E_g = \frac{1}{2}(M+m)v^2 + (M+m)gx + \frac{1}{2}kx^2. \tag{5.10}$$

We also fix the position x (in the ground phase) at which the impulse is applied. Note that given x and E_g, $v \geq 0$ can be solved from (Equation 5.10). The net change in energy $\Delta E_{\text{net}}(p)$ can be expressed as a function of impulse strength p as follows. The solutions of the jumper and trampoline in flight phase are given by:

$$x_j(t) = x + (v + \frac{p}{m})t - \frac{1}{2}gt^2 \tag{5.11}$$

$$x_p(t) = A\sin(\omega t + \phi) - \frac{Mg}{g} \tag{5.12}$$

$$A = \sqrt{\left(x + \frac{Mg}{k_g}\right)^2 + \left(\frac{Mv-p}{M\omega}\right)^2} \tag{5.13}$$

$$\phi = \tan^{-1}\left(\frac{x + \frac{Mg}{k_g}}{\frac{Mv-p}{M\omega}}\right) \tag{5.14}$$

$$\omega = \sqrt{\frac{k_g}{M}} \tag{5.15}$$

Here $x_j(t)$ and $x_p(t)$ are the positions of the jumper and the trampoline respectively. The coefficients A , ϕ and ω represent the amplitude, phase shift and frequency and can be obtained from the system parameters and appropriate boundary conditions. Let $T_p > 0$ be the smallest time such that $x_j(T_p) = x_p(T_p)$ (i.e. T_p is the duration of the flight phase). Here, $x_j(t)$ and $x_p(t)$ are given by (Equation 5.11)-(Equation 5.12). Then

$$\Delta E_{\text{net}}(p) = \Delta E_{g\to f}(p) + \Delta E_{f\to g}(\dot{x}_p(T_p), \dot{x}_j(T_p)), \tag{5.16}$$

with $\Delta E_{g\to f}(\cdot)$ and $\Delta E_{f\to g}(\cdot,\cdot)$ respectively from (Equation 5.6) and (Equation 5.8).

Thus, by Proposition Equation 5.9, we need to find $p > 0$ such that $\Delta E_{net}(p) = 0$. This can be done numerically by a nonlinear root finding method such as fsolve in MATLAB.

Remark 5.3.1. *There are multiple values of p satisfying* (Equation 5.9) *for a fixed x (position where the impulse is applied) and ground phase energy E_g. This gives rise to different* types *of periodic orbits, differing in the duration of the ballistic phase. This will be discussed in more detail below.*

5.3.3 Timing Diagram

Suppose the ground phase energy E_g is fixed, but the position $x \leq 0$ at which the impulse p is applied is varied. As E_g is fixed, we can obtain the pre-impulse velocity $v(x) \geq 0$ from (Equation 5.10). Then, for each x there is a $p(x)$ that satisfies $\Delta E_{\text{net}}(p) = 0$, ensuring periodicity. Shown in Figure 5.2 is a plot of the impulse $p(x)$ (obtained from (Equation 5.9)) versus the departure position x for a *fixed* ground phase energy E_g. These plots are called *timing diagrams* since they details what the impulse $p(x)$ must be to generate a periodic orbit for a given departure position. The relevance for the name "timing diagram" stems from the fact the position x of a periodic motion of a mass-spring system can be related to the time along the orbit. The different curves in Figure 5.2 represent timing diagrams of p versus x for different ground phase energies. In Figure 5.3 different periodic orbits are plotted along the timing diagram for a fixed ground phase energy of $E_g = -300\text{J}$.

5.3.4 Periodic Orbit Types

In Remark 5.3.1 it was mentioned that there could be multiple solutions of p satisfying (Equation 5.9), for fixed E_g and x. This gives rise to different *types* of orbits which we now define.

Definition 5.3.1. *Let T_n be the period of oscillation of the trampoline. A periodic motion of the hybrid system of type κ is such that the duration of the flight phase T_f satisfies $\kappa T_n \leq T_f \leq (\kappa + 1)T_n$ where $\kappa \in \mathbb{N} \cup \{0\}$.*

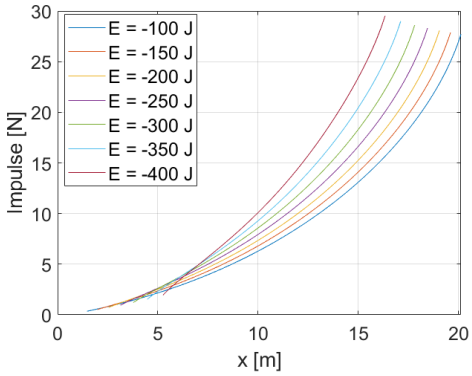

(a) Timing Diagram for different E_g

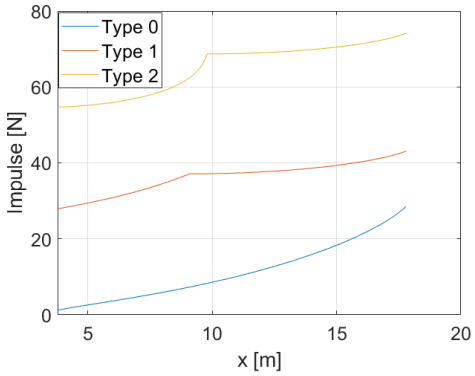

(b) Timing Diagram for different types

Figure 5.2: Plot of Timing Diagrams.

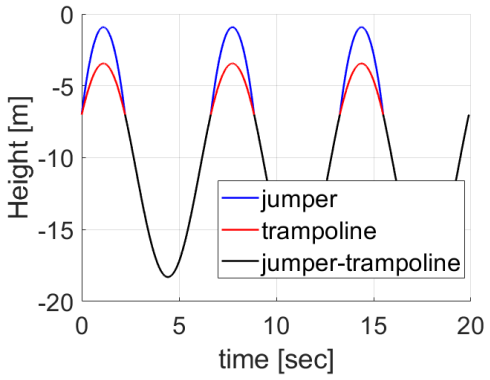

(a)

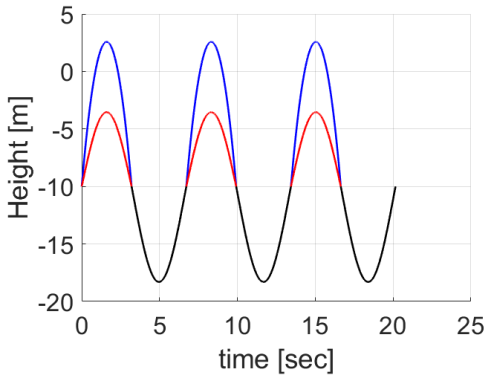

(b)

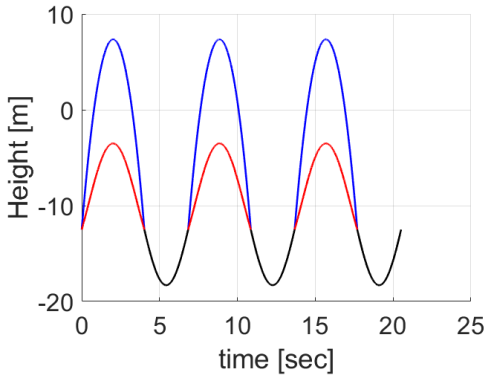

(c)

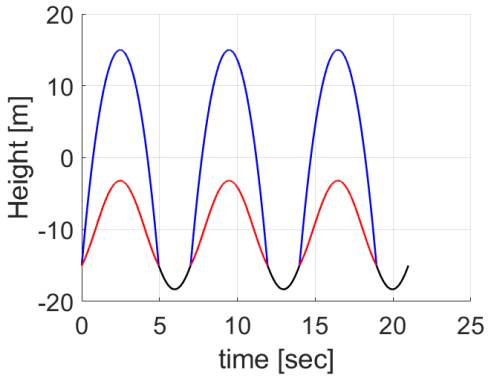

(d)

Figure 5.3: Plot of trajectories of the jumper and trampoline for orbits along the Timing Diagram for $E_g = -300\text{J}$. Throughout this chapter the blue and red curves represent the flight phase trajectory of the jumper and trampoline respectively. The black curve represents the ground phase trajectory of the combined jumper-trampoline mass.

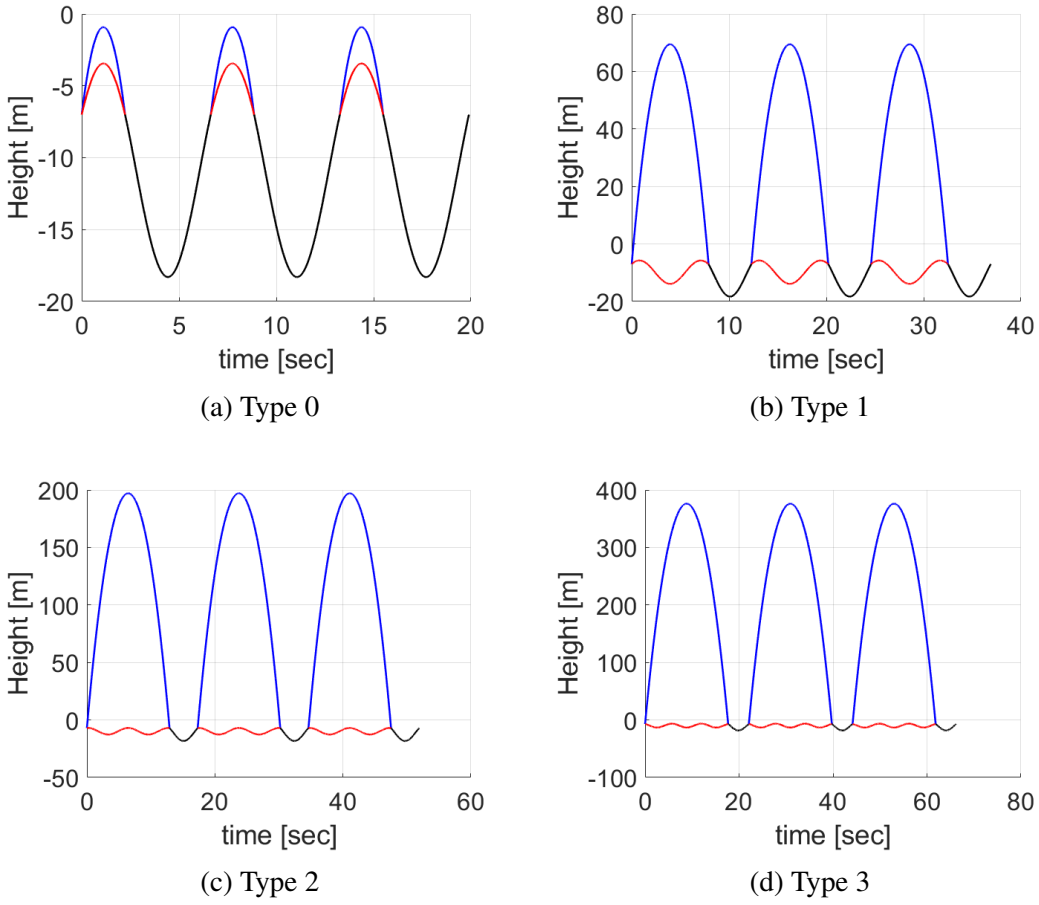

(a) Type 0

(b) Type 1

(c) Type 2

(d) Type 3

Figure 5.4: Plot of Orbits of different types for fixed $E_g = -300\text{J}$.

Referring to Figure 5.4 we see that we have periodic orbits of types zero, one, two and three respectively. All of these orbits have the same ground phase energy of $E_g = -300J$. These were obtained from numerical solutions of (Equation 5.9), for the same x which is the position of the impulse application. The smallest p gives rise to type zero, the next larger solution to type one, etc.

Timing Diagrams

We can construct timing diagrams corresponding to orbits of higher types. The timing diagrams in Figure 5.2a were for orbits of type zero. In Figure 5.2b, we show timing diagrams for orbits of type zero, one, and two all for a fixed ground phase energy of $E_g = -300\text{J}$.

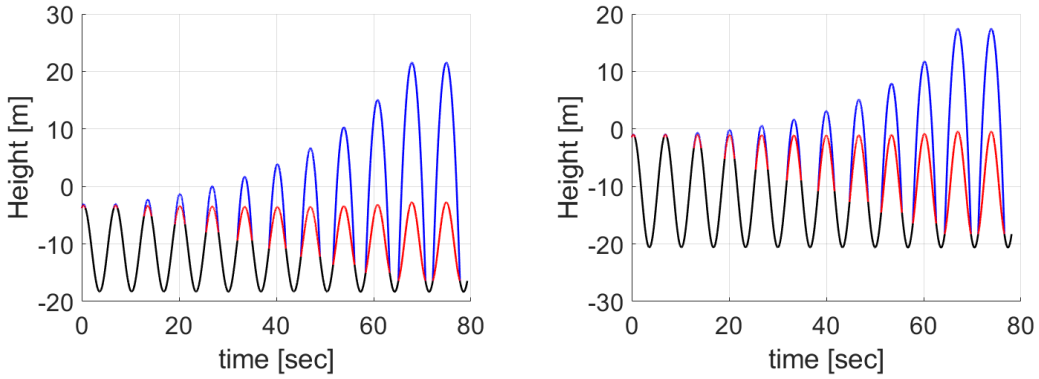

(a) $E_g = -300\text{J}$ (b) $E_g = -100\text{J}$

Figure 5.5: Raccordation with timing diagram.

5.4 Graceful Transitions

In this section, we synthesize graceful transitions between periodic orbits. First, the timing diagram will be used to obtain transitions between orbits lying on the same timing diagram. Subsequently, an optimization problem is proposed the solution of which will yield a graceful transition between periodic orbits of different types and energy.

5.4.1 Raccordation based on Timing Diagram

We denote by $\mathcal{O}(x_{\text{init}})$ and $\mathcal{O}(x_{\text{final}})$ two different periodic orbits on a timing diagram with timing x_{init} and x_{final} respectively. Suppose a raccordation is required in N hops. We choose successive departure points x_j given by

$$x_j = x_{\text{init}} + \frac{j}{N+1}\left(x_{\text{final}} - x_{\text{init}}\right)$$

where j is an integer satisfying $1 \leq j \leq N$. Then, at the jth hop the impulse $p(x_j)$ at position x_j is applied whenever the departure velocity is positive. This will yield a feasible transition by virtue of the timing diagram. Because of the continuity of the timing diagram, the transition will be also graceful for N sufficiently large.

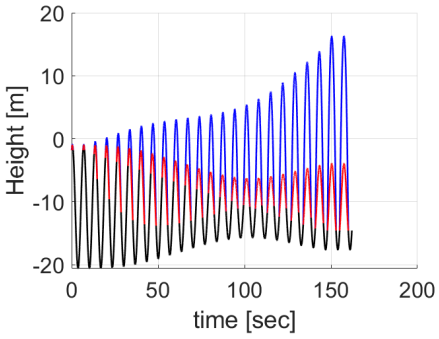

(a) Raccordations

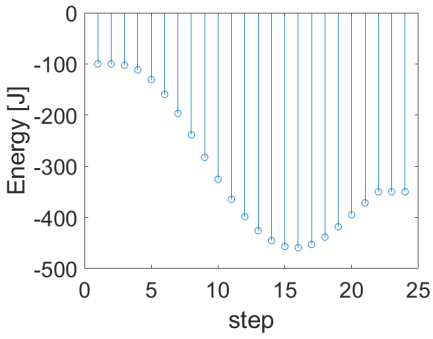

(b) Energy

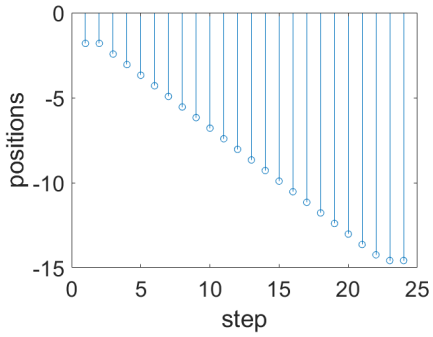

(c) Position

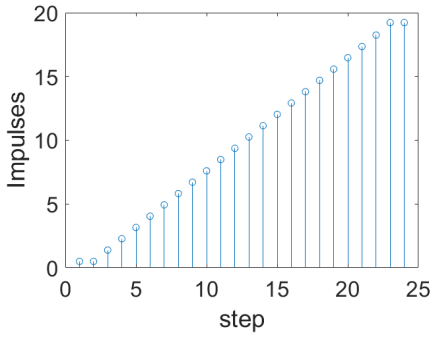

(d) Impulses

Figure 5.6: Raccordation between Orbits of Type 0.

5.4.2 Optimization Problem for Raccordations

We seek to obtain transitions in N hops. Define

$$S = \left\{x_i, v_i, p_i, T_i^F, x_i', v_i', T_i^G\right\}_{i=1}^{N} \tag{5.17}$$

Here x_i represents the combined jumper-trampoline ground phase terminal position, v_i represents the combined jumper-trampoline ground phase terminal velocity, p_i represents the impulse strength, T_i^F represents the flight phase duration, x_i' represents the ground phase initial position, v_i' represents the ground phase initial velocity and T_i^G represents the ground phase duration. The subscript i is present to represent the fact that these are the variables for the i-th hop of the raccordation. S is the vector of all variables stacked together which

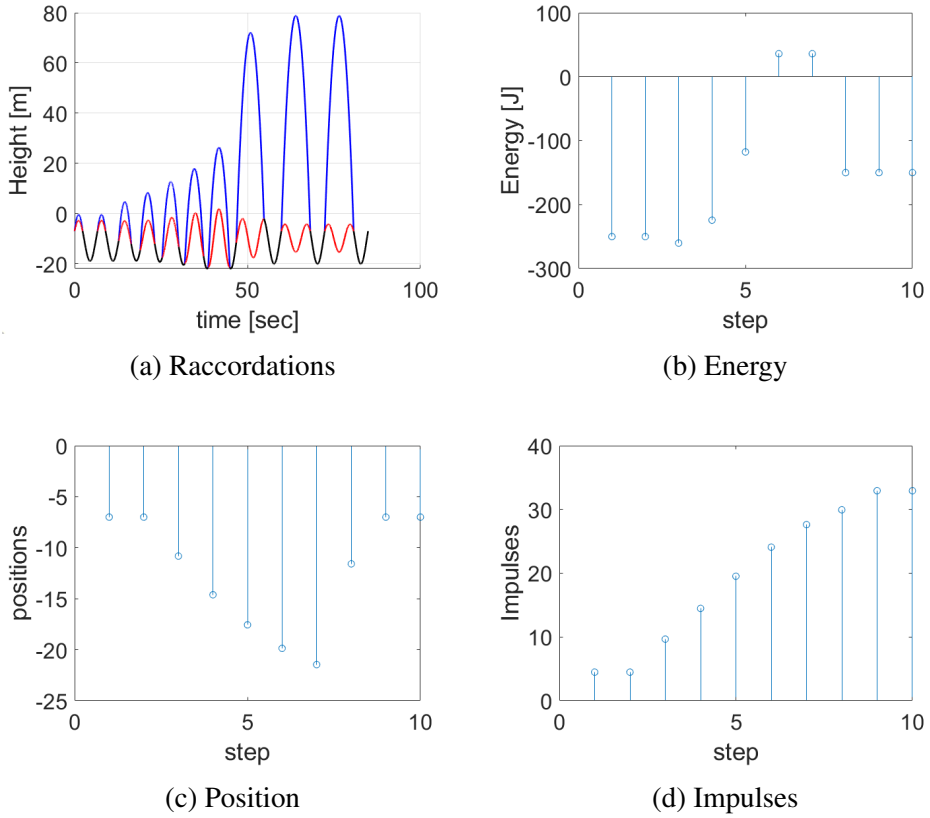

(a) Raccordations (b) Energy

(c) Position (d) Impulses

Figure 5.7: Raccordation between Orbits of Type 0 and Type 1.

is the decision vector for the optimization problem below.

$$\min_{S} \mathcal{J}(S) = \sum_{i=1}^{N} w_p(p_i - p_{i-1})^2 + w_x(x_i - x_{i-1})^2 \tag{Obj}$$

$$\text{subject to} \qquad A_i^F \sin(\omega^F T_i^F + \phi_i^F) - \frac{Mg}{k_g} - x_i' = 0 \tag{C1}$$

$$x_i + (v_i + \frac{p_i}{m})T_i^F - \frac{1}{2}g(T_i^F)^2 - x_i' = 0 \tag{C2}$$

$$v_i' = \Delta\left(v_i + \frac{p_i}{m} - gT_i^F, A_i^F\omega_i^F\cos(\omega^F T_i^F + \phi_i^F)\right) \tag{C3}$$

$$A_i^G \sin(\omega^G T_i^G + \phi_i^G) - \frac{(M+m)g}{k_g} = x_{i+1} \tag{C4}$$

$$A_i^G\omega_i^G\cos(\omega^G T_i^G + \phi_i^G) - v_{i+1} = 0 \tag{C5}$$

where, in (Equation C3)

$$\Delta(v_p, v_j) = \frac{Mv_p + mv_j}{M+m} \tag{5.18}$$

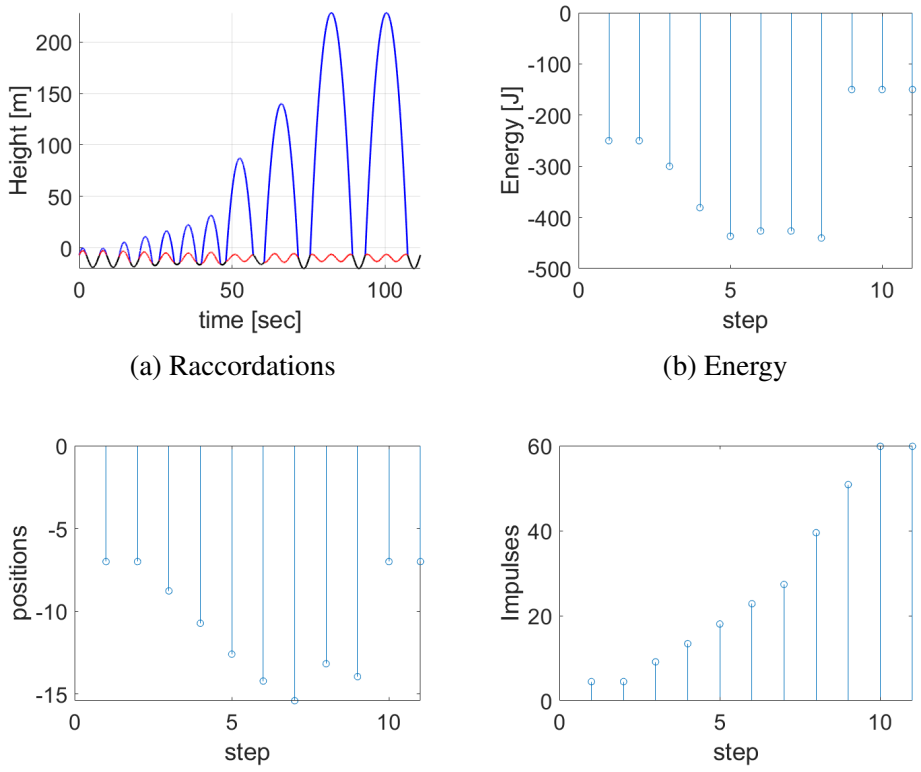

(a) Raccordations (b) Energy

(c) Position (d) Impulses

Figure 5.8: Raccordation between Orbits of Type 0 and Type 2.

as the reset map for the velocities. We also have the following expressions for A_i^F, ω^F, ϕ_i^F,A_i^G, ω^G, ϕ_i^G,

$$A_i^F = \sqrt{\left(x_i + \frac{Mg}{k_g}\right)^2 + \left(\frac{Mv_i - p_i}{M\omega^F}\right)^2} \tag{5.19}$$

$$\phi_i^F = \tan^{-1}\left(\frac{x_i + \frac{Mg}{k_g}}{\frac{Mv_i - p_i}{M\omega^F}}\right) \tag{5.20}$$

$$\omega^F = \sqrt{\frac{k_g}{M}} \tag{5.21}$$

$$A_i^G = \sqrt{\left(x_i' + \frac{(M+m)g}{k_g}\right)^2 + \left(\frac{v_i'}{\omega^G}\right)^2} \tag{5.22}$$

$$\phi_i^G = \tan^{-1}\left(\frac{x_i' + \frac{(M+m)g}{k_g}}{\frac{v_i'}{\omega^G}}\right) \tag{5.23}$$

$$\omega^G = \sqrt{\frac{k_g}{M+m}} \tag{5.24}$$

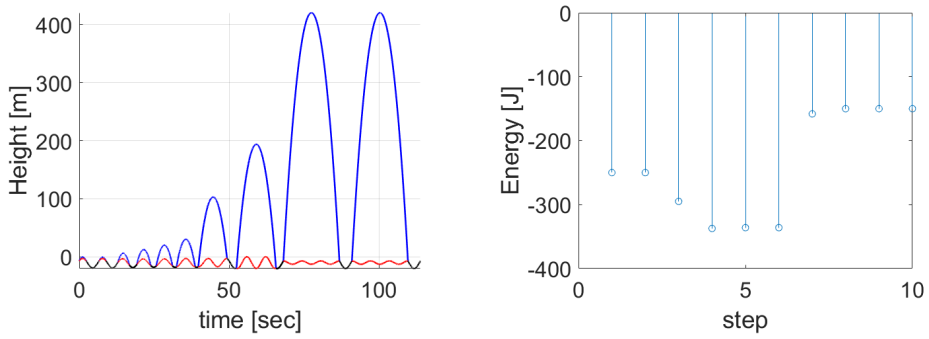

(a) Raccordations

(b) Energy

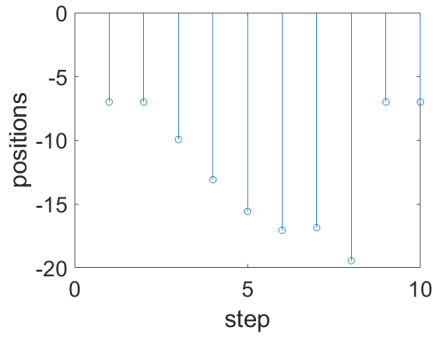

(c) Position

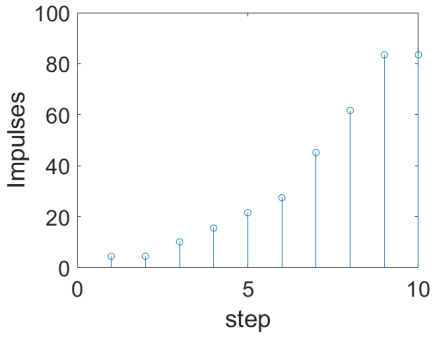

(d) Impulses

Figure 5.9: Raccordation between Orbits of Type 0 and 3.

the optimization objective (Equation Obj) is motivated by the desire to make a transition between the two orbits $\mathcal{O}_1$ and $\mathcal{O}_2$ as gracefully as possible, i.e., with minimal variation of the given periodic behaviors. To this end, we minimize the change in impulse strength and the points of application of the impulse. Note that if $\mathcal{O}_2 = \mathcal{O}_1$, then the cost in (Equation Obj) is zero. The constraints expressed in (Equation C1) - (Equation C5) are just the closed form expressions for the solutions of the dynamics in the flight and ground phase. This is a *kernel method* (see § 2.2) since we can view this as minimizing $\langle \mathbb{O}_p w, \mathbb{O}_p w \rangle_W$ (a weighted metric) where

$$\mathbb{O}_p w = \begin{bmatrix} (\mathbf{I} - \mathbf{S_1})p \\ (\mathbf{I} - \mathbf{S_1})x \end{bmatrix} \tag{5.25}$$

with $\mathbf{S_1}$ being a shift operator that shifts a sequence x to the left. Finally, (Equation Obj) - (Equation C5) can be expressed as a Nonlinear Program

$$\min_{S} \mathcal{J}(S) \tag{5.26}$$

$$s.t. \quad \mathcal{F}(S) = 0 \tag{5.27}$$

$$\text{lb} \leq S \leq \text{ub} \tag{5.28}$$

We solved this problem numerically with fmincon in MATLAB.

5.4.3 Examples

We provide a few examples to the solution of the optimization problem described. Throughout Figure 5.6-Figure 5.9 (a) represents the trajectories of the system. (b) represents the ground phase energy of the system at each hop. (c) represents the position at which the impulse is applied. (d) shows the strength of the impulse. Shown in Figure 5.6 - Figure 5.9 are raccordations between an initial orbit of type 0 and final orbits of type 0, type 1, type 2 and type 3 respectively. We note that even as the strength of the impulses increase (we are injecting energy), the ground phase energy of the system across multiple hops does not necessarily do so as energy is also lost during impacts. The impulses do not increase linearly, but they transfer the system from the initial to the final orbit.

5.5 Rimless Wheel with Impulse

Shown in Figure 5.10 is a schematic of a rimless wheel. The rimless wheel is a popular reduced order model used for understanding locomotion [58, 59] due to the fact that is easy to analyze and can be used for fast motion planning. In this section, we consider the motion of a rimless wheel on hard flat ground. We also consider an impulsive input that can be applied to the system when two spokes are on the ground. Such an input is depicted in Figure 5.10 and the strength of the impulse is denoted by p. The impulses serve

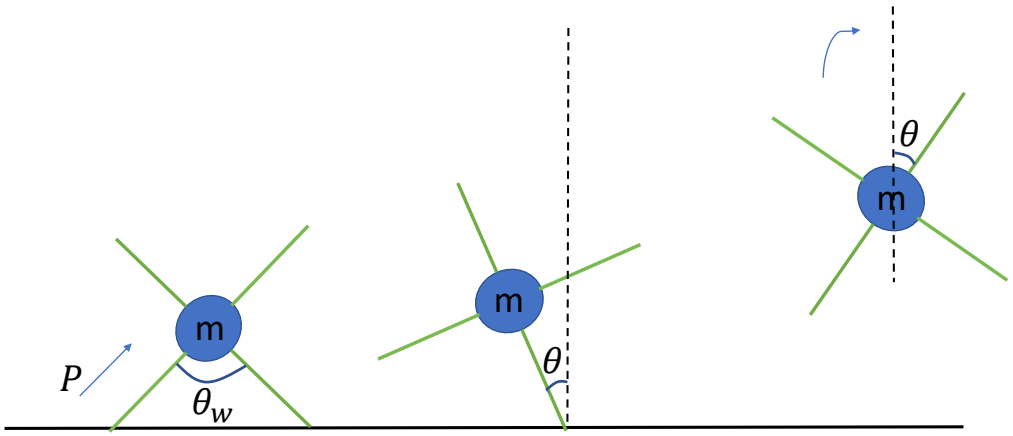

Figure 5.10: Schematic of a 2D Rimless wheel with impulsive kicks.

to inject energy into the system, while the impact of the spokes with the ground dissipates energy. The primary motivation to investigate this system is to consider transitions between different types of periodic orbits, i.e. a periodic orbit with only a ground phase, and a second periodic orbit which contains both a ground phase and a flight phase. We believe that this system could serve as a stepping stone to study transitions between walking to running for bipedal robots. For the system depicted in Figure 5.10 the length of the spoke is L. The angle between spokes is θ_w.

5.5.1 System Model

We now describe the system model. We can model this as a hybrid system with a ground phase and an aerial phase respectively.

Ground Phase

From Newton's laws we have

$$mL^2\ddot{\theta} = mgL\sin(\theta) \tag{5.29}$$

which can also be written as

$$\ddot{\theta} = \frac{g}{L}\sin(\theta) \tag{5.30}$$

which is the same as the dynamics of a pendulum. We provide conditions for completing a step, where a step is defined as the wheel successfully traversing forward in the horizontal direction while rotating about the spoke in contact with the ground. From energy conservation, the kinetic energy will get completely converted to potential energy when the wheel has a spoke completely vertical

$$\frac{1}{2}m\left(L\dot{\theta}_{\min}\right)^2 = mgL\left(1-\cos(\theta_w)\right). \tag{5.31}$$

In other words, the minimum angular velocity is

$$\dot{\theta}_{\min} = \sqrt{\frac{2g}{L}\big(1-cos(\theta_w)\big)} \tag{5.32}$$

if $\dot{\theta}(0) > \dot{\theta}_{\min}$, the rimless wheel completes a step. The acceleration (along the vertical direction) of the mass is given by

$$\ddot{y} = -L\sin(\theta)\ddot{\theta} - L\dot{\theta}^2\cos(\theta) \tag{5.33}$$

The normal force exerted by the ground on the mass is given by

$$\begin{aligned} N &= mg + m\ddot{y} && (5.34)\\ &= mg - mL\sin(\theta)\ddot{\theta} - mL\dot{\theta}^2\cos(\theta) && (5.35)\\ &= \left(mg\cos(\theta) - mL\dot{\theta}^2\right)\cos(\theta) && (5.36) \end{aligned}$$

The wheel is in the ground phase as long as $N \geq 0$ i.e. as long as

$$\|\dot{\theta}\| \leq \sqrt{\frac{g\cos(\theta)}{L}} \tag{5.37}$$

when $N = 0$, transition to flight phase occurs.

Ground Phase to Ground Phase Impact: In the event that $N \geq 0$ throughout the ground phase, transition to flight does not occur, resulting in an additional spoke hitting the ground. In that case, by conservation of angular momentum,

$$\dot{\theta}^{+} = \dot{\theta}^{-} cos(\theta_w) \tag{5.38}$$

where $\dot{\theta}^{-}$ is the angular velocity just before impact and $\dot{\theta}^{+}$ is the angular velocity just after impact.

Flight Phase

To model the dynamics in the flight phase, we use the generalized coordinates $q = [x, y, \theta]^{\top}$, where x and y represent the Cartesian position of the mass. θ represents the rotation of the spoke w.r.t. vertical as shown in Figure 5.10.

Ground Phase to Flight Phase Reset: Since the generalized coordinates is three dimensional as opposed to being one dimensional in the ground phase, we have the reset map from the ground phase to the flight phase given by $q = \Delta_q(\theta)$, where

$$\Delta_q(\theta) = \begin{bmatrix} L\sin(\theta) + p_x \\ L\cos(\theta) \\ \theta \end{bmatrix} \tag{5.39}$$

where p_x is the x position of the ground contact point. Then it also follows that

$$\dot{q} = \frac{\partial \Delta_q}{\partial \theta}(\theta)\dot{\theta} \tag{5.40}$$

Dymamics: The dynamics of the system is given once again by Newton's Laws

$$\ddot{x} = 0 \tag{5.41}$$

$$\ddot{y} = -g \tag{5.42}$$

$$\ddot{\theta} = 0. \tag{5.43}$$

During the flight phase, all spokes are above the ground. Whenever, any of the spokes touch the ground, the system transits back to the ground phase as discussed below.

Flight Phase to Ground Phase Reset: From Appendix A we know that the position components q are continuous during impact, however, the velocity components undergo a discontinuous change due to inelastic impact. We can represent this as

$$\begin{bmatrix} q^+ \\ \dot{q}^+ \end{bmatrix} = \begin{bmatrix} q \\ \Delta_{\dot{q}}(q)\dot{q}^- \end{bmatrix} \tag{5.44}$$

We need to reset the state from the three dimensional position components q to the one dimensional quantity θ for the subsequent ground phase dynamics. This can be done by

$$\theta^+ = \Delta_\theta(q^+) = \tan^{-1}\left(\frac{x^+ - p_x}{y^+}\right) \tag{5.45}$$

where p_x is the x position of the point of contact of the spoke with the ground. The angular velocity can be given as

$$\dot{\theta}^+ = \frac{\partial \Delta_\theta}{\partial q}(q^+)\dot{q}^+. \tag{5.46}$$

This completes the full reset map.

Control Input

The control input can only be applied when two spokes are on the ground. The change in the angular velocity is again obtained from Newton's laws

$$\dot{\theta}_{\text{after}} = \dot{\theta}_{\text{cur}} + \frac{p}{mL}\sin(\theta_w) \tag{5.47}$$

where p denotes the strength of the impulse. Given a desired angular velocity $\dot{\theta}_{\text{des}}$, we can solve for the impulses using (Equation 5.47) as

$$p = \frac{mL}{\sin(\theta_w)}\left(\dot{\theta}_{\text{after}} - \dot{\theta}_{\text{cur}}\right) \tag{5.48}$$

where $\dot{\theta}_{\text{cur}}$ represents the current angular velocity just before application of the impulse.

5.5.2 Determination of Periodic Orbits

The impulsive control input can only be applied when two spokes are on the ground, which occurs during a ground phase to ground phase transition or (in the unlikely case of) a flight phase to ground phase transition with two spokes on the ground. *Thus to generate a periodic orbit we need to*

1. Choose a $\dot{\theta}^{+}_{\text{des}}$ at the start of a ground phase.
2. Simulate the hybrid system forward until it reaches a spot where two spokes are on the ground.
3. Choose the impulse p according to (Equation 5.48).

5.5.3 Transitions

We can assume that the orbits are respectively characterized by their angular velocities $\dot{\theta}^{+}_{\text{init}}$ and $\dot{\theta}^{+}_{\text{fin}}$ respectively. We find a transition in M steps. To find a control input to steer the

system from orbit $\mathcal{O}_1$ to $\mathcal{O}_2$, we choose

$$\dot{\theta}_i^+ = \dot{\theta}_{\text{init}}^+ + \frac{i}{M}(\dot{\theta}_{\text{fin}}^+ - \dot{\theta}_{\text{init}}^+) \tag{5.49}$$

where $i = 1, 2, \cdots, M-1$. Once the $\dot{\theta}_i^+$ are determined, we can obtain the impulses as

$$p_i = \frac{mL}{\sin(\theta_w)}(\dot{\theta}_i^+ - \dot{\theta}_i^-) \tag{5.50}$$

where $\dot{\theta}_i^-$ are the angular velocities of the wheel at the ith step obtained by forward evaluation of the dynamics.

5.5.4 Results

Shown in Figure 5.11 are a plot of two different periodic orbits of this system. The blue curves represent the ground phase of the system, while the red curves represent the flight phase of the system. The components plotted are the Cartesian position of the mass, and it's angular position. Shown in Figure 5.12 are the transitions between these types of orbits. One can see the wheel moves progressively faster by looking at the velocity plots v_x in Figure 5.12. One can also inspect the vertical motion (y[m]) of the rimless wheel in Figure 5.12.

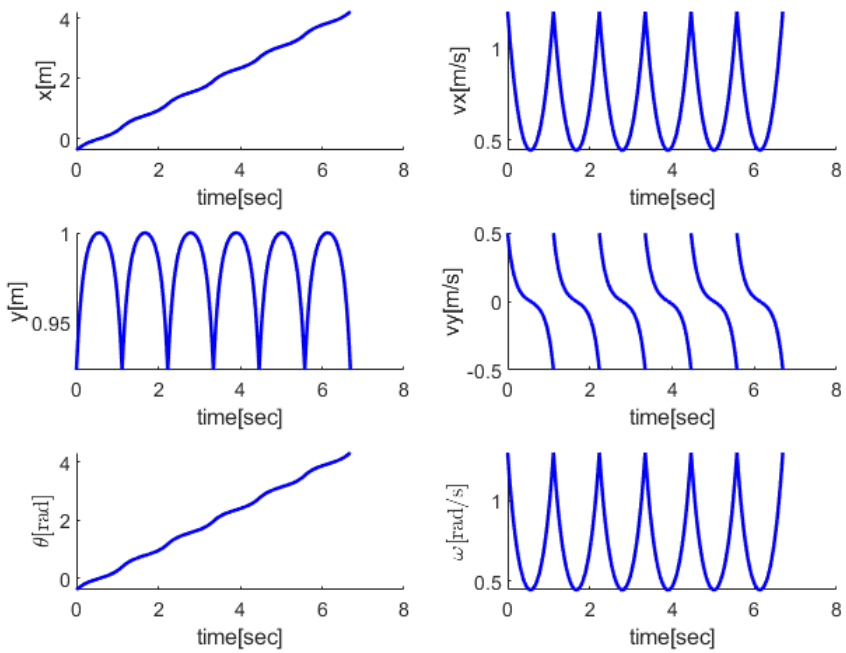

(a) Periodic Orbit with only ground phase

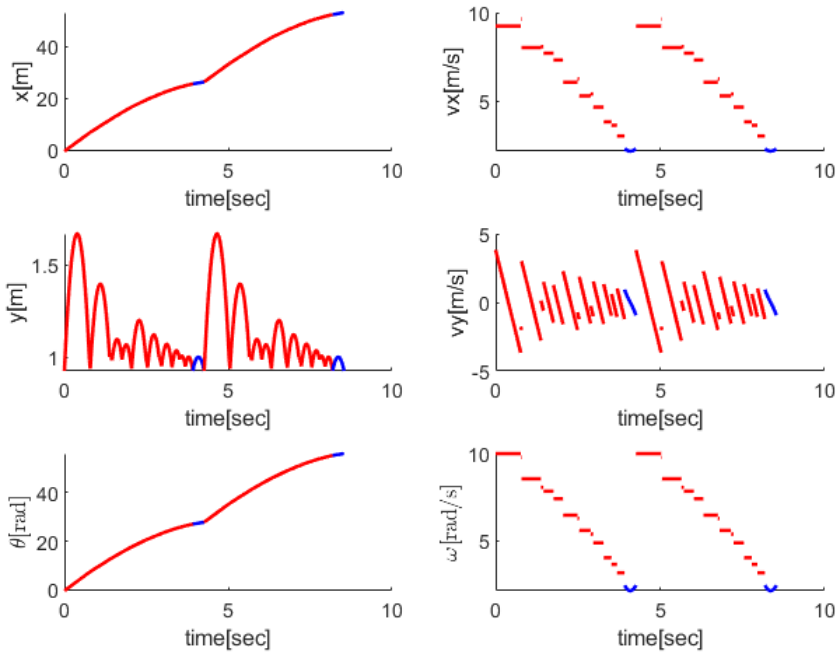

(b) Periodic Orbit with both Ground and Flight Phase

Figure 5.11: Plot of Periodic Orbits. Red and blue curves represent flight and ground phase respectively.

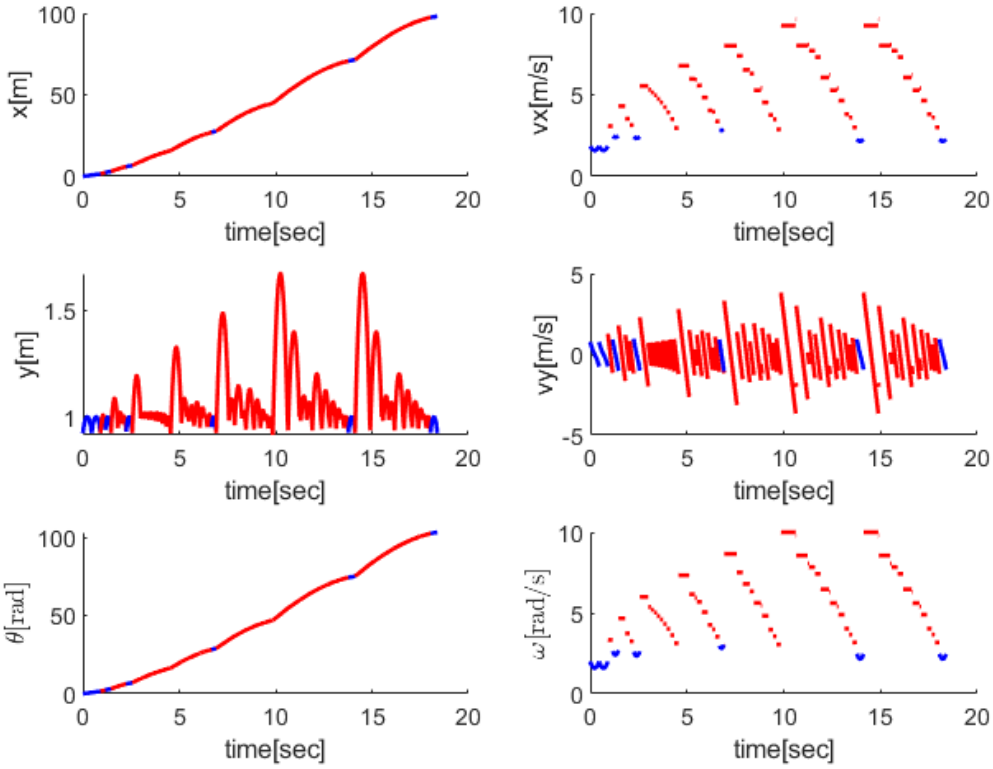

Figure 5.12: Plot of Transitions for the rimless wheel.

CHAPTER 6

KERNEL METHOD FOR HOPPING ROBOTS ON GRANULAR TERRAIN

6.1 Introduction

In this chapter, we continue our study of hopping robots initiated in Chapter 5. We consider hopping robots on deformable, granular terrain. This also furnishes more involved examples of hybrid dynamical systems for which we demonstrate the kernel method. The raccordations obtained in this chapter are between periodic orbits that traverse the same domain sequences in the same order. As a result, these methods are not directly extensible to transitions between gaits of different types, e.g. walking to running.

The first system we consider is a hopping robot on granular media as depicted in Figure 6.1. Granular media is a substrate whose forces have both solid-like and fluid like behaviors [60]. Several methods exist for describing such forces such as discrete element methods (DEM) and Coloumb friction based resistive force theories (RFT). However, these models have drawbacks such as being too computationally expensive to simulate quickly, or not being accurate for certain object-substrate interactions (like high speed intrusions) [60]. More recently added mass models have been proposed to describe substrate forces of granular media [61]. These models are relatively simple, and have been demonstrated to be accurate [61, 60] on experimental platforms. We use this as a model for the substrate force for the hopping robot in Figure 6.1. We include this in our optimization to determine periodic orbits and for transitioning between orbits.

The second system we consider is a 2D kicker on deformable terrain. Here a simple one-way spring is used as a model of the granular substrate force owing to the complexities of rotational, longitudinal and vertical dynamics, as opposed to the added mass model. The periodic orbits and transitions between them are determined via numerical optimization.

6.2 Obtaining Graceful Transitions

We refer the reader to § 2.4 for our definition of hybrid systems and the associated terminology. We denote by $\mathcal{D} = \bigcup_i \mathcal{X}_i$, i.e it is the union of all the domains of the hybrid system.

Definition 6.2.1. *A Cycle is a trajectory of the hybrid system with the initial domain the same as the final domain. Two Cycles are of the same type if their domain sequences are the same.*

Definition 6.2.2. *A* periodic orbit $\gamma : [0, T] \to \mathcal{D}$ *of a hybrid system is a cycle such that* $(\gamma(T), u(T)) \in \mathcal{G}(q_k, q_1)$ *and* $R(q_K, q_1)\gamma(T) = \gamma(0)$. *Here* $\mathcal{G}(\cdot,\ \cdot)$ *and* $\mathcal{R}(\cdot,\ \cdot)$ *denote the guard set and the reset map respectively.*

A periodic orbit is a cycle with the initial point same as the final point. Note that a cycle is more general than a periodic orbit. Let $\gamma_1 : [0, T_1] \to \mathcal{D}$ and $\gamma_2 : [0, T_2] \to \mathcal{D}$ be two periodic orbits of the Hybrid System $\mathcal{H}$ generated by control signals v_1 and v_2 respectively. Let N be a given positive integer. We formulate an optimal control problem that captures the notion of a graceful transition from γ_1 to γ_2 in N cycles.

We say that a function $x : [0, T] \to \mathcal{D}$ is a transition in N cycles from the periodic orbit γ_1 to the orbit γ_2 if

- $x(t)$ is a solution of the hybrid system $\mathcal{H}$ for some $u(t)$ and consists of N cycles.
- $x(t)$ starts at the initial orbit, i.e. $x(0) = \gamma_1(0)$.
- $x(t)$ ends at the start of the final orbit, i.e. the guard condition $(x(T), u(T)) \in \mathcal{G}(q_K, q_1)$ holds and the reset map condition $\mathcal{R}(q_K, q_1)x(T) = \gamma_2(0)$ holds.

We denote by $x^i_j : [t^{i-1}_j, t^i_j] \to \mathcal{X}_{q_i}$ the portion of the transition $x(t)$ which lies completely in the domain $\mathcal{X}_{q_i}$ during the jth cycle with t^{i-1}_j, the point of entry into $\mathcal{X}_{q_i}$ and $\left(x^i_j(t^i_j), u(t^i_j)\right) \in G(q_i, q_{i+1})$ i.e. t^i_j is the time of departure from $\mathcal{X}_{q_i}$. Here $j = 0, \cdots, N+1$

is the index of the cycle and $i = 1, \cdots, K$ represents the ith domain *during* the jth cycle. Here, the zeroth cycle $x_0(t)$ denotes the initial periodic orbit $\gamma_1(t)$ and the $(N+1)$th cycle $x_{N+1}(t)$ denotes the final periodic orbit $\gamma_2(t)$.

Let Z be any set. To any function $f : [t_1, t_2] \to Z$ we denote by $Sf : [0, 1] \to Z$ to be the function defined by

$$Sf(t) = f\left((t_2 - t_1)t + t_1\right) \tag{6.1}$$

Definition 6.2.3. *The transition $x(t)$ from γ_1 to γ_2 is said to be* graceful *if it minimizes the cost functional*

$$J(x) = \sum_{j=1}^{N+1} \sum_{i=1}^{K} \int_0^1 (Sx_j^i - Sx_{j-1}^i)^\top W_j^i (Sx_j^i - Sx_{j-1}^i) dt. \tag{6.2}$$

where W_j^i is a sequence of positive semidefinite matrices.

Hence we need to determine a function $x(t)$ that minimizes (Equation 6.2) subject to the constraints that it be a transition from $\gamma_1(t)$ to $\gamma_2(t)$.

The motivation for the cost function can be seen as follows: The cost is a measure of the difference between the signals $x_j^i(t)$ and $x_{j-1}^i(t)$ for each domain i. Thus we expect the first cycles $x_1^i(t)$ to be close to the initial periodic orbit $\gamma_1^i(t)$ in each domain. We also have a similar situation for x_N^i and γ_2^i. Thus a minimizing function of eqn (Equation 6.2) can be expected to start out at periodic orbit γ_1 and gradually change to reach the periodic orbit γ_2 by keeping the differences in consecutive cycles small. Since the signals $x_j^i(t)$ and $x_{j-1}^i(t)$ may be defined on different intervals, we use the scaling operator to ensure that Sx_j^i and Sx_{j-1}^i are defined on $[0, 1]$ in the cost function (Equation 6.2).

Remark 6.2.1. *Instead of the cost (Equation 6.2) one can also minimize the difference between a general function of the scaled and translated states, by replacing the scaled version of the states Sx_j^i by $h(Sx_j^i)$ in* (Equation 6.2)*. This can be used when we don't require all of the states to be periodic but only a subset of it's components.*

Remark 6.2.2. *One can also consider the case where the the vector fields f^i depend on a set of parameters p, i.e $f^i = f^i(x, u; p)$. Assume that γ_j for $j = 1, 2$ are two distinct periodic orbits satisfying $\dot{\gamma}^i_j = f^i(\gamma^i_j, v^i_j; p_j)$ in each $\mathcal{X}_{q_i}$. Assuming that the parameter set p changes from p_1 to p_2 at $t = t_0$ when $(\gamma_1(t_0), u(t_0)) \in \mathcal{G}(X_{q_1}, X_{q_2})$, we can use the same cost (Equation 6.2) to obtain a graceful transition from the orbit γ_1 to γ_2. In the example hybrid system of the 2D actuated rod discussed in § 6.4, the parameter set p will represent the type of terrain. The terrain changing will represent the parameter set p changing. As the rod enters the second terrain at $t = 0$, the dynamics constraint is given by $f^i(x, u; p_2)\ \forall i$. The number of cycles, N, in transition period is one of the design parameter. In contrast, K is a fixed quantity and is a property of the hybrid system.*

6.2.1 Transforming the optimal control problem

We write the optimal control problem (Equation 6.2) in an equivalent standard form. We know that $x^i_j(t)$ satisfies the differential equation

$$\dot{x}^i_j = f^i\left(x^i_j, u^i_j\right) \tag{6.3}$$

for some function $u^i_j : [t^{i-1}_j,\ t^i_j] \to U$. Let us define $\bar{x}^i_j = Sx^i_j$ and $\bar{u}^i_j = Su^i_j$. Then one can easily verify that

$$\frac{d}{dt}\bar{x}^i_j = (t^i_j - t^{i-1}_j) f^i(\bar{x}^i_j, \bar{u}^i_j) \tag{6.4}$$

Let us also define $\tau^i_j = t^i_j - t^{i-1}_j$. Then the optimization problem (Equation 6.2) can be written as

$$\min_{x^i_j, u^i_j, \tau^i_j} \sum_{j=1}^{N+1} \sum_{i=1}^{K} \int_0^1 (\bar{x}^i_j - \bar{x}^i_{j-1})^\top W^i_j (\bar{x}^i_j - \bar{x}^i_{j-1}) dt. \tag{6.5}$$

subject to the dynamical system constraints:

$$\frac{d\bar{x}^i_j}{dt} = \tau^i_j f^i(\bar{x}^i_j, \bar{u}^i_j) \tag{6.6}$$

and the initial constraint:

$$\bar{x}_1^1(0) = \gamma_1(0). \tag{6.7}$$

Assuming that the domain $\mathcal{X}_{q_i}$ admits defining functions $d^i(x) \leq 0$ for all $x \in \mathcal{X}_{q_i}$ (in some ambient space), we can write the domain constraint as

$$d^i\left(\bar{x}_j^i(t)\right) \leq 0. \tag{6.8}$$

Similarly assuming that the guard set in each domain admits a defining functions $g^i(x) = 0$ and $m^i(x, u) < 0$ we write the guard conditions as

$$g^i(\bar{x}_j^i(1)) = 0. \tag{6.9}$$

$$m^i(\bar{x}_j^i(1), \bar{u}_j^i(1)) < 0. \tag{6.10}$$

If we denote the reset map in the guard set of the ith domain by R^i the reset condition is (for $i = 1, \cdots, K-1$).

$$\bar{x}_j^{i+1}(0) = R^i\left(\bar{x}_j^i(1)\right). \tag{6.11}$$

For $i = K$ and $j = 1, \cdots, N$ the reset condition takes the form

$$\bar{x}_{j+1}^1(0) = R^K\left(\bar{x}_j^K(1)\right). \tag{6.12}$$

For $j = N$, (Equation 6.12) is actually the final constraint. We can also consider τ_j^i as a state variable by introducing $\dot{\tau}_j^i = 0$ with the inequality constraint $\tau_j^i > 0$. If we define X_s to be the vector obtained by stacking the states $X_s = \{x_1^1, \tau_1^1, \ \ldots, x_N^K, \tau_N^K\}$ and U_s to be the vector of inputs $U_s^\top = \{u_1^1, u_1^2, \ \ldots, u_N^K\}$ then the optimal control problem (Equation 6.5) becomes

$$\min_{X_s, U_s} \int_0^1 L(X_s) dt. \tag{6.13}$$

subject to the constraints

$$\dot{X}_s = F(X_s, U_s). \tag{6.14}$$

$$b(X_s(0), X_s(1)) = 0. \tag{6.15}$$

$$p(X_s(t)) \leq 0. \tag{6.16}$$

$$m_s(X_s(1), U_s(1)) < 0. \tag{6.17}$$

where $L(X_s)$ is an equivalent expression for the integrand of (Equation 6.2) using the augmented states, b represents reset conditions and equality guard constraints, m_s represents strict inequality guard constraints, and p represents domain constraints.

Transcription of Optimal Control Problem to Nonlinear Programming Problem

The optimal control problem detailed above can be transcribed into nonlinear programming problems by using a MATLAB based software, OPTRAGEN [41]. The resulting nonlinear program was solved by IPOPT 3.12.6, a software using interior point method to solve the nonlinear program [62].

6.3 1D Hopper

Our aim in this section is to obtain graceful transitions for the 1D Hopper jumping on deformable granular media. More detailed physics of the hopper can be found in [60, 61].

6.3.1 Granular Media Model

The visualization of 1D Hopper jumping on deformable granular media is shown in Figure 6.1. As the foot intrudes the granular media, the grain on the ground gets compacted forming a cone shape, which behaves as if a mass was added to the foot (Figure 6.1b). Throughout this subsection we assume that $z_f \leq 0$ where z_f is the position of the foot

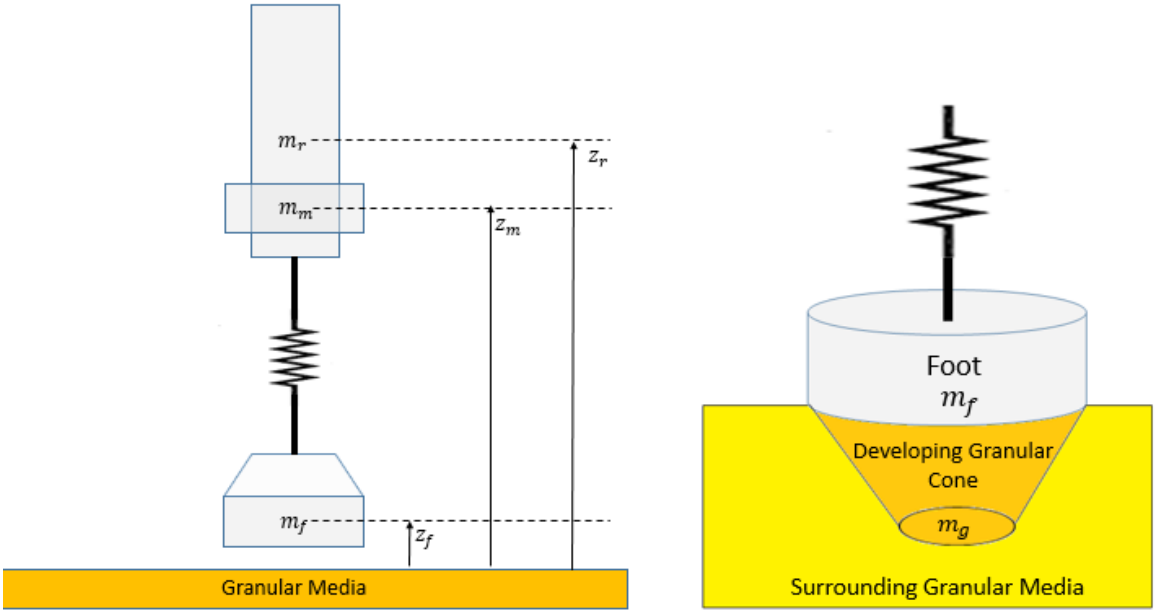

Figure 6.1: (a) A sketch of the 1D jumping hopper. (b) Depiction of the added mass model of the granular media.

(Figure 6.1a). The added mass model can be written as

$$A_{flat}(z_f) = \pi \left(R + \frac{\mu z_f}{\tan(\theta)} \right)^2 \tag{6.18}$$

$$A_{cone}(z_f) = \frac{\pi R^2 - A_{flat}(z_f)}{\cos(\theta)}. \tag{6.19}$$

The added mass m_g to the foot is then given by

$$m_g(z_f) = -c_g \phi \rho \mu \int_0^{z_f} A_{flat}(s) ds. \tag{6.20}$$

Finally the substrate force exerted by the granular media on the foot is given by

$$\psi_g(z_f, \dot{z}_f) = \frac{k_{sh}}{\pi R^2} \int_0^{z_f} A_{flat}(s) ds + \sigma_{rft} \int_0^{z_f} A_{cone}(s) - b \dot{m}_g \dot{z}_f. \tag{6.21}$$

$$F_g = \psi_g(z_f, \dot{z}_f) - m_g \ddot{z}_f \tag{6.22}$$

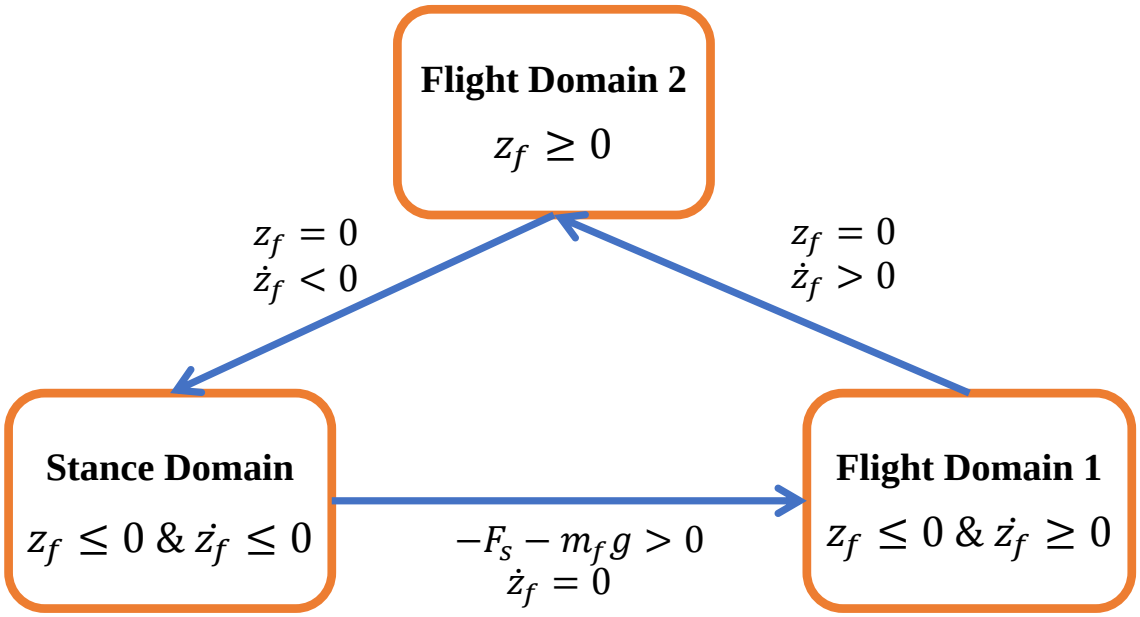

Figure 6.2: Schematic Description of Hybrid System for 1D Hopper.

The values and meaning of all parameters can be found in [60].

6.3.2 Hybrid System Model of Hopper.

We define the configuration space of the system to be $q^\top = [z_m, z_r, z_f]$ where z_m is the motor position, z_r is the rod position, z_f is the foot position (Figure 6.1a). The states are given by $x^\top = \left[q^\top, \dot{q}^\top\right]$. We denote by $u = F_m$ the motor force. The spring force can be written as

$$F_s(x) = k_s(z_f - z_r + \ell_0) - c_s(\dot{z}_r - \dot{z}_f) \tag{6.23}$$

where k_s is the spring coefficient and c_s is the damping coefficient. Three discrete domains $Q = (Stance, Flight1, Flight2)$, the guard condition G, and each domain are shown in Figure 6.2.

Stance domain

During the stance domain, the model can be written as

$$M_{gr}(q)\ddot{q} + C_{gr}(q, \dot{q}) = Bu. \tag{6.24}$$

where $M_{gr} = diag(m_m, m_r, m_f + m_g)$ and $C_{gr} = [m_m g, -F_s + m_r g, +F_s + m_f g - \psi_g(z_f, \dot{z}_f)]$ and B is given by $B^\top = [1, -1, 0]$. We assume that $z_f \leq 0$ (foot is penetrating the media) and $\dot{z}_f \leq 0$ (the granular media has no restorative motion). The substrate force must always be positive i.e $F_g \geq 0$. The transition to the flight domain occurs when the foot velocity $\dot{z}_f = 0$. To prevent zeno executions we assume that the spring force is large enough to lift the foot against it's weight i.e $-F_s - m_f g > 0$.

Flight Domain 1

In the Flight Domain 1 the equations are:

$$M_{fl}(q)\ddot{q} + C_{fl}(q, \dot{q}) = Bu. \tag{6.25}$$

M_{fl} is given by M_{gr} with $m_g = 0$. C_{fl} is given by C_{gr} with $\psi_g = 0$. Once the granular media is deformed, it has no restoring force and it stays deformed. In this domain, the foot position needs to satisfy $z_f^{end} \leq z_f \leq 0$ where z_f^{end} is the final foot position at the end of the stance domain and zero is the undeformed (initial) level of the granular media. More concretely In Flight Domain 1, the foot has lost contact with the deformed media. Instead of imposing $z_f^{end} \leq z_f \leq 0$ as the constraint we introduce a stronger set of constraints $z_f \leq 0$ and $\dot{z}_f \geq 0$, i.e we want the foot position to monotonically increase from z_f^{end} up to zero. Transition from Flight Domain 1 to Flight Domain 2 occurs when the foot position $z_f = 0$ and the foot velocity $\dot{z}_f > 0$.

Flight Domain 2

In the Flight Domain 2 the dynamics equation is the same as Flight Domain 1, i.e is given by (Equation 6.25). The force experienced by the hopper foot when it reintrudes the granular media is not well known. For this reason, we assume that the hopper *sees new ground* as the foot position z_f rises above zero. For this reason, we assume that we reinitialize the granular media to its undeformed level (which is zero) whenever the foot position z_f rises above zero. For the purposes of vertical 1D hopping, this is not physically possible but it would be true if there was a horizontal component of motion (see § 6.4). Thus Flight Domain 2 defined by the foot position $z_f(t) \geq 0$. Transition from Flight Domain 2 to Stance Domain occurs when the foot position $z_f = 0$ (comes in contact with new ground) and the foot velocity $\dot{z}_f < 0$. Transition from Flight Domain 2 back to the Stance Domain occurs when the foot position $z_f = 0$ and foot velocity $\dot{z}_f < 0$.

6.3.3 Results

We have here a hybrid system with three domains: Stance Domain, Flight Domain 1 and Flight Domain 2. We show in Figure 6.3 a transition between two distinct periodic orbits. The initial periodic orbit is shown in blue and was obtained by *minimizing* the integral of the actuator velocity $\int \dot{z}_m^2 dt$ (minimizing the energy of the input typically yields oscillatory solutions), subject to the hybrid dynamics constraints and periodicity constraints. This results in a low jump height of 1.2 mm, where jump height is defined as the maximum position of the foot z_f above zero (the undeformed level of granular media). The final periodic orbit shown in pink, was obtained by *maximizing* the integral of the foot position $\int z_f^2 dt$. This results in a high jump height of 36 mm. Figure 6.3 show a graceful transition of all the state components from the initial periodic orbit to the final one. One can see the jump height gradually rising from 1.2 mm to 36 mm in $N = 3$ cycles. Similar transitions occur for the other components e.g $z_r(t)$ and $z_m(t)$. Throughout all cycles, an actuator bound of $-80N \leq u \leq 80N$ was given where u is the force provided by the motor.

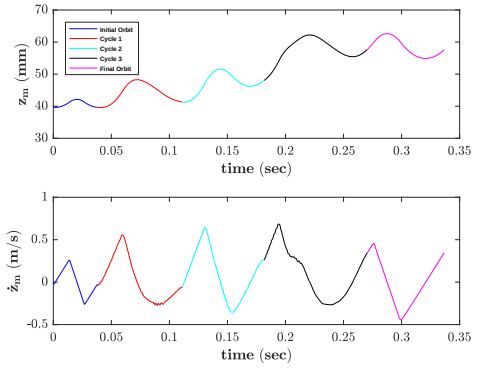

(a) z_m and $\dot{z}_m$

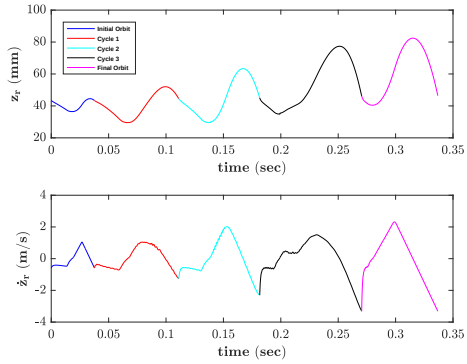

(b) z_r and $\dot{z}_r$

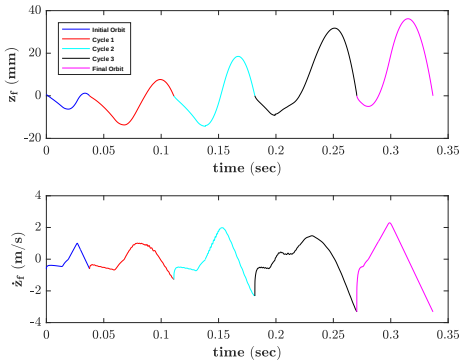

(c) z_f and $\dot{z}_f$

Figure 6.3: Plot of state trajectories for raccordation.

Parameter Values

The mass of the motor $m_m = 0.948$ Kg, the mass of the rod was $m_r = 0.165$ Kg, the mass of the foot was assumed to be $m_f = 0.044$ Kg. The spring constant was assumed to be $k_s = 2730$ N/m and natural length 5 cm. The damping coefficient b_s was assumed to be 500 N s/m. The foot is a circular disk (see Figure 6.1b) with diameter 7.6 cm. All other parameters pertaining to the granular media can be found in [60]. We used the cost (Equation 6.2) with the weight values $W_j^i = diag(0.1, 0.05, 5)$ for $j = 1, 2, 3$ cycles and $i = 1, 2, 3$ domains.

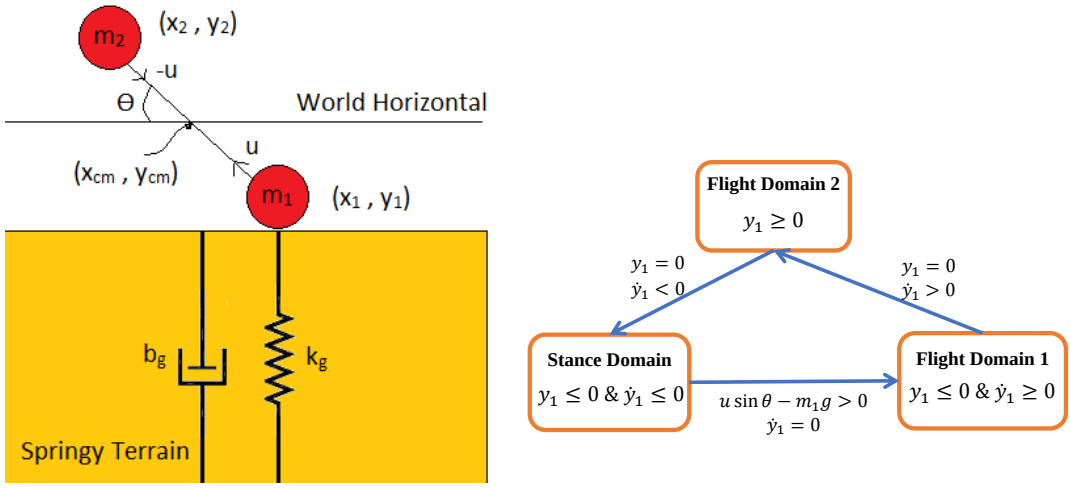

(a) (b)

Figure 6.4: Schematic of an actuated rod and it's hybrid system description

6.4 2D Actuated Jumper on Springy Terrain

Figure 6.4 shows a 2D rod with two point masses m_1 and m_2 moving on elastic, deformable terrain. The two masses are connected by a massless rod that is actuated by a force u. The substrate force exerted by the media will be approximated by a simple one way spring damper model instead of (Equation 6.22). The distances from masses m_1 and m_2 to the Center of Mass (CoM) is denoted by ℓ_1 and ℓ_2 respectively. From Figure 6.4 and definition of ℓ_1, we see that the position of mass m_1 which we denote by $[x_1, y_1]$ is given by $[x_1, y_1] = [x_{cm} + \ell_1 \cos\theta, y_{cm} - \ell_1 \sin\theta]$. We note that this model is a simplification of the rimless wheel, described in [63] and [64] where its potential multiple gaits, by individual actuation of the spokes, were demonstrated. Here we take the model of the rimless wheel with actuated spokes a bit further by allowing each spoke to enable a kicking acting (as opposed to slower extension) in the radial direction (i.e. similar to the above 1-D hopper).

6.4.1 Hybrid System Model

We have $q^\top = [x_{cm}, y_{cm}, \theta, \ell_1]^\top$ and $x^\top = [q^\top, \dot{q}^\top]$. We define $m_{tot} = m_1 + m_2$ and $c = m_1(1 + \frac{m_1}{m_2})$. Three discrete states $Q = (Stance, Flight1, Flight2)$, the guard condition

G, and each domain are shown in Figure 6.4.

Stance domain

In the stance domain, the dynamics model is given by (Equation 6.24). Since the terrain can only deform, the substrate force acts only when foot velocity is negative ($\dot{y}_1 \leq 0$). Hence the domain is defined by the constraint $d^1(t) \leq 0$ where $d^1(x) = [y_{cm} - \ell_1 \sin\theta, \dot{y}_{cm} - \ell_1\dot{\theta}\cos\theta - \dot{\ell}_1 \sin\theta]^\top$. Transition from stance domain occurs when the velocity of mass m_1 becomes zero $\dot{y}_1 = 0$ and when the input force is larger than the weight of mass m_1 i.e $u\sin\theta - m_1 g > 0$.

Flight Domain 1

In the flight domain, the dynamics are given by eq (Equation 6.25). As in the 1D case, the mass m_1 has left contact with the deformed terrain in this domain, and is in flight. Recalling that y_1 is the vertical position of mass m_1, Flight Domain 1 is defined by $d^2(x) \leq 0$ where $d^2(x) = [y_1, -\dot{y}_1]^\top$. Transition to Flight Domain 2 occurs when $y_1 = 0$ and $\dot{y}_1 > 0$.

Flight Domain 2

Once the position of mass m_1 rises above zero, we assume that the rod *sees new ground* as it is traversing horizontally. Hence we reset the terrain to it's original undeformed state. Consequently Flight Domain 2 is defined by $d^3(x) \leq 0$ where $d^3(x) = y_1$. Transition to stance domain occurs when position of mass one $g^3(x) = y_1 = 0$ and velocity $m^3(x,u) = \dot{y}_1 < 0$. In all the domains (Stance Domain, Flight Domain 1 and Flight Domain 2) we add constraints to ensure that the vertical position of mass m_2 given by $y_2(t) > 0$. We are only interested in finding controls $u(t)$ where a stance domain can only occur when mass m_1 is on the ground (and never m_2). The reset map is trivial in all cases.

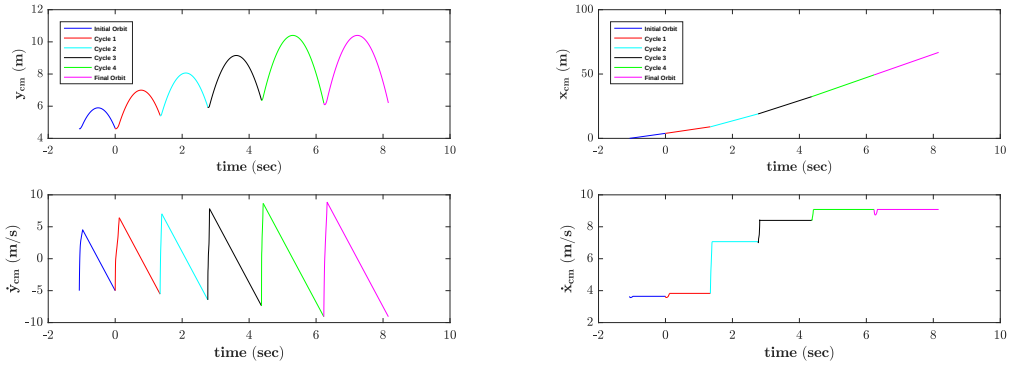

(a) (b)

Figure 6.5: Raccordation for the actuated rod showing the cartesian states.

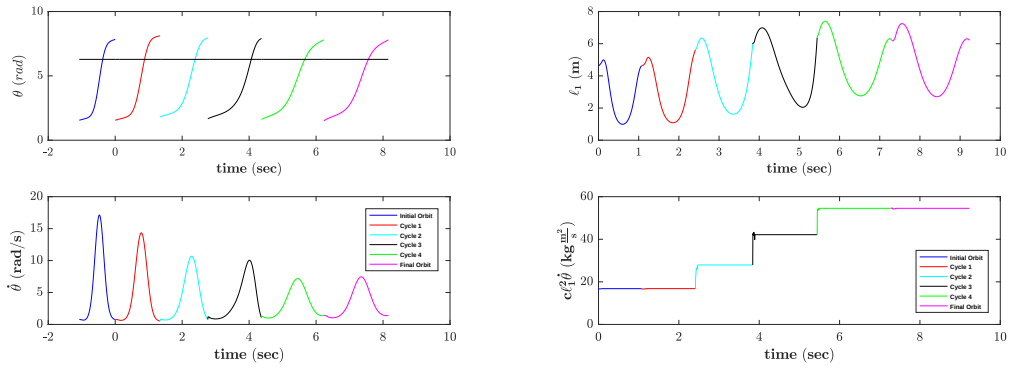

(a) (b)

Figure 6.6: Raccordation for the actuated rod showing the radial and angular states.

6.4.2 Results

As before, we have a hybrid system with three domains. We have shown the raccordations in Figure 6.5 - Figure 6.6. The blue and pink parts of the figures are periodic in all the state components except x_{cm} and θ as we move forward horizontally and rotate in the clockwise direction. For the initial and final gaits we do have however that the final angle $\theta(t_f)$ and the initial angle $\theta(t_i)$ differ as $\theta(t_f) = \theta(t_i) + 2\pi$ as we identify angles differing by integer multiples of 2π. The initial gait (cycle) shown in blue was obtained for $k_g = 500$ N/m and $b_g = 100$ N s/m. The performance index being minimized was the integral of $\dot{\ell}_1^2$. At $t = 0$ we assume that the *terrain changes* to a 'harder granular media'. To model this, we

assumed $k_g = 1000$ N/m and $b_g = 200$ N s/m. We minimized the same performance index integral of $\dot{\ell}_1^2$ to obtain the final gait shown in pink. Figure 6.5-Figure 6.6 show a graceful transition between these two distinct orbits. The rod makes a full revolution in each cycle. One can see in the figures a gradual transition in y_{cm} from a smaller jump height to a larger jump height. A similar situation occurs for the horizontal velocity $\dot{x}_{cm}$ where it gradually transitions from a low $\dot{x}_{cm}$ to a high $\dot{x}_{cm}$. The raccordation is done in $N = 4$ cycles.

Parameter Values

As mentioned above, the terrain is assumed to change, hence we need to use the parameters $k_g = 1000$ N/m and $b_g = 200$ N s/m during the raccordation interval. Other parameter values are $f_g = 500$ N s/m. Mass $m_1 = 0.2085$ Kg and $m_2 = 0.9484$ Kg. The function used for the raccordation was not the full state but was taken to be $h(x) = [\dot{x}_{cm}, y_{cm}, c\ell_1^2\dot{\theta}]$. The final component of $h(x)$ is just the angular momentum about CoM. All the weights W_j^i were the identity.

CHAPTER 7
IMAGE METHOD FOR BIPEDAL ROBOTS

7.1 Introduction

In this chapter, we use the image method (see § 2.3) to synthesize graceful transitions for bipedal robots. As mentioned in § 2.3 and in chapter 4, we require a parameterized family of periodic orbits $\mathcal{O}(\alpha)$. Thus, we first set up a parameterized optimal control problem to obtain parameterized periodic orbits. Subsequently, a reference trajectory is constructed *offline* based on work in [65, 66]. Subsequently, an *online* tracking controller is constructed to track this reference that takes into account the ground contact forces and actuator limits. Finally, this is also illustrated on an underactuated planar bipedal robot is provided to indicate how this can be extended to underactuated hybrid systems. Throughout this chapter, we only focus on the case of transitions between walking gaits.

7.2 Walking Robot Model

The robot shown in Figure 7.1 is fully actuated i.e. all joints are actuated. The robot has only a single support phase where the stance foot is flat on the ground and the non stance foot is above the ground. Once the non stance foot impacts on the ground, the stance foot is assumed to lift off instantaneously and we relabel legs to label the non stance leg as the stance leg and vice versa, thereby exploiting the symmetry of the walking behavior. With these modeling assumptions one can define a hybrid system model of the robot by

$$\mathcal{H} = (\mathcal{D}, \mathcal{G}, \Delta, f, g) \tag{7.1}$$

The details of $\mathcal{H}$ are provided below.

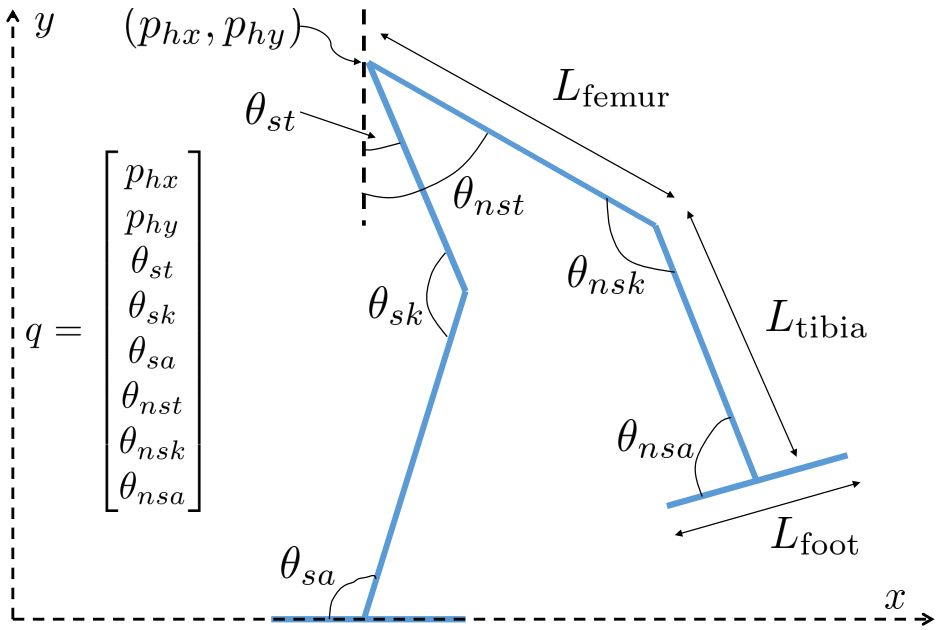

Figure 7.1: Schematic of the planar 5 dof walking robot

7.2.1 Robot Dynamics

We use floating base coordinates of the walking robot as shown in Figure 7.1. The configuration space is $\mathcal{Q} = \mathbb{R}^2 \times \mathbb{T}^6$. In local coordinates, q is depicted in Figure 7.1. The function defining the holonomic constraints is given as follows $h(q) = (p_{\text{sfx}}^{\text{com}}(q), p_{\text{sfy}}^{\text{com}}(q), \theta_{\text{sf}}(q))$ where $p_{\text{sfx}}^{\text{com}}(q)$, $p_{\text{sfy}}^{\text{com}}(q)$ denote the (global) horizontal and vertical position and $\theta_{\text{sf}}(q)$ is the global orientation of the stance foot link with respect to the horizontal. In the single support phase, the stance foot is flat on the ground, so $p_{\text{sfx}}^{\text{com}}(q) = \text{constant}$, $p_{\text{sfy}}^{\text{com}}(q) = 0$ and $\theta_{\text{sf}}(q) = 0$ are the holonomic constraints. The equations of motion for the robot in floating base coordinates can be written as [32]

$$M(q)\ddot{q} + C(q,\dot{q})\dot{q} + G(q) = Bu + \frac{\partial h}{\partial q}^{\top} \lambda \tag{D1}$$

$$\frac{\partial h}{\partial q}\ddot{q} + \frac{d}{dt}\left(\frac{\partial h}{\partial q}\right)\dot{q} = 0 \tag{D2}$$

Table 7.1: Inertial Parameters of the Robot

Link Name	Mass (kg)	Inertia ($kg\ m^2$)	Length (m)
Torso	36.044	0	0
Femur	9.149	0.331	0.4000
Tibia	3.000	0.149	0.4000
Foot	0.625	0.100	0.1600

The inertial parameters of the robot are shown in Table 7.1. The matrix $M(q)$ represent the generalized mass matrix, $C(q, \dot{q})$ represent the terms due to Coriolis Forces, and $G(q)$ represents the generalized forces due to gravity. λ are *forces of constraint* and can be explicitly obtained by substituting $\ddot{q}$ from (Equation D1) into (Equation D2). B is a matrix that maps joint torques to generalized forces and has full rank. The continuous dynamics of the robot are represented by (Equation D1) - (Equation D2). When the non stance foot impacts flat on the ground, we relabel legs and declare the non stance foot prior impact as the stance foot after impact. This corresponds to a relabeling in the configuration space

$$q^+ = \Delta_q q^- \tag{7.2}$$

Δ_q is a relabeling matrix that does not change the global coordinates and $\Delta_q^2 = I$. The post impact joint velocity can be obtained from the pre impact joint velocity by solving

$$\begin{bmatrix} M(q) & -\frac{\partial p_{\text{nsf}}}{\partial q}^\top \\ \frac{\partial p_{\text{nsf}}}{\partial q} & 0 \end{bmatrix} \begin{bmatrix} v^+ \\ \delta\lambda \end{bmatrix} = \begin{bmatrix} M(q)\dot{q}^- \\ 0 \end{bmatrix} \tag{7.3}$$

as in [32]. Here $p_{\text{nsf}}(q)$ represents the global x, y position and orientation of the center of mass of the non stance foot link. We also relabel joint velocities to obtain

$$\dot{q}^+ = \Delta_q v^+ \tag{7.4}$$

Hence the reset map can be represented as a function

$$(q^+, \dot{q}^+) = \Delta(q^-, \dot{q}^-) \tag{7.5}$$

where

$$\Delta(q, \dot{q}) = \begin{bmatrix} \Delta_q q \\ \Delta_{\dot{q}}(q)\dot{q} \end{bmatrix} \tag{7.6}$$

is obtained from (Equation 7.2)-(Equation 7.4). The domain of the single support phase can be formally represented as

$$\mathcal{D} = \left\{ (q, \dot{q}) \in TQ \,\middle|\, p^{\text{left}}_{\text{nsfy}}(q) \geq 0, \;\; p^{\text{right}}_{\text{nsfy}}(q) \geq 0 \right\} \tag{7.7}$$

where $p^{\text{left}}_{\text{nsfy}}(q)$ and $p^{\text{right}}_{\text{nsfy}}(q)$ represent the vertical position of the left end and right end of the non-stance foot link. TQ represents the tangent bundle of the robot configuration space Q where the full state (representing generalized positions and velocities) evolves. The Guard Set can be represented as

$$\mathcal{G} = \left\{ (q, \dot{q}) \in TQ \,\middle|\, p^{\text{left}}_{\text{nsfy}}(q) = 0, \;\; p^{\text{right}}_{\text{nsfy}}(q) = 0, \;\; dp^{\text{com}}_{\text{nsfy}}(q)\dot{q} < 0 \right\} \tag{7.8}$$

Finally, f and g can be obtained from (Equation D1) - (Equation D2) as

$$\dot{x} = f(x) + g(x)u \tag{7.9}$$

where $x = (q, \dot{q}) \in TQ$.

7.2.2 Contact Forces

In order for the model described earlier to be valid, the stance foot must remain flat on the ground and not slip. This imposes constraints on the contact forces. From the definition of the holonomic constraints we see that $\lambda(1)$ represents the total (tangential) frictional force on the robot, $\lambda(2)$ is the total normal force exerted by the ground on the robot and $\lambda(3)$ is the net moment exerted by the ground contact forces on the stance foot center of mass. Since the stance foot is not slipping, the friction cone constraint must be satisfied

$$-\mu\lambda(2) \leq \lambda(1) \leq \mu\lambda(2) \tag{D3}$$

Also the total normal force must be positive

$$\lambda(2) \geq 0 \tag{D4}$$

Since the stance foot is not rotating the *Zero Moment Point (ZMP) constraint* must be satisfied [32]

$$-\frac{L_{\text{foot}}}{2}\lambda(2) \leq \lambda(3) \leq \frac{L_{\text{foot}}}{2}\lambda(2) \tag{D5}$$

where L_{foot} is the total length of the foot. If the ZMP constraint is violated the stance foot rotates and our assumption that the robot is fully actuated is no longer valid.

7.3 Obtaining Parameterized Periodic Orbits

In this section, we discuss the optimization problem involved in finding a continuous family of dynamically feasible periodic orbits $(q(t,\alpha), \dot{q}(t,\alpha))$ for each parameter α varying from $[0,1]$.

7.3.1 Physically motivated parameter set

A physically inspired parameter which changes the performance of walking gaits is proposed. Suppose that $d_{\text{total}}(\alpha)$ is the step length, i.e. the total distance traveled by the non-stance foot over a step and $v_{\text{avg}}(\alpha)$ is the average speed indexed by $\alpha \in [0, 1]$,

$$v_{\text{avg}}(\alpha) = v_l + \alpha(v_u - v_l) \tag{7.10}$$

$$d_{\text{total}}(\alpha) = d_l + \alpha(d_u - d_l) \tag{7.11}$$

and v_l, v_u, d_l and d_u are fixed parameters such that we get walking speeds in $[v_l, v_u]$ and different step lengths in $[d_l, d_u]$. The period of each gait can also be indexed by α,

$$T(\alpha) = \frac{d_{\text{total}}(\alpha)}{v_{\text{avg}}(\alpha)}. \tag{7.12}$$

7.3.2 Finding a family of orbits via optimization

Given the above performance parameters the periodic gait for each α is obtained by considering the trajectory optimization problem. The performance index used is

$$\mathcal{J}_\alpha(u) = \frac{1}{mgd_{\text{total}}} \int_0^{T(\alpha)} u^\top(t)u(t)\, dt \tag{7.13}$$

where m is the total mass of the robot, g is the acceleration due to gravity and d_{total} is the step length. Since we are interested in finding periodic orbits, we need to add the following constraints

$$(q(T(\alpha)), \dot{q}(T(\alpha))) \in \mathcal{G} \tag{CO1}$$

i.e. the switching surface is reached at the end of the step. We also need to add the reset map constraint

$$(q(T(\alpha)+), \dot{q}(T(\alpha)+)) = \Delta\left(q(T(\alpha)-), \dot{q}(T(\alpha)-)\right) \tag{CO2}$$

and the periodicity constraint

$$\begin{bmatrix} \pi_1(q(T(\alpha)+)) \\ \dot{q}(T(\alpha)+) \end{bmatrix} = \begin{bmatrix} \pi_1(q(0)) \\ \dot{q}(0) \end{bmatrix} \tag{CO3}$$

where π_1 is the projection of q onto the last $n-1$ coordinates (as the first coordinate is the hip x position which is monotonically increasing). The α in the second tuples of $q(t,\alpha)$ is ignored for the sake of brevity. In addition,(Equation 7.10) constrains the average walking speed and (Equation 7.11) constrains the step length based on α.

The overall optimization problem is formulated as

$$\begin{aligned} &\min_{u(t)} \mathcal{J}_\alpha(u) \\ s.t.\ &\text{(Equation D1)} - \text{(Equation D5)}, \\ &\text{(Equation CO1)} - \text{(Equation CO3)} \\ &\text{(Equation 7.10)} - \text{(Equation 7.11)} \end{aligned} \tag{7.14}$$

We stress here that in this optimization α is a user defined fixed value between $[0,1]$. Different values of α give gaits of different step lengths and walking speeds. The solution to the optimization problem (Equation 7.14) is an open loop control denoted $u(t,\alpha)$ and a corresponding periodic orbit $(q(t,\alpha),\dot{q}(t,\alpha))$ for $0 \leq t \leq T(\alpha)$ where $T(\alpha)$ is the period of the periodic orbit. Please see Figure 7.2 where the vertical yellow lines denote the periodic orbits $\mathcal{O}(\alpha)$ for each α. We also note that if we define the set $F = \cup_\alpha \mathcal{O}(\alpha) \times \{\alpha\}$, then $F \subset TQ \times A$ and $\pi : F \to A$ is a *fiber bundle* of periodic orbits over A where $A = [0,1]$. The green surface in Figure 7.2 is the set F. The reader can perhaps visualize pictorially that F (the green surface) comprises of infinitely many yellow vertical lines (periodic orbits $\mathcal{O}(\alpha)$).

Remark 7.3.1. *The trajectory optimization problem* (Equation 7.14) *is solved numerically*

using direct collocation methods. This works by first transcribing the infinite dimensional optimization problem into a finite dimensional optimization by parameterizing the states and control as splines and enforcing modeling and path constraints at a discrete set of points. The problem is then converted to a finite dimensional Nonlinear Program (NLP) over the spline coefficients which can be solved efficiently with solvers like IPOPT [62]. Several frameworks for transcribing exist such as the ones described in [31],[33]. We used the one described in [33].

7.4 Static Raccordation

From section 7.3 we obtain a continuous family of periodic orbits denoted as $(q(t,\alpha), \dot{q}(t,\alpha))$ where $0 \leq \alpha \leq 1$. Fix a *raccordation interval* (transition duration) $[0, R]$. Choose a smooth monotonic function $\alpha_{ar} : [0, R] \to [0, 1]$ such that $\alpha_{ar}(0) = 0$ and $\alpha_{ar}(R) = 1$, where the subscript *ar* stands for area law (a particular choice of the smooth monotonic function in [65]). It is worth to mention that the theory proposed in this paper holds for any choice of smooth monotonic function.

Definition 7.4.1. *The Static Raccordation is defined as*

$$\begin{aligned} x_{sr}(t) &= (q_{sr}(t), v_{sr}(t)) \\ &= (q(\beta(t), \alpha_{ar}(t)), \dot{q}(\beta(t), \alpha_{ar}(t))) \end{aligned} \tag{7.15}$$

where $\beta(t) = t - t_p$ and t_p is the previous time such that $x_{sr}(t_p^-) \in \mathcal{G}$.

Note that for each t, $(x_{sr}(t), \alpha_{ar}(t)) \in \pi^{-1}(\alpha_{ar}(t)) \subset F$ where $\pi : F \to A$ is the bundle projection. Thus pictorially, the static raccordation can be thought of as starting at the initial orbit $\mathcal{O}(0)$ and ends at the final orbit $\mathcal{O}(1)$ while $x_{sr}(t) \in \mathcal{O}(\alpha_{ar}(t))$ for $\forall t$. This picture is depicted in Figure 7.2 where all the state space, TQ, is compressed in one dimension for the visualization purpose. Each vertical line (yellow) with the arrow shows

the periodic orbit for a given parameter α_{ar}, and the orange lines represents that static raccordation connecting two orbits.

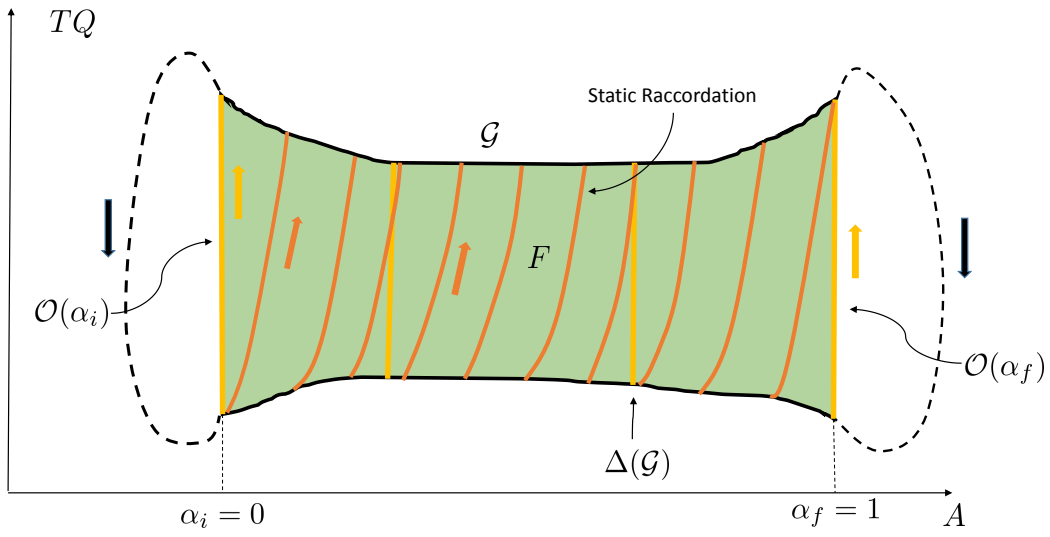

Figure 7.2: Picture of Static Raccordation

7.4.1 Generation of Static Raccordations

Although the conceptual idea of static raccordation is simple, generation of such a path is challenging due to the hybrid structure of the model. In this section, an numerical algorithm to generate a static raccordation is considered.

First, at a given time t, to evaluate $q_{sr}(t)$, we first need to evaluate $\alpha_{ar}(t)$, and solve the optimization problem (Equation 7.14) with $\alpha = \alpha_{ar}(t)$ to access the periodic orbit, $O(\alpha_{ar}(t))$. This gives us the optimal trajectory $(q(\tau, \alpha_{ar}(t)), \dot{q}(\tau, \alpha_{ar}(t)))$. We then evaluate $q(\tau, \alpha_{ar}(t))$ at $\tau = \beta(t) = t - t_p$.

Observe that at each time t, the position (or joint angles) of static raccordation in (Equation 7.15) stays in its corresponding orbit but it does not satisfies the kinematic constraints as

$$v_{sr}(t) = \frac{d}{d\tau} q(\beta(\tau), \alpha_{ar}(t))|_{\tau=t} \tag{7.16}$$

whereas

$$\frac{d}{dt}q_{sr}(t) = v_{sr}(t) + \frac{\partial q_{sr}}{\partial \alpha}(\beta(t), \alpha_{ar}(t))\dot{\alpha}_{ar}(t) \tag{7.17}$$

and so $\dot{q}_{sr}(t) \neq v_{sr}(t)$. Therefore, the static raccordation given by (Equation 7.15) is dynamically infeasible.

7.5 Feasible Reference Trajectory Generation via Static Raccordation

In this section, a new raccordation is proposed which can be shown to be dynamically feasible i.e. satisfying the continuous dynamics. The error in the discrete reset map can be made arbitrarily small by slowing down the speed of parameter sweeping of α_{ar}.

Let the new raccordation be defined as

$$x_{tr}(t) = (q_{sr}(t), \dot{q}_{sr}(t)) \tag{7.18}$$

where q_{sr} is the static raccordation.

Sweeping the α_{ar} from 0 to 1, the new raccordation is obtained by $x_{tr}(t) = (q_{sr}(t), \dot{q}_{sr}(t))$, where this trajectory will be used as a reference trajectory to follow in Sec section 7.6. Note that there exist a finite set with $0 \in \{t_1, t_2, ..., t_n\}$ from the construction of $\beta(t)$, such that $x_{tr}(t_i^-) \in \mathcal{G}$ for all i. Also in the open interval (t_i, t_{i+1}) we have that $x_{tr}(t) \in \mathcal{D}$ and $x_{tr}(t) \notin \mathcal{G} \cup \Delta(\mathcal{G})$.

7.5.1 Continuous Dynamics

We show that the trajectory $x_{tr}(t) = (q_{sr}(t), \dot{q}_{sr}(t))$ satisfies the continuous dynamics. First, we check that the holonomic constraints is satisfied. Note that on $t_i \leq t \leq t_{i+1}$ we have

$$h(q_{sr}(t)) = h(q(\beta(t), \alpha_{ar}(t))) = 0 \quad \forall t \tag{7.19}$$

because $q(\tau, \alpha_{ar}(t))|_{\tau=\beta(t)}$ is obtained from the trajectory optimization (Equation 7.14). Differentiating (Equation 7.19) we see

$$\frac{dh}{dq}(q_{sr})\dot{q}_{sr} = 0 \tag{7.20}$$

$$\frac{dh}{dq}(q_{sr})\ddot{q}_{sr} + \frac{d}{dt}\left(\frac{dh}{dq}(q_{sr})\right)\dot{q}_{sr} = 0 \tag{7.21}$$

Thus, we see that $(q_{sr}(t), \dot{q}_{sr}(t))$ satisfies (Equation D2). To see that $(q_{sr}, \dot{q}_{sr})$ satisfies (Equation D1), we need to find $u_{tr}(t)$ and $\lambda_{tr}(t)$ such that

$$M(q_{sr})\ddot{q}_{sr} + C(q_{sr}, \dot{q}_{sr}) + G(q_{sr}) = \begin{bmatrix} B & \frac{dh}{dq}^{\top}(q_{sr}) \end{bmatrix} \begin{bmatrix} u_{tr} \\ \\ \lambda_{tr} \end{bmatrix}$$

But, since the system is *fully actuated* the matrix $\left[B, \frac{dh}{dq}\right]$ has full rank, and we can solve for u_{tr} and λ_{tr}. Thus $x_{tr} = (q_{sr}, \dot{q}_{sr})$ satisfies the continuous dynamics (Equation D1) - (Equation D2). We see that the trajectory $x_{tr} = (q_{sr}(t), \dot{q}_{sr}(t))$ can be made to satisfy the continuous dynamics in $t_i \leq t \leq t_{i+1}$.

7.5.2 Discrete Dynamics

We now examine whether $x_{tr}(t)$ satisfies the discrete dynamics on this discrete set $\{t_1, t_2, ..., t_n\}$.

Theorem 7.5.1. *With $x_{tr}(t) = (q_{sr}(t), \dot{q}_{sr}(t))$, let t_i be a point such that $x_{tr}(t_i^-) \in \mathcal{G}$. Then the following is true:*

1. *The position component of x_{tr} is invariant under reset at t_i, i.e.*

$$\pi_1 q_{sr}(t_i^+) = \pi_1 \Delta_q \left(q_{sr}(t_i^-)\right).$$

2. *The error for the velocity component $e = \dot{q}_{sr}(t_i^+) - \Delta_{\dot{q}}\dot{q}_{sr}(t_i^-) \to 0$ as $\dot{\alpha} \to 0$.*

Proof. First, note that $x_{tr}(t_i^-) \in \mathcal{G} \iff x_{sr}(t_i^-) \in \mathcal{G}$ where x_{sr} is from Defini-

tion 1. We know from (Equation 7.15) that the static raccordation x_{sr} takes values in $\mathcal{O}(\alpha_{ar}(t))$ for each $t \in [0, R]$. Thus $x_{sr}(t_i^-) \in \mathcal{G}$ precisely when $\lim_{t\to t_i^-} \beta(t) = T(\alpha_{ar}(t_i))$,where $T(\alpha_{ar})$ is the period of the orbit $O(\alpha_{ar})$. Since $\beta(t)$ is reset to zero at t_i, we have $\lim_{t\to t_i^+} \beta(t) = 0$, and so

$$q_{sr}(t_i^+) = \lim_{t\to t_i^+} q(\beta(t), \alpha_{ar}(t)) = q(0, \alpha_{ar}(t_i)) \tag{7.22}$$

holds where $q(\cdot, \alpha)$ is the solution of (Equation 7.14).

On the other hand, $t \leq t_i$ implies that

$$q_{sr}(t_i^-) = \lim_{t\to t_i^-} q(\beta(t), \alpha_{ar}(t)) = q(T(\alpha_{ar}(t_i))^-, \alpha_{ar}(t_i)) \tag{7.23}$$

where $T(\alpha_{ar}(t_i))^- := \lim_{\epsilon\to 0+} T(\alpha_{ar}(t_i)) - \epsilon$. Now, since $\mathcal{O}(\alpha_{ar})$ is a periodic orbit,

$$\pi_1 q(0, \alpha_{ar}(t)) = \pi_1 \Delta_q q(T(\alpha_{ar}(t_i))^-, \alpha_{ar}(t_i)) \tag{7.24}$$

holds where Δ_q is the relabeling matrix. Combining (Equation 7.22) - (Equation 7.24), we obtain

$$\pi_1 q_{sr}(t_i^+) = \pi_1 \Delta_q q_{sr}(t_i^-) \tag{7.25}$$

We have established that the position component of $x_{tr}(t)$ is invariant under the reset map.

Next, we turn to the velocity component $\dot{q}_{sr}(t)$. Looking at (Equation 7.17) we see that

$$\frac{dq_{sr}(t_i^+)}{dt} = v_{sr}(t_i^+) + \frac{\partial q}{\partial \alpha}(0^+, \alpha_{ar}(t_i))\dot{\alpha}(t_i) \tag{7.26}$$

The left limit of $\dot{q}_{sr}(t)$ at t_i is

$$\frac{dq_{sr}(t_i^-)}{dt} = v_{sr}(t_i^-) + \frac{\partial q}{\partial \alpha}(T(\alpha_{ar})^-, \alpha_{ar}(t_i))\dot{\alpha}(t_i) \tag{7.27}$$

We know that because $O(\alpha_{ar})$ is a periodic orbit and because the reset map is fiber wise

linear on TQ (see (Equation CO3) and (Equation 7.6))

$$v_{sr}(t_i^+) = \Delta_{\dot{q}}(q_{sr}(t_i^-))v_{sr}(t_i^-) \tag{7.28}$$

This implies that the error

$$e = \dot{q}_{sr}(t_i^+) - \Delta_{\dot{q}}(q_{sr}(t_i^-))\dot{q}_{sr}(t_i^-) \tag{7.29}$$

is given by (using (Equation 7.26) - (Equation 7.27))

$$e = \left(\frac{\partial q}{\partial \alpha}(0^+, \alpha_{ar}(t_i)) - \Delta_{\dot{q}}\frac{\partial q}{\partial \alpha}(T(\alpha_{ar})^-, \alpha_{ar}(t_i))\right)\dot{\alpha}(t_i) \tag{7.30}$$

Since $q(t, \alpha)$ is smooth we can assume a bound on the jacobian $\|\frac{\partial q}{\partial \alpha}(t, \alpha)\|$ for $0 \leq \alpha \leq 1$, and $0 \leq t \leq T(\alpha)$. This means that the error e can be made to go to zero by making $\dot{\alpha}$ go to zero. □

7.6 Dynamic Raccordation

The previous sections dealt with the computation of a reference trajectory, a computationally intensive process that is done *offline*. With the reference trajectory at hand, we use *online* QP based controllers to track this reference trajectory. This QP based tracking controller is discussed in the current section. However, before discussing the QP based controller, we discuss our implementation on how to track $x_{tr}(t) = (q_{sr}(t), \dot{q}_{sr}(t))$.

7.6.1 Tracking Control Scheme

Let $x_{tr}(t)$ be the reference trajectory obtained from Sec section 7.5. Suppose that the switching times are given by $\{t_1, t_2, ..., t_n\}$ such that $x_{tr}(t_i^-) \in \mathcal{G}$, $x_{tr}(t) \in \mathcal{D}$ and $x_{tr}(t) \notin \mathcal{G} \cup \Delta(\mathcal{G})$ whenever $t \in (t_i, t_{i+1})$ for all i. Observe that there are n steps in the raccordation. Since the dynamics are hybrid, there are no guarantees that the actual switching time, is

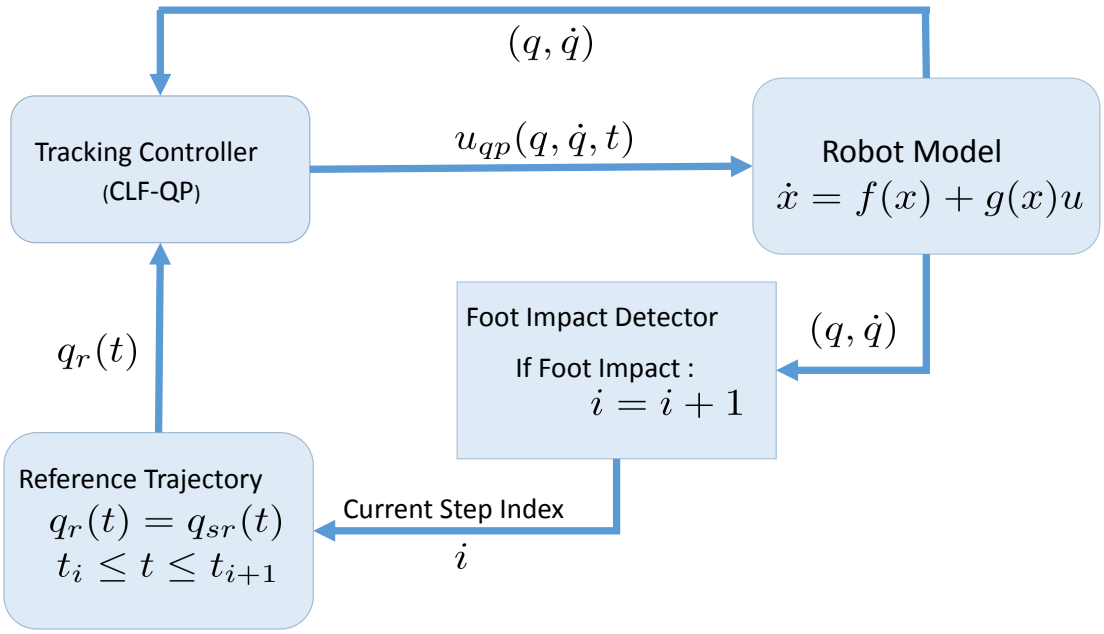

Figure 7.3: Schematic of Tracking Control Architecture. Given the current step i, $q_{sr}(t)$ for $t_i \leq t \leq t_{i+1}$ is given as a reference trajectory to the CLF-QP.

matched to the above prescribed switching time. In this section, we propose an architecture, to select the appropriate reference step to follow despite mismatches in switching time.

Our desired output is

$$y_r(t) = Hq_r(t) + H_{\text{bias}} \tag{7.31}$$

Following the methodology proposed in [67], we now construct a (time dependent) Control Lyapunov Function (CLF) and construct a feedback controller $u_{qp}(q, \dot{q}, t)$ to decrease it by solving a Quadratic Program (QP) at each state $(q, \dot{q})$. Let the output coordinates be defined as η, and satisfies

$$\eta(q, \dot{q}, t) = \begin{bmatrix} \eta_1 \\ \eta_2 \end{bmatrix} = \begin{bmatrix} y(q) - y_r(t) \\ \dot{y}(q, \dot{q}) - \dot{y}_r(t) \end{bmatrix}. \tag{7.32}$$

We know that the feedback linearization control

$$u_{fl}(q,\dot{q},t) = -L_g L_f \eta_1^{-1}(q,\dot{q},t)\Big(L_f^2\eta_1(q,\dot{q},t)+ \frac{d}{dt}\frac{\partial \eta_1}{\partial t}(q,t) + K_p\eta_1 + K_d\dot{\eta}_1\Big) \tag{7.33}$$

yields the dynamics

$$\dot{\eta} = A\eta \tag{7.34}$$

when $(q,\dot{q})$ satisfies the continuous dynamics and

$$A = \begin{bmatrix} 0 & I \\ -K_p & -K_d \end{bmatrix}. \tag{7.35}$$

whereK_p and K_d are positive gains. Since the system (Equation 7.34) is exponentially stable, we can guarantee that $\eta \to 0$ under (Equation 7.33) to succesfully achieve tracking. This shows the existence of the Control Lyapunov Function (CLF).

Now, we use (Equation 7.34) to construct a Control Lyapunov Function (CLF) for the system. Let P solve the Lyapunov Equation

$$A^\top P + PA = -Q \tag{7.36}$$

and

$$I_\epsilon = \begin{bmatrix} \epsilon I & 0 \\ 0 & I \end{bmatrix}. \tag{7.37}$$

Define

$$V_\epsilon(q,\dot{q},t) = \eta^\top I_\epsilon P I_\epsilon \eta \tag{7.38}$$

Then V_ϵ is a valid one parameter family of CLFs dependent on ϵ [67] which determines the convergence rate.

Among many benefits of using online CLF-QP, our main objective to use the optimization framework is to include ground contact force constraints and input bounds as a part of state feedback control law. Therefore, the cost function is formulated such that it allows to check if the current feedback linearization controller allows dynamically feasible contact force constraints and input bounds (if not find a nearby controller which are feasible). Hence the cost function is chosen as $J(u) = (u - u_{fl}(q, \dot{q}, t))^2$. Let the free parameter in the numerical optimization program be $p = [\ddot{q}, u, \lambda]^\top$.

This objective is quadratic in p, i.e $(u-u_{fl}(q, \dot{q}, t))^2 = \frac{1}{2}p^\top H_{\text{obj}}(q, \dot{q}, t)p + F_{\text{obj}}^\top(q, \dot{q}, t)p$ and the dynamics constraints in (Equation D1) - (Equation D2) can be formulated as equality constraints $c_{\text{dyn}}(q, \dot{q})p = d_{\text{dyn}}(q, \dot{q})$ for some $c_{\text{dyn}}(q, \dot{q}) \in \mathbb{R}^{11\times 16}$ and $d_{\text{dyn}}(q, \dot{q}) \in \mathbb{R}^{11}$. The constraints for ground forces (Equation D3) - (Equation D5) can be written as $c_{\text{grf}}p \leq d_{\text{grf}}$ for some constant $c_{\text{grf}} \in \mathbb{R}^{5\times 16}$ and $d_{\text{grf}} \in \mathbb{R}^5$. The constraints for CLF is given by

$$\frac{\partial V_\epsilon}{\partial q}\dot{q} + \frac{\partial V_\epsilon}{\partial \dot{q}}\ddot{q} + \frac{\partial V_\epsilon}{\partial t} \leq -\gamma_{\text{clf}}\epsilon V_\epsilon \tag{7.39}$$

can be written as $c_{\text{clf}}(q, \dot{q}, t)p \leq d_{\text{clf}}(q, \dot{q}, t)$ where $c_{\text{clf}}(q, \dot{q}) \in \mathbb{R}^{1\times 16}$ and $d_{\text{clf}} \in \mathbb{R}$. The input saturation constraints $-u_{max} \leq u \leq u_{max}$ can be written as $c_{sat}p \leq d_{sat}$ where $c_{\text{sat}} \in \mathbb{R}^{2\times 16}$ and $d_{\text{sat}} \in \mathbb{R}^2$. Finally, the overall Control Lyapunov Function based Quadratic Program (CLF-QP) [67] is formulated as

$$\begin{aligned} p^*(q, \dot{q}, t) = \arg\min_p \frac{1}{2}p^\top H_{\text{obj}}(q, \dot{q}, t)p + F_{\text{obj}}^\top(q, \dot{q}, t)p \\ s.t. \quad c_{\text{dyn}}(q, \dot{q})p = d_{\text{dyn}}(q, \dot{q}) \\ c_{\text{grf}}p \leq d_{\text{grf}} \\ c_{\text{clf}}(q, \dot{q}, t)p \leq d_{\text{clf}}(q, \dot{q}, t) \\ c_{\text{sat}}p \leq d_{\text{sat}} \end{aligned} \tag{7.40}$$

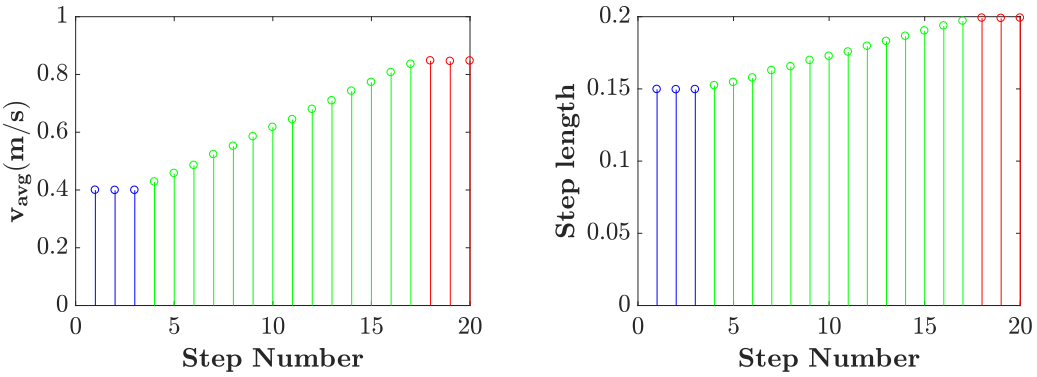

(a) Average speed (b) Step length

Figure 7.4: Average speed and step length vs number of steps

The applied feedback control is a function of $(q, \dot{q})$ and is given by,

$$u_{qp}(q, \dot{q}, t) = \pi_u p^*(q, \dot{q}, t) \tag{7.41}$$

where π_u is the projection of p onto u. This QP must be solved at each step of the ode integration for all $(q, \dot{q})$. The solution of the hybrid system (Equation D1) - (Equation D5) undergoing impacts (Equation 7.5) with the control input $u_{qp}(q, \dot{q}, t)$ is denoted $x_d(t) = (q_d(t), \dot{q}_d(t))$ and is called the *dynamic raccordation*.

7.6.2 Results

In this section, we demonstrate the raccordation method in simulation. The parameter $v_l = 0.40$ m/s and $v_u = 0.85$ m/s in (Equation 7.10). The parameter $d_l = 0.15$ m and $d_u = 0.20$ m in (Equation 7.11). Varying $0 \leq \alpha \leq 1$ gives us a variety of gaits with varying average walking speeds and step lengths. The raccordation interval R was chosen to be 4 seconds. The monotonic function $\alpha_{ar}(t)$ was selected based on the area law, according to [65]. The position component of the reference trajectory $q_{sr}(t)$ was computed which involves solving a very large number of trajectory optimization problems.

The solution of the hybrid system (where $u_{qp}(x, t)$ is obtained from the CLF-QP given by (Equation 7.40)) is denoted as $x_d(t) = (q_d(t), \dot{q}_d(t))$ (the dynamic raccordation). The

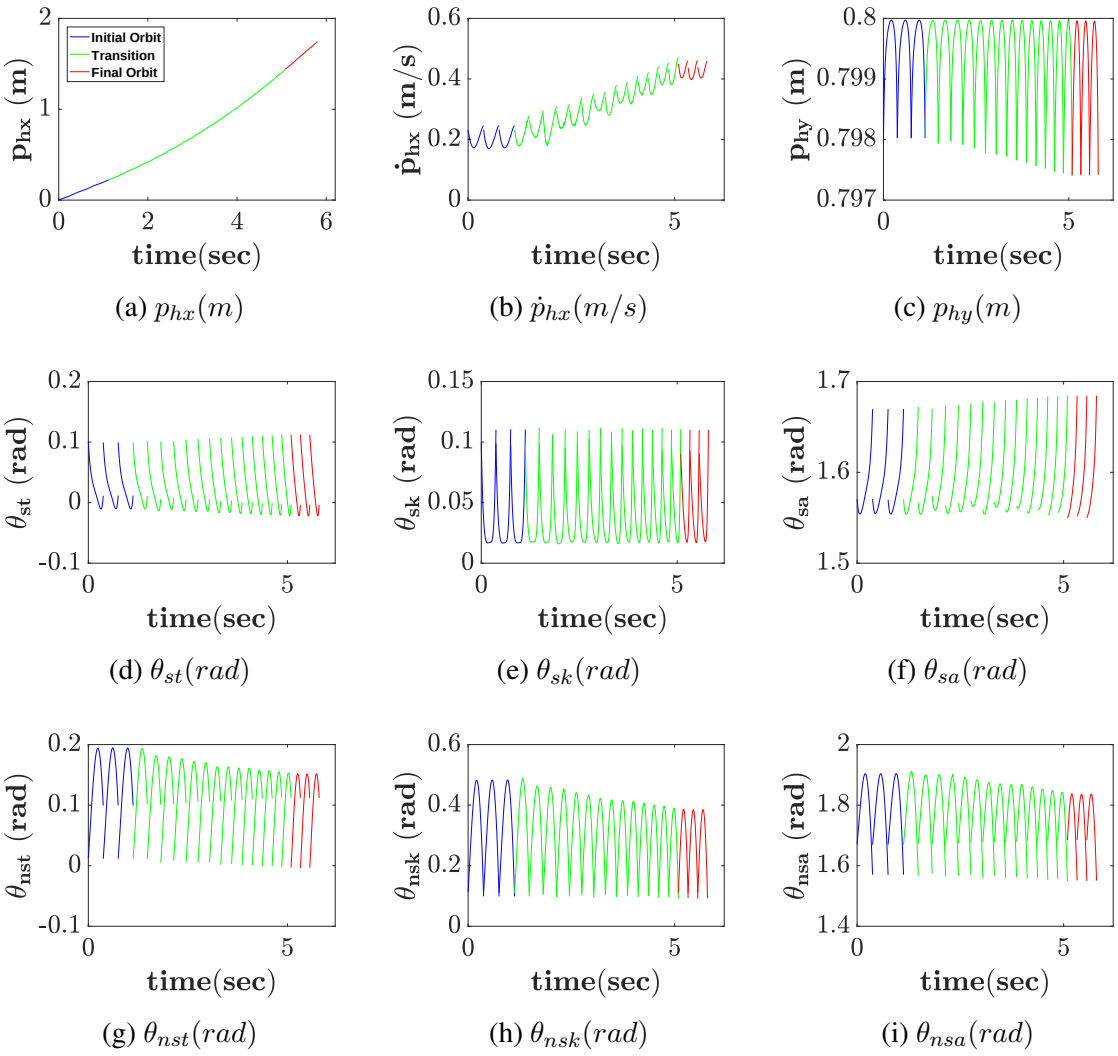

(a) $p_{hx}(m)$ (b) $\dot{p}_{hx}(m/s)$ (c) $p_{hy}(m)$

(d) $\theta_{st}(rad)$ (e) $\theta_{sk}(rad)$ (f) $\theta_{sa}(rad)$

(g) $\theta_{nst}(rad)$ (h) $\theta_{nsk}(rad)$ (i) $\theta_{nsa}(rad)$

Figure 7.5: Plot of joint coordinates for transitions between the orbits $\mathcal{O}(0)$ and $\mathcal{O}(1)$.

initial orbit consists of the first three steps and is depicted in blue. The final orbit consists of the last three steps and is depicted in red, the transition steps are $N = 14$ depicted in green. The total number of steps when we include 3 steps of the initial and final orbit as seen in Figure 7.4. The average speed of $x_d(t)$ changes gradually from $v_l = 0.4$ m/s to $v_u = 0.85$ m/s. Similarly the step length of $x_d(t)$ changes from $d_l = 0.15$ m to $d_u = 0.20$ in Figure 7.4.

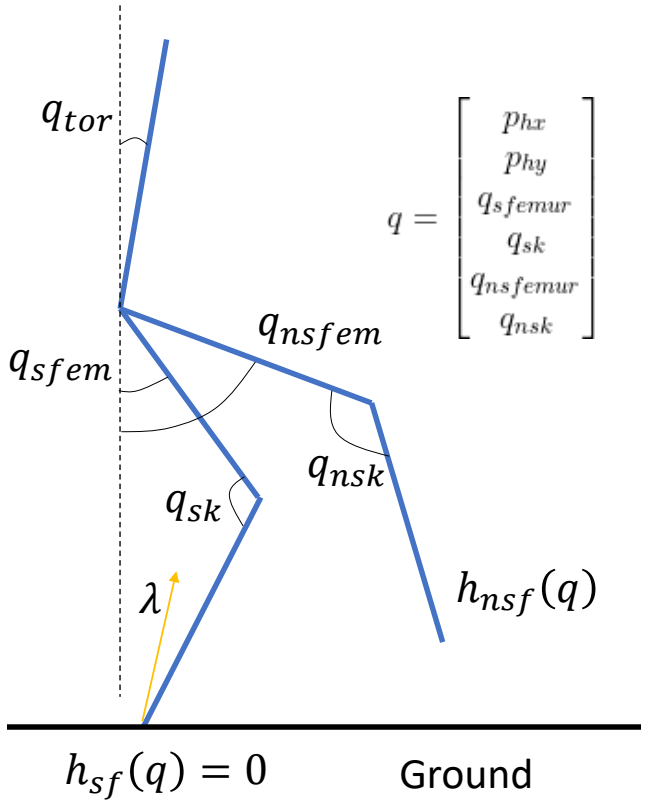

Figure 7.6: Schematic of the planar underactuated walking robot

7.7 Extension to Underactuated Bipeds

We consider the case where the robot is underactuated. Shown in Figure 7.6 is a walking robot with point feet. As a result the robot is underactuated since it does not have an ankle and *does not* have direct control of the angle of the tibia with respect to the ground. More concretely, we have

$$\text{rank}(B) < \dim(\mathcal{Q}) - \text{number of holonomic constraints}$$

where B is the actuation matrix and $\mathcal{Q}$ is the configuration space.

7.7.1 Correction to the static raccordation

We saw in § 7.4.1 that the static raccordation does not respect kinematic considerations. Namely, from (Equation 7.17) we know that

$$\frac{d}{dt}q_{sr} \neq v_{sr}.$$

Thus, the static raccordation cannot satisfy the dynamics equations for bipedal robots since they have second order dynamics. Recall from § 7.4.1 that the static raccordation can be split up into *steps* as depicted in Figure 7.2. Thus we seek to solve a sequence of optimization problems to *correct* each step of the static raccordation, i.e. find a dynamically feasible trajectory as close as possible to the static raccordation. We would thus like to set up an optimal control problem to achieve this. For what follows below we denote by

$$x^i_{\text{ref}}(t) = \begin{bmatrix} q^i_{\text{ref}}(t) \\ \dot{q}^i_{\text{ref}}(t) \end{bmatrix} \tag{7.42}$$

the reference of the ith step of the static raccordation. To this end, we formulate the following optimization problem.

$$\min \mathcal{J} = \int_0^{T^i} (x - x^i_{\text{ref}}(t))^\top Q (x - x^i_{\text{ref}}(t)) dt + (x - x^i_{\text{ref}}(T^i))^\top Q_f (x - x^i_{\text{ref}}(T^i)) \tag{7.43}$$

subject to

$$q(0) = q^i_{\text{ref}}(0) \tag{7.44}$$

$$\dot{q}(0) = \dot{q}_{\text{init}} \tag{7.45}$$

$$q^{i+1}_{\text{ref}}(0) = \Delta_q q(T_i) \tag{7.46}$$

$$\|\dot{q}^{i+1}_{\text{ref}}(0) - \Delta_{\dot{q}}(q(T^i))\dot{q}(T^i)\| < \epsilon \tag{7.47}$$

$$\text{Robot Dynamics} : \quad \text{(Equation D1)} - \text{(Equation D5)},$$

$$\text{(Equation CO1)} - \text{(Equation CO2)} \tag{7.48}$$

The (Equation 7.44) is the initial condition for the joint position. (Equation 7.45) is the initial condition for the joint velocity. Here, $\dot{q}_{\text{init}}$ is an initial condition provided to the optimization as follows: for the first step of the static raccordation, $\dot{q}_{\text{init}} = \dot{q}_{sr}(0)$. For all other subsequent steps,

$$\dot{q}_{\text{init}} = \Delta_{\dot{q}}(q_{\text{prev}}(T^i))\dot{q}_{\text{prev}}(T^i) \tag{7.49}$$

where $q_{\text{prev}}(t)$ and $\dot{q}_{\text{prev}}(t)$ are the solutions of the optimal control problem (Equation 7.43) - (Equation 7.48) obtained in the preceding step. This serves to ensure that stitching together the solutions of these optimization problems across multiple steps results in a dynamically feasible trajectory that also respects the discrete dynamics of the hybrid system. (Equation 7.46) - (Equation 7.47) are final constraints on the trajectory. (Equation 7.47) is formulated as an inequality constraint to avoid infeasibility of the optimal control problem. Finally (Equation 7.48) includes the robot dynamics (the continuous dynamics of the hybrid system). Stitching together the trajectories of the various steps results in a dynamically feasible trajectory of the hybrid system.

Remark 7.7.1. *The optimization problem* (Equation 7.43) - (Equation 7.48) *obtains trajectories that satisfy the continuous dynamics for a single step. The initial and final boundary constraints, serve to ensure that all the discrete reset maps are satisfied and the trajecto-*

ries can be stitched together. However, it is also possible to formulate a (larger) optimal control problem that includes the full dynamics across multiple steps, and have the cost (Equation 7.43) *summed over multiple steps. This approach is expected to yield trajectories closer to the static raccordation. We follow the single step approach as it is cheaper computationally.*

7.7.2 Tracking the Reference

Let the continuous dynamics of the robot be represented as

$$\dot{x} = f(x, u) \tag{7.50}$$

Given a dynamically feasible reference trajectory $(x_{\text{ref}}(t), u_{\text{ref}})$ we can linearize around the trajectory :

$$\dot{\delta x} = \left.\frac{\partial f}{\partial x}\right|_{x_{\text{ref}}(t), u_{\text{ref}}(t)} \delta x \quad + \quad \left.\frac{\partial f}{\partial u}\right|_{x_{\text{ref}}(t), u_{\text{ref}}(t)} \delta u \tag{7.51}$$

We can stabilize the trajectory via Time Varying Linear Quadratic Controller (TV-LQ):

$$\min \mathcal{J} = \int_0^{T_p} (\delta x)^\top Q(\delta x) + (\delta u)^\top R(\delta u)\ dt + (\delta x)^\top Q_f(\delta x) \tag{7.52}$$

subject to

$$\dot{\delta x} = A(t)\delta x + B(t)\delta u \tag{7.53}$$

where

$$A(t) = \left.\frac{\partial f}{\partial x}\right|_{x_{\text{ref}}(t), u_{\text{ref}}(t)} \tag{7.54}$$

$$B(t) = \left.\frac{\partial f}{\partial u}\right|_{x_{\text{ref}}(t), u_{\text{ref}}(t)} \tag{7.55}$$

The optimal solution is :

$$\delta u(\delta x, t) = -R^{-1}(t)B^{\top}(t)P(t)\delta x \tag{7.56}$$

$$-\dot{P}(t) = P(t)A(t) + A^{\top}(t)P(t) - P(t)B(t)R^{-1}(t)B^{\top}(t)P(t) \tag{7.57}$$

The final closed loop control is given by

$$u(x,t) = u_{\text{ref}}(t) + \delta u(\delta x, t) \tag{7.58}$$

$$= u_{\text{ref}}(t) - R^{-1}(t)B^{\top}(t)P(t)\left(x - x_{\text{ref}}(t)\right) \tag{7.59}$$

7.7.3 Results

In Figure 7.7 we show the raccordations for the planar underactuated robot by following the above mentioned approach. The black dotted lines in the figure represents the *static raccordation*. However, we know that it does not satisfy the dynamics. The blue, green and red curves represent the trajectories of the hybrid system under the control law (Equation 7.59). The blue curve represents the initial walking gait. The red curve represents the final walking gait. The green curve represents the trajectories during the transition.

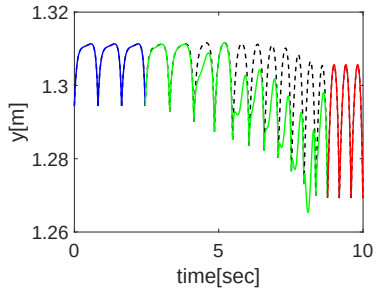

(a)

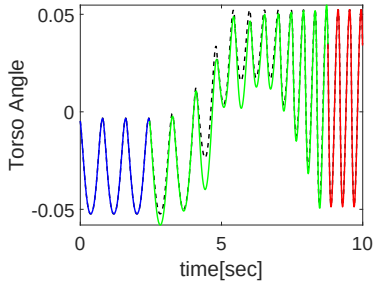

(b)

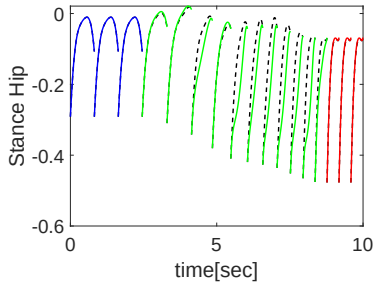

(c)

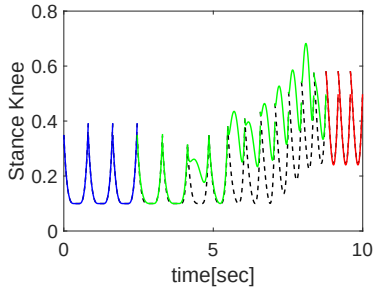

(d)

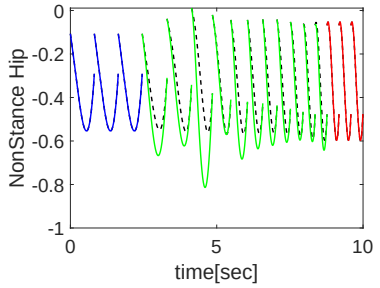

(e)

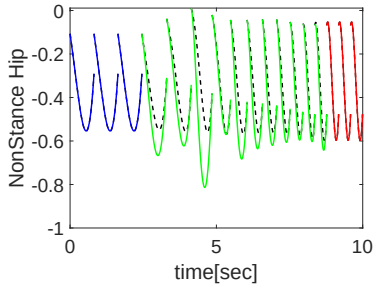

(f)

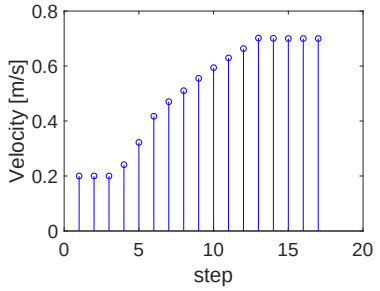

(g)

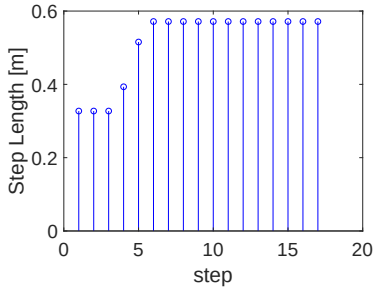

(h)

Figure 7.7: Plot of raccordations for the under-actuated robots.

CHAPTER 8

OPTIMAL TRANSITIONS BASED ON PARTIAL HYBRID ZERO DYNAMICS

8.1 Introduction

In this chapter, we focus primarily on the energy efficiency of locomotion. It is well known that existing methods based on zero moment point methods are not energy efficient. In this chapter, we utilize the partial hybrid zero dynamics (PHZD) framework [68] to generate energy efficient stable periodic walking gaits. A popular measure for energy efficiency for bipedal robots is the mechanical cost of transport [69]. We generate periodic orbits on the PHZD manifold by minimizing cost of transport. The solution to this optimization problem actually gives an *infinite* family of walking gaits indexed by walking speed on the PHZD manifold [68]. However, these gaits are not energy efficient as we demonstrate with an empirical simulation study. We show the importance of optimizing a PHZD manifold for each walking speed as it significantly improves energy efficiency, especially during transitions. Once again, we focus only on walking gaits.

8.2 Partial Hybrid Zero Dynamics Optimization

We discuss in this section the optimization problem involved in finding a continuous family of stable periodic orbits, based on the PHZD framework. We first discuss about the controller design and then we discuss the optimization problem involved.

8.2.1 Controller Design

The controller on the robot seeks to drive certain outputs to zero as we now describe. We define

$$z_1(q) = p_{hx} - p_{\text{sfx}}^{\text{com}}(q) \tag{8.1}$$

to be the horizontal displacement of the hip with respect to stance foot center of mass. We have the relative degree one output

$$y_1(q, \dot{q}, v_f) = z_2(q, \dot{q}) - v_f \tag{8.2}$$

where $z_2(q, \dot{q})$ represents the hip velocity given by

$$z_2(q, \dot{q}) = \frac{\partial z_1}{\partial q}(q)\dot{q} \tag{8.3}$$

and $v_f \in \mathbb{R}$ represents a desired fixed walking speed. The (vector) relative degree two outputs are

$$y_2(q) = y^a(q) - y^d(\tau(q), \alpha) \tag{8.4}$$

where $y^a(q)$ represents the "actual outputs" given by

$$y^a(q) = \begin{bmatrix} \frac{\pi}{2} + \theta_{nst} - \theta_{nsk} + \theta_{nsa} \\ \theta_{sk} \\ \theta_{nst} - \theta_{st} \\ \theta_{nsk} \end{bmatrix} \tag{8.5}$$

and $y^d(t, \alpha)$ represent the desired outputs given by Bezier polynomials

$$y^d(t, \alpha) = \sum_{k=1}^{M} \alpha_k \frac{M!}{k!(M-k)!} t^k (1-t)^{M-k} \tag{8.6}$$

where each α_k is a 4×1 vector and $\alpha = \{\alpha_k\}_{k=1}^{M}$ is a column vector of all the α_k stacked together and the parameter $M = 6$. $\tau(q)$ is monotonic throughout a step and is known as the phase variable and is given by

$$\tau(q) = \frac{z_1(q) - z_1^+}{z_1^- - z_1^+} \tag{8.7}$$

where the parameters z_1^+ and z_1^- are chosen to ensure that $\tau(q) \in [0,1]$ throughout a step, i.e., they are chosen based upon the initial and final position of the robot during a step. With these outputs the feedback control

$$u_\epsilon(q,\dot{q},\alpha,v_f) = \mathcal{A}_\alpha^{-1}(q,\dot{q}) \left(\begin{bmatrix} 0 \\ L_f^2 y_2(q,\dot{q}) \end{bmatrix} + \begin{bmatrix} L_f z_2(q,\dot{q}) \\ 2\epsilon L_f y_2(q,\dot{q}) \end{bmatrix} + \begin{bmatrix} \epsilon\left(z_2(q,\dot{q}) - v_f\right) \\ \epsilon^2 y_2(q) \end{bmatrix} \right) \tag{8.8}$$

where the decoupling matrix

$$\mathcal{A}_\alpha(q,\dot{q}) = \begin{bmatrix} L_g z_2(q,\dot{q}) \\ L_g L_f y_2(q,\dot{q},\alpha) \end{bmatrix} \tag{8.9}$$

yields the output dynamics

$$\dot{y}_1 + \epsilon y_1(q,\dot{q},v_f) = 0 \tag{O1}$$

$$\ddot{y}_2 + 2\epsilon \dot{y}_2(q,\dot{q},\alpha) + \epsilon^2 y_2(q,\alpha) = 0. \tag{O2}$$

Here $L_f y$ represents the lie derivative of the output y along the vector field f. The parameter ϵ serves as a controller gain parameter and serves to control the rate of the output to zero. Because we have rendered these dynamics stable, the solutions converge to the (1-dimensional) surface defined by these functions being identically zero, i.e., to the *full zero dynamics* surface:

$$FZ_\alpha = \Big\{ (q,\dot{q}) \in TQ \Big| y_1(q,\dot{q},v_f) = 0, \; y_2(q,\alpha) = \dot{y}_2(q,\dot{q},\alpha) = 0 \Big\} \tag{8.10}$$

We are interested in varying the desired velocity, v_f, and thus we wish to consider the surface where the output y_1 is allowed to vary but the output y_2 is identically zero. This is termed the *partial zero dynamics* surface and given by:

$$PZ_\alpha = \left\{ (q, \dot{q}) \in TQ \middle| y_2(q, \alpha) = \dot{y}_2(q, \dot{q}, \alpha) = 0 \right\} \tag{8.11}$$

The control given by (Equation 8.8) renders both FZ_α and PZ_α forward invariant. However, in the presence of impacts, we only enforce invariance of PZ_α as discussed in the optimization problem below. We note that on PZ_α, the dynamics of the system

$$\dot{x} = f(x) + g(x)u_\epsilon(x, \alpha, v_f) \tag{8.12}$$

can be represented by a second order system

$$\begin{aligned} \dot{z}_1 &= z_2 \\ \dot{z}_2 &= -\epsilon(z_2 - v_f) \end{aligned} \tag{8.13}$$

and the state $(q, \dot{q})$ can be reconstructed as

$$(q, \dot{q}) = (\phi_{PZ}(z_1), \psi_{PZ}(z_1)z_2) \tag{8.14}$$

Finally, we note that given $(z_1^-, z_2^-) \in \mathcal{G} \cap PZ_\alpha$, we can obtain the equivalent $(q^-, \dot{q}^-) \in \mathcal{G} \cap PZ_\alpha$ according to (Equation 8.14), then apply the reset map to obtain $(q^+, \dot{q}^+) = \Delta(q^-, \dot{q}^-)$ and finally $(z_1^+, z_2^+) = (z_1(q^+), z_2(q^+, \dot{q}^+))$ where $z_1(q)$ and $z_2(q, \dot{q})$ are given in (Equation 8.1) and (Equation 8.3). We thus obtain:

$$\left(z_1^+, z_2^+\right) = \Delta_{PZ}\left(z_1^-, z_2^-\right) \tag{8.15}$$

We have thus constructed a reduced order two dimensional hybrid system (assuming hybrid invariance) inside the full hybrid system with continuous dynamics given by (Equation 8.13) and reset map given by (Equation 8.15).

8.2.2 Optimization

With the controller design in place, we now discuss an optimization problem to find a PZ_α that contains a periodic orbit that is optimal with respect to a prescribed performance index, subject to physical constraints. The performance index is taken as (motivated by the cost of transport [69])

$$\mathcal{J}_1 = \frac{1}{mgd}\int_0^T u^\top u \ dt \tag{8.16}$$

where m is the total mass of the robot, g is the acceleration due to gravity and d is the step length, i.e the total horizontal distance traveled by the non stance foot over a step. We also would like to obtain parameters α satisfying

$$\Delta(\mathcal{G} \cap PZ_\alpha) \subset PZ_\alpha \tag{N1}$$

This makes the partial zero dynamics surface hybrid invariant, thereby creating *partial hybrid zero dynamics* (PHZD). As discussed in [68], we only enforce impact invariance of the relative degree two outputs, since there is a discontinuous change in the cartesian velocities of the links across impacts. In contrast, the cartesian positions of the links are always continuous. We thus allow for change in the relative degree one outputs (which is the hip velocity) to account for this. To ensure the trajectory begins in PZ_α we enforce

$$y_2(q(0), \alpha) = \dot{y}_2(q(0), \dot{q}(0), \alpha) = 0 \tag{N2}$$

We also have the boundary condition

$$(q(T^-), \dot{q}(T^-)) \in \mathcal{G} \tag{N3}$$

i.e the switching surface is reached at the end of a step. Finally, we also have domain constraints which are inequality constraints

$$(q(t), \dot{q}(t)) \in \mathcal{D}, t \in [0, T] \tag{N4}$$

The optimization problem solved is

$$\begin{aligned} &\min_{\alpha} \mathcal{J}_1(\alpha, v_f) \\ s.t.\ &\text{(Equation D1)} - \text{(Equation D5)}, \\ &\text{(Equation O1)} - \text{(Equation O2)}, \\ &\text{(Equation N1)} - \text{(Equation N4)} \end{aligned} \tag{8.17}$$

Note that we did not explicitly enforce periodicity constraints, however by [68] for large ϵ in (Equation 8.8) there will be a stable periodic orbit in PZ_α. The end result of the optimization problem is a set of coefficients α that result in stable walking.

Remark 8.2.1. *It is important to note that the parameter v_f given in* (Equation O1) *is a user defined parameter that determines how fast the robot travels. The solution α^* to* (Equation 8.16) *depends on v_f. Different choices of v_f would yield different Bezier coefficients α^*. We denote the solution as $\alpha(v_f)$ and the resulting surface as $PZ_{\alpha(v_f)}$ henceforth.*

8.3 Transitions between Orbits

In this section, we first discuss transitions between periodic orbits that live on a fixed surface $PZ_{\alpha(v_f)}$ where v_f is a fixed desired walking speed. Subsequently, we discuss transitions between periodic orbits that are in distinct PHZD surfaces.

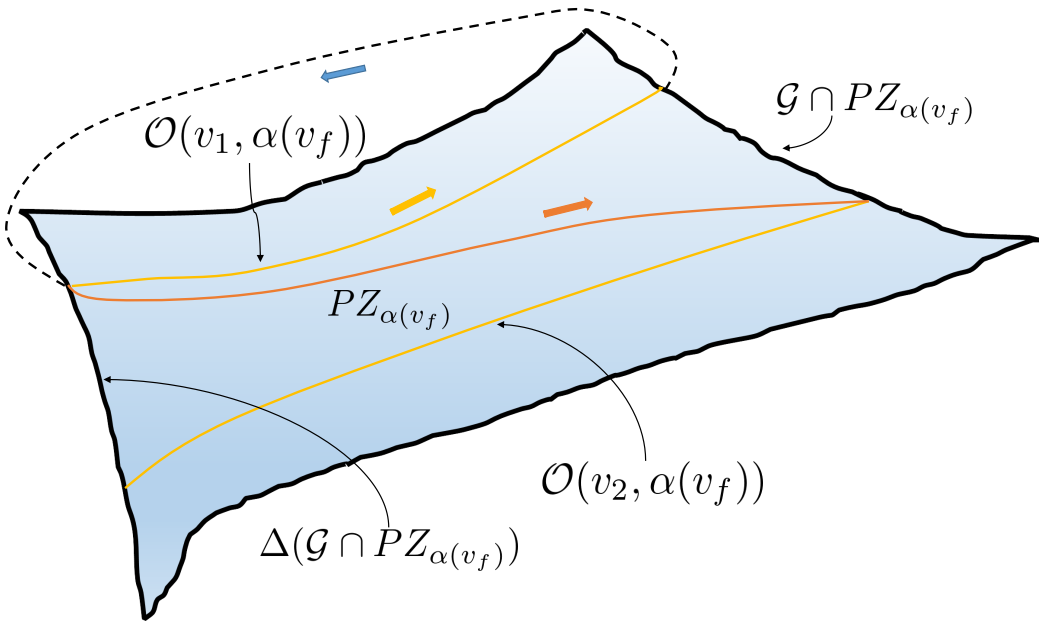

Figure 8.1: Sketch of Transitions on $PZ_{\alpha(v_f)}$. Yellow lines are Periodic Orbits and orange line is transition.

8.3.1 Transitions between orbits on same PHZD

We assume that we can solve (Equation 8.17) for a user defined fixed v_f obtaining a fixed optimal $\alpha(v_f)$ and hence a PHZD surface $PZ_{\alpha(v_f)}$. However, by results of [68], we get an infinite family of stable periodic orbits on $PZ_{\alpha(v_f)}$ for different values of walking speeds v_d (which replaces v_f in (Equation 8.2) but $\alpha(v_f)$ in (Equation 8.4) is fixed as before) as depicted in Figure 8.1. We denote such periodic orbits by $\mathcal{O}(v_d, \alpha(v_f))$. Two such periodic orbits $\mathcal{O}(v_1, \alpha(v_f))$ and $\mathcal{O}(v_2, \alpha(v_f))$ are depicted in Figure 8.1 for different velocities v_1 and v_2. The orange line depicts a transition between these orbits. Given the two distinct periodic orbits $\mathcal{O}(v_1, \alpha(v_f))$ and $\mathcal{O}(v_2, \alpha(v_f))$ on $PZ_{\alpha(v_f)}$, we discuss an optimization problem to transition between them.

To obtain transitions, we use the feedback control given by (Equation 8.8) where $v_f \in$

$\mathbb{R}$ is replaced by a function of time $v_d(t)$ which result in the dynamics on $PZ_{\alpha(v_f)}$ given by

$$\dot{z}_1 = z_2 \tag{8.18}$$

$$\dot{z}_2 = -\epsilon(z_2 - v_d(t)) \tag{8.19}$$

where the full state can still be reconstructed according to (Equation 8.14). Hence, we can view (Equation 8.18) as a *controlled hybrid system* [70] with control input $v_d(t)$ where the reset map is still given by (Equation 8.15). This control input enables us to transition between any two periodic orbits on $PZ_{\alpha(v_f)}$, while still staying in $PZ_{\alpha(v_f)}$. We want to transition between orbits in N steps in an optimal manner, where N is a user defined parameter. We formulate the objective function

$$\mathcal{J}_2 = \frac{1}{mgd_{\text{total}}} \int_{t_0}^{t_N} \phi(t)\, dt \tag{8.20}$$

where N represents the number of steps in the transitions, d_{total} represents the total horizontal distance traveled by the non stance foot over N steps, and $\phi(t)$ represents the control effort given by

$$\phi(t) = u_{\alpha(v_f)}(z_1(t), z_2(t), v_d(t))^\top u_{\alpha(v_f)}(z_1(t), z_2(t), v_d(t)) \tag{8.21}$$

The control $u_{\alpha(v_f)}(z_1(t), z_2(t), v_d(t))$ is obtained from (Equation 8.14) and (Equation 7.33). The states $(z_1(t), z_2(t))$ are continuous at all times except at a discrete set of times denoted $\{t_k\}$, $1 \leq k \leq N$. At these impact times we need to have the discrete reset map

$$\begin{bmatrix} z_1(t_k^+) \\ z_2(t_k^+) \end{bmatrix} = \Delta_{PZ} \left(\begin{bmatrix} z_1(t_k^-) \\ z_2(t_k^-) \end{bmatrix} \right) \tag{T2}$$

We also impose continuity of $v_d(t)$ at the points of impact, namely

$$v_d(t_k^+) = v_d(t_k^-) \tag{T3}$$

for $0 \leq k \leq N$ where $v_d(t_0^-) = v_1$ represents the initial walking speed and $v_d(t_N^+) = v_2$ represents final walking speed. We also impose the boundary conditions ensuring we start at the initial orbit and end at the final orbit.

$$(z_1(t_0), z_2(t_0)) \in \mathcal{O}\left(v_1, \alpha(v_f)\right) \tag{T4}$$

$$\left(z_1(t_N^+), z_2(t_N^+)\right) \in \mathcal{O}\left(v_2, \alpha(v_f)\right) \tag{T5}$$

Hence, the overall optimization problem solved is

$$\begin{aligned} &\min_{v_d(t)} \mathcal{J}_2(v_d(t)) \\ s.t\ \ &\text{(Equation 8.18)} - \text{(Equation 8.19)} \\ &\text{(Equation T2)} - \text{(Equation T5)} \end{aligned} \tag{8.22}$$

Remark 8.3.1. *We note that since* (Equation 8.18)-(Equation 8.19) *is an exponentially stable linear system, appropriately ramping $v_d(t)$ from v_1 to v_2 will effect a transition from $O(v_1, \alpha(v_f))$ to a neighborhood of $O(v_2, \alpha(v_f))$ in N steps and it would do so exponentially fast. However, it is not* optimal *with respect to $\mathcal{J}_2(v_d(t))$ which we illustrate in the subsequent sections.*

8.3.2 Transition between orbits on different PHZD surfaces

The periodic orbit $\mathcal{O}(v_f, \alpha(v_f)) \subset PZ_{\alpha(v_f)}$ is optimal w.r.t $\mathcal{J}_1(\alpha, v_f)$ by definition of $\alpha(v_f)$ in subsection 8.3.1. However, the orbits $\mathcal{O}(v_d, \alpha(v_f)) \subset PZ_{\alpha(v_f)}$ are not optimal for $\mathcal{J}_1(\alpha, v_d)$ where $v_d \neq v_f$ (see Remark 8.2.1). This motivates optimizing several PHZD surfaces PZ_α for various walking speeds v_d and constructing transition controllers between

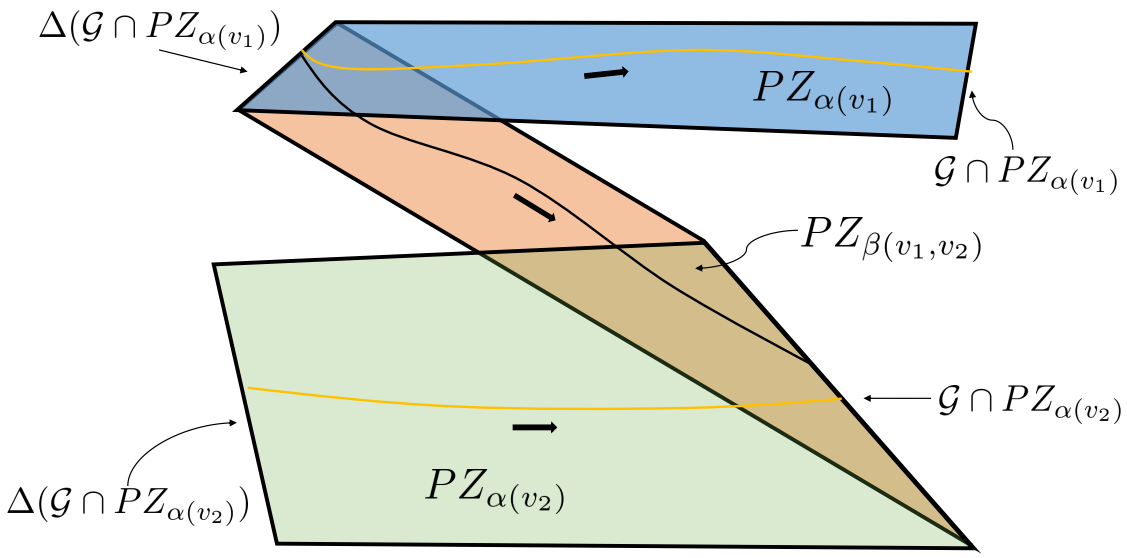

Figure 8.2: Sketch of connecting PHZD surface PZ_β between $PZ_{\alpha(v_1)}$ and $PZ_{\alpha(v_2)}$.

them. This is pictorially depicted in Figure 8.2 where the yellow lines denote periodic orbits on optimized surfaces $PZ_{\alpha(v_1)}$ and $PZ_{\alpha(v_2)}$. The periodic orbits on these surfaces are denoted by $\mathcal{O}(v_1, \alpha(v_1))$ and $\mathcal{O}(v_2, \alpha(v_2))$. We connect $PZ_{\alpha(v_1)}$ and $PZ_{\alpha(v_2)}$ over a single step. The objective function used is given by $\mathcal{J}_1$ given in (Equation 8.16) where u is given in (Equation 7.33) is a function of β (the bezier coefficients) and $v_d(t)$. This means that on the connecting surface PZ_β, the dynamics evolve as in (Equation 8.18). However, the constraint (Equation N1) is replaced by

$$\Delta(\mathcal{G} \cap PZ_{\alpha(v_1)}) \subset PZ_\beta \tag{8.23}$$

$$\Delta(\mathcal{G} \cap PZ_\beta) \subset PZ_{\alpha(v_2)} \tag{8.24}$$

The optimization problem solved is

$$\begin{aligned} &\min_{\beta, v_d(t)} \mathcal{J}_1(\beta, v_d(t)) \\ s.t\ &\text{(Equation D1)} - \text{(Equation D5)}, \\ &\text{(Equation O1)} - \text{(Equation O2)}, \\ &\text{(Equation 8.23)} - \text{(Equation 8.24)}, \\ &\text{(Equation N3)} - \text{(Equation N4)} \end{aligned} \tag{8.25}$$

Optimizing (Equation 8.25) results in a (optimized connecting) PHZD surface denoted $PZ_{\beta(v_1,v_2)}$ shown in Figure 8.2. To implement (Equation 8.24), we do the following, we first impose the constraint $(q(0^-), \dot{q}(0^-)) \in \mathcal{G} \cap PZ_{\alpha(v_1)}$ by

$$\begin{bmatrix} y_2(q(0^-), \alpha(v_1)) \\ p^{\text{com}}_{\text{nsfy}}(q(0^-)) \\ h(q(0^-)) \\ dy_2(q(0^-), \alpha(v_1))\dot{q}(0^-) \\ dh(q(0^-))\dot{q}(0^-) \end{bmatrix} = 0 \tag{8.26}$$

where h is the holonomic constraints and $p^{\text{com}}_{\text{nsfy}}$ defines the switching surface. The constraints $(q(0^+), \dot{q}(0^+)) = \Delta(q(0^-), \dot{q}(0^-))$ are added, i.e., $(q(0^+), \dot{q}(0^+))$ is related to $(q(0^-), \dot{q}(0^-))$ by the reset map and the transversality condition $dp^{com}_{nsfy}(q(0^-))\dot{q}(0^-) < 0$ is also added. Finally we add

$$\begin{bmatrix} y_2(q(0^+), \beta) \\ dy_2(q(0^+), \beta)\dot{q}(0^+) \end{bmatrix} = 0 \tag{8.27}$$

These set of constraints ensure $\Delta(\mathcal{G} \cap PZ_{\alpha(v_1)}) \subset PZ_\beta$ by Theorem 1 of [68]. By a similar set of constraints we can achieve $\Delta(\mathcal{G} \cap PZ_\beta) \subset PZ_{\alpha(v_2)}$.

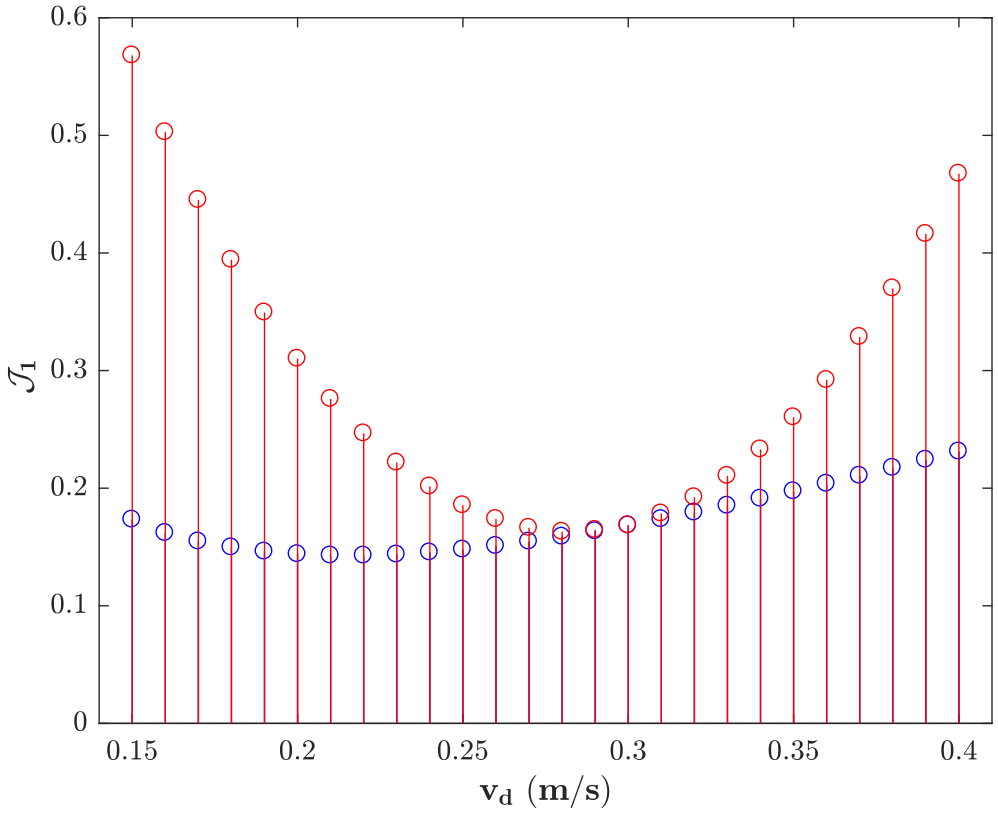

Figure 8.3: Comparison of objective function $\mathcal{J}_1$ for the periodic orbits $\mathcal{O}\left(v_d, \alpha(v_d)\right)$ i.e. $\mathcal{J}_1(u_{\alpha(v_d)}(z_1, z_2, v_d))$ (blue) and $\mathcal{O}\left(v_d, \alpha(v_f)\right) \subset PZ_{\alpha(v_f)}$ i.e. $\mathcal{J}_1(u_{\alpha(v_f)}(z_1, z_2, v_d))$ (red) respectively. $v_f = 0.3$ m/s is fixed.

8.4 Results

This section provides the simulation results for the 5 DOF robot explained in § 7.2. We first compare the performance index $\mathcal{J}_1$ of the orbits $\mathcal{O}(v_d, \alpha(v_f))$ i.e. the cost of transport given by $\mathcal{J}_1(u_{\alpha(v_f)}(z_1, z_2, v_d))$ (depicted in Figure 8.1) and the periodic orbits $\mathcal{O}(v_d, \alpha(v_d))$ i.e, $\mathcal{J}_1(u_{\alpha(v_d)}(z_1, z_2, v_d))$ (depicted in Figure 8.2) for different values of v_d. In this paper, we chose $v_f = 0.3\ m/s$ and solved (Equation 8.17) to obtain $PZ_{\alpha(v_f)}$. The performance index of these orbits is shown in red in Figure 8.3. We also solved (Equation 8.16) for different v_d to obtain the orbits $O(v_d, \alpha(v_d))$ shown in blue in Figure 8.3. We see that the performance index $\mathcal{J}_1$ for $\mathcal{O}(v_d, \alpha(v_f))$ gets larger as v_d further deviates from v_f as

Table 8.1: Comparison of Performance Metrics for 3 step Transition Controllers

Speed Transition	Performance Index			Performance Improvement	
	$\mathcal{J}_2(u_1)$	$\mathcal{J}_2(u_2)$	$\mathcal{J}_2(u_3)$	$\frac{\mathcal{J}_2(u_1)-\mathcal{J}_2(u_2)}{\mathcal{J}_2(u_1)} \times 100$	$\frac{\mathcal{J}_2(u_2)-\mathcal{J}_2(u_3)}{\mathcal{J}_2(u_2)} \times 100$
$0.15 \rightarrow 0.20$ m/s	0.9862	0.7062	0.3033	28.3908	57.0518
$0.15 \rightarrow 0.22$ m/s	0.9687	0.7297	0.3544	24.6650	51.4321
$0.15 \rightarrow 0.24$ m/s	0.9864	0.7849	0.4138	20.4228	47.2799
$0.15 \rightarrow 0.26$ m/s	1.0351	0.8662	0.4993	16.3183	42.3574
$0.15 \rightarrow 0.28$ m/s	1.1123	0.9791	0.5961	11.9716	39.1176
$0.15 \rightarrow 0.30$ m/s	1.2244	1.1251	0.7116	8.1151	36.7523
$0.30 \rightarrow 0.25$ m/s	0.3346	0.3149	0.2681	5.8885	14.8619
$0.30 \rightarrow 0.23$ m/s	0.3835	0.3509	0.3101	8.5029	11.6272
$0.30 \rightarrow 0.21$ m/s	0.4444	0.4128	0.3519	7.1226	14.7529
$0.30 \rightarrow 0.19$ m/s	0.5327	0.4962	0.4324	6.8565	12.8577
$0.30 \rightarrow 0.17$ m/s	0.6540	0.6026	0.5308	7.8580	11.9150
$0.30 \rightarrow 0.15$ m/s	0.7989	0.7311	0.6434	8.4821	11.9956

mentioned in Remark 8.2.1.

Definition of Performance Index

In this paper, all the controllers are designed to achieve transitions in $N = 3$ steps. The performance index used is

$$\mathcal{J}_2 = \frac{1}{mgd_{\text{total}}} \int_0^T u^\top u \, dt \tag{8.28}$$

where d_{total} is the total step length of the robot. Here $[0, T]$ is defined such that it is exactly the duration of *five* steps of the robot, the first step being the initial periodic orbit, the subsequent three steps being the transitions and the fifth step being the final orbit. The motivation for including one step of the initial and final orbit in the performance index calculation is to enable us to compare transitions $\mathcal{O}(v_1, \alpha(v_f)) \rightarrow \mathcal{O}(v_2, \alpha(v_f))$ and $\mathcal{O}(v_1, \alpha(v_1)) \rightarrow \mathcal{O}(v_2, \alpha(v_2))$.

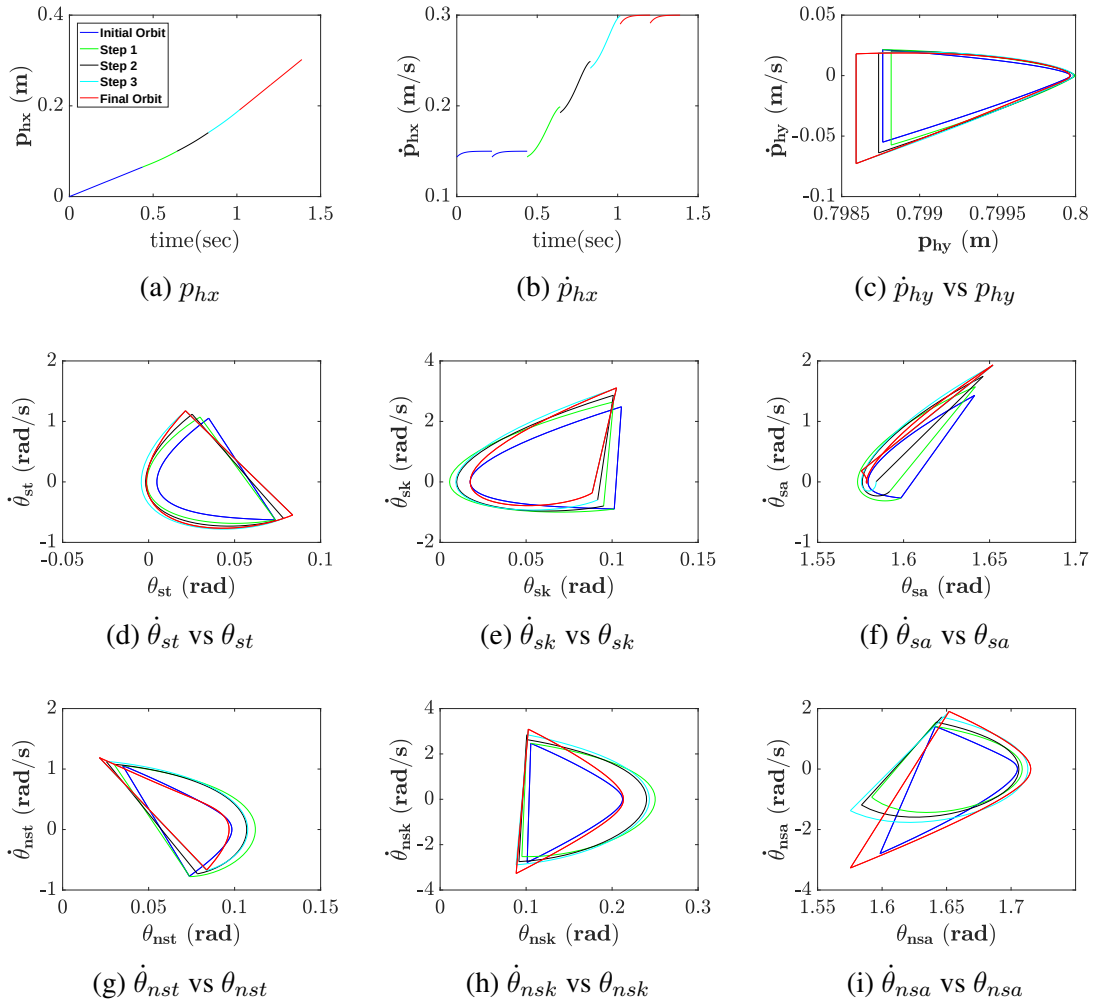

(a) p_{hx} (b) $\dot{p}_{hx}$ (c) $\dot{p}_{hy}$ vs p_{hy}

(d) $\dot{\theta}_{st}$ vs θ_{st} (e) $\dot{\theta}_{sk}$ vs θ_{sk} (f) $\dot{\theta}_{sa}$ vs θ_{sa}

(g) $\dot{\theta}_{nst}$ vs θ_{nst} (h) $\dot{\theta}_{nsk}$ vs θ_{nsk} (i) $\dot{\theta}_{nsa}$ vs θ_{nsa}

Figure 8.4: Plot of states for 3 step transitions from 0.15 m/s to 0.30 m/s

8.4.1 Comparison between Transition Controllers on $PZ_{\alpha(v_f)}$

In Remark 8.3.1, we stated that we could use a linear ramp to transition between $\mathcal{O}(v_1, \alpha(v_f))$ and $\mathcal{O}(v_2, \alpha(v_f))$ since the dynamics of the robot on $PZ_{\alpha(v_f)}$ is an exponentially stable system given by (Equation 8.18). That is given initial and final velocities v_1 and v_2, the control input is $v_d^1(t) = c_1 t + c_2$ is applied to the system (Equation 8.18) such that at time $t = t_i$ we have $v_d^1(t_i) = v_1$ and after three steps of transitions we have $v_d^1(t_f) = v_2$ where $[t_i, t_f]$ is the transition duration. The full control is given by $u_1(t) = u_{\alpha(v_f)}(z_1, z_2, v_d^1(t))$ where $z_1(t)$ and $z_2(t)$ are the solutions of (Equation 8.18) with v_d^1 as a control input.

Solving (Equation 8.22) gives the optimal input denoted $v_d^2(t)$ that transfers the system

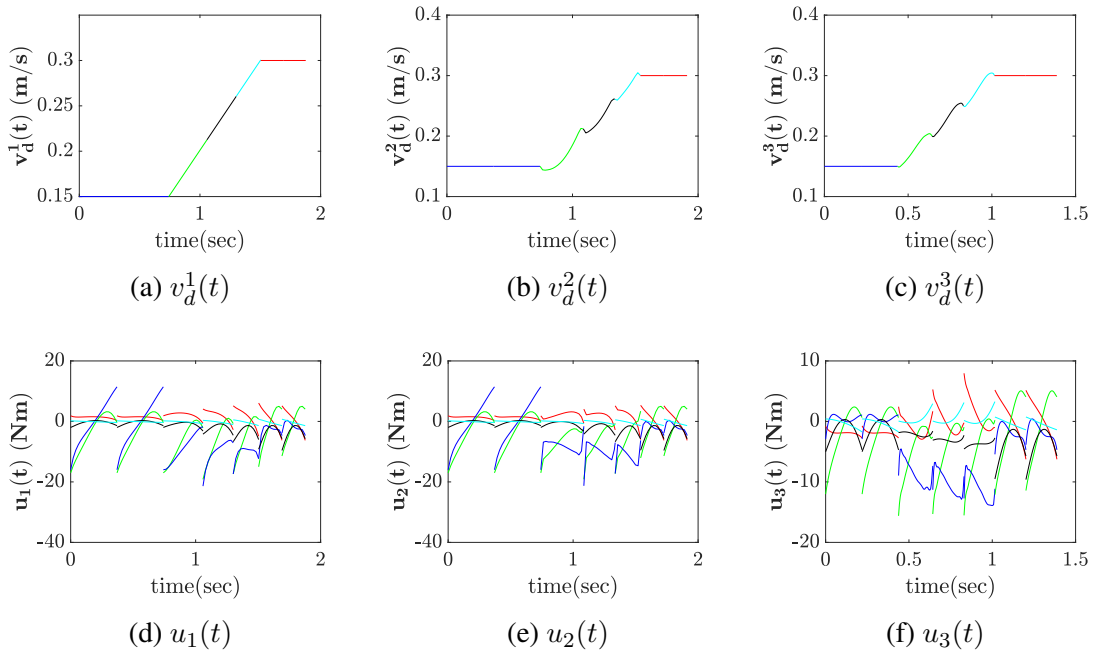

(a) $v_d^1(t)$ (b) $v_d^2(t)$ (c) $v_d^3(t)$

(d) $u_1(t)$ (e) $u_2(t)$ (f) $u_3(t)$

Figure 8.5: Plot of reduced control $v_d^i(t)$ (top row) and full control $u_i(t)$ (bottom row) , $i = 1, 2, 3$.

from $O(v_1, \alpha(v_f))$ to $\mathcal{O}(v_2, \alpha(v_f))$ subject to being in $PZ_{\alpha(v_f)}$ in 3 steps. Given the control $v_d^2(t)$, we can get the full control $u_2(t) = u_{\alpha(v_f)}(z_1, z_2, v_d^2(t))$. The performance index $\mathcal{J}_2$ given in (Equation 8.28) is evaluated on both u_1 and u_2. The results are illustrated in Table Table 8.1. We see that for increasing transitions ($v_1 < v_2$), there is a lot of improvement when the gap between $v_2 - v_1$ is small but it decreases with increasing gap between $v_2 - v_1$. For decreasing transitions ($v_1 > v_2$). In all cases the performance improvement is larger than 5 percent.

8.4.2 Comparison between Optimal Transition Controllers on $PZ_{\alpha(v_f)}$ and Transition Controllers connecting different PHZD surfaces

We obtain one step optimal controllers to transition between orbits $\mathcal{O}(v_1, \alpha(v_1)) \subset PZ_{\alpha(v_1)}$ and $\mathcal{O}(v_2, \alpha(v_2)) \subset PZ_{\alpha(v_2)}$ by solving (Equation 8.25) to obtain $\beta(v_1, v_2)$ and a $v_d(t)$. The full control over one step is then $u_{\beta(v_1,v_2)}(z_1, z_2, v_d(t))$ We then compose these controllers to obtain multi step transitions. For example, to obtain a transition $0.15 \rightarrow 0.30$ m/s, we

obtain *one step* transition controllers $0.15 \rightarrow 0.20$ m/s , $0.20 \rightarrow 0.25$ m/s and $0.25 \rightarrow 0.30$ m/s and execute these controllers one after the other. The resulting net transition controller (over all the three steps) is denoted $u_3(t)$ and the corresponding reduced controller is $v_d^3(t)$. The resulting performance index $\mathcal{J}_2$ given in (Equation 8.28) is evaluated to obtain $\mathcal{J}_2(u_3)$. This approach was followed for several different cases and is illustrated in Table Table 8.1. We see that for increasing transitions there is a tremendous improvement of $\mathcal{J}_2(u_3)$ over $\mathcal{J}_2(u_2)$. The reason is because u_2 attempts to transition from $\mathcal{O}(v_1, \alpha(v_f)) \rightarrow \mathcal{O}(v_2, \alpha(v_f))$. But $\mathcal{O}(v_1, \alpha(v_f))$ has a very high performance index $\mathcal{J}_1$ for $v_1 = 0.15$ m/s (see Figure 8.3). On the other hand $v_f = 0.30$ m/s so for decreasing transitions ($0.30 \rightarrow 0.15$ m/s for example) the performance improvement is comparatively lower. In all cases the improvement was over 11.91 percent.

In Figure 8.4 we show a plot of transitions in 3 steps from $0.15 \rightarrow 0.30$ m/s with the control $u_3(t)$. The blue curves represent the initial orbit, the red curves represent the final orbit and all other colors represent a step in the transitions. As seen in Figure 8.4(b), the hip velocity $\dot{p}_{hx} = z_2(q, \dot{q})$ given in (Equation 8.3) changes from about 0.15 m/s to 0.30 m/s. The corresponding $u_3(t) \in \mathbb{R}^5$ is plotted in Figure 8.5(f). The reduced order control $v_d^3(t)$ is plotted in Figure 8.5(c). As a comparison, $u_1(t)$ and $u_2(t)$ are also plotted in Figure 8.5 that achieve transitions $0.15 \rightarrow 0.30$ m/s, along with their corresponding reduced controllers.

8.4.3 Solving the Optimization Problems

All the optimal control problems (Equation 8.17), (Equation 8.22) and (Equation 8.25), were solved numerically using the method of direct collocation. The method works by considering the state and control as polynomials and enforcing dynamics and path constraints at a discrete set of points. This results in a finite dimensional Non Linear Program (NLP) that can be solved by solvers such as IPOPT [62]. The FROST toolkit achieves this transcription and is described in detail in [33]. We used the FROST toolkit throughout this chapter.

CHAPTER 9
CONCLUSION AND FUTURE WORK

This thesis focused on applying the Gluskabi raccordation frameowrk to synthesize transitions between periodic motions of smooth nonlinear systems and hybrid systems. The kernel method was used in the context of hopping gaits and the image method was used for walking gaits. The kernel method typically involves solving a single optimal control problem which can be readily related to an abstract notion of gracefulness by minimizing a carefully chosen objective. However, the kernel method could become numerically challenging to perform as the raccordation interval increases, the number of hopping steps or walking steps during transition increases, or if the system complexity increases. In contrast, the image method (typically) involves solving a sequence of (parameterized) optimization problems to generate a family of periodic orbits (an orbit library). Relatively computationally inexpensive controllers or optimal control problems can be formulated to stay close to this orbit family while transiting between periodic orbits. However, generating an orbit library is (currently) computationally intensive and must be done *offline* and also requires careful formulation of a parameterized optimal control problem to shape the orbit library.

Future work involves the problem of transitions between types of gaits, i.e. between walking to running for bipedal robots, or trotting to bounding for quadrupeds. Efforts to mitigate the computational complexity of solving a single large optimal control problem (in the case of Kernel method) and a large sequence of optimization problems (in the case of the Image method) are interesting directions to pursue. We also briefly focused on energy efficency of locomotion in the final chapter of this thesis. The relation of energy efficiency of locomotion to a notion of gracefulness (if any) remains to be examined. In recent years, control barrier functions have emerged as a promising tool to guarantee safety of the system. The relation of safety and gracefulness is also another direction to pursue.

Appendices

APPENDIX A

IMPACT DYNAMICS

In order to make the thesis more self contained, we briefly provide details on the robot impact dynamics. We follow the derivation provided in [58]. For the purposes of this derivation, we assume that we can compute a smooth distance function $\phi(q)$ that represents the distance between the two objects. $\phi(q) = 0$ means that the two objects are in contact and $\phi(q) > 0$ means the objects are not in contact. In the example of the bipedal robot, $\phi(q)$ could represent the height of the non stance foot above the ground. We denote by $J = \frac{\partial \phi}{\partial q}$. We can write

$$M(q)\ddot{q} + C(q, \dot{q}) = Bu + J^{\top}(q)\lambda \tag{A.1}$$

where $\lambda = 0$ when $\phi(q) > 0$ and $\lambda \neq 0$ only when $\phi(q) = 0$. Let t_c be the first time when $\phi(q(t_c)) = 0$. Then,

$$\int_{t_c^-}^{t_c^+} \Big(M(q)\ddot{q} + C(q, \dot{q})\Big)dt = \int_{t_c^-}^{t_c^+} \Big(Bu + J^{\top}(q)\lambda\Big)dt \tag{A.2}$$

Since $M(q)$, $C(q, \dot{q})$ and u are constants we have

$$M\dot{q}^+ - M\dot{q}^- = J^{\top} \int_{t_c^-}^{t_c^+} \lambda dt \tag{A.3}$$

multiplying both sides by $J(q)M^{-1}$, we get

$$J\dot{q}^+ - J\dot{q}^- = JM^{-1}(q)J^{\top} \int_{t_c^-}^{t_c^+} \lambda dt \tag{A.4}$$

On the other hand, after impact we have $\phi(q(t)) = 0$. this means

$$J(q)\dot{q}^+ = \lim_{t \downarrow t_c} \frac{d}{dt}\phi(q(t)) = 0 \tag{A.5}$$

Using this in (Equation A.4), we get

$$\int_{t_c^-}^{t_c^+} \lambda dt = -\left(JM^{-1}J^\top\right)^\dagger J(q)\dot{q}^- \tag{A.6}$$

Substituting this in (Equation A.3), we get

$$M\dot{q}^+ = \left(M - J^\top\left(JM^{-1}J^\top\right)^\dagger J\right)\dot{q}^- \tag{A.7}$$

$$\dot{q}^+ = \left(I - M^{-1}J^\top\left(JM^{-1}J^\top\right)^\dagger J\right)\dot{q}^- \tag{A.8}$$

we can represent this as

$$\dot{q}^+ = \Delta_{\dot{q}}(q)\dot{q}^-. \tag{A.9}$$

The position variables are *continuous* across the collisions, namely

$$q^+ = q^- = q \tag{A.10}$$

Remark A.0.1. *In the case of bipedal robots, the position variables are also discontinuous due to relabeling the left and right legs. This means*

$$q_{\text{relabel}} = Rq^+ \tag{A.11}$$

$$\dot{q}_{\text{relabel}} = R\dot{q}^+ \tag{A.12}$$

where q^+ and $\dot{q}^+$ are given by (Equation A.10) - (Equation A.9).

Remark A.0.2. *$\dot{q}^+$ can also be obtained by solving*

$$\begin{bmatrix} M(q) & -J^\top(q) \\ J(q) & 0 \end{bmatrix} \begin{bmatrix} \dot{q}^+ \\ \int_{t_c^-}^{t_c^+} \lambda dt \end{bmatrix} = \begin{bmatrix} M(q)\dot{q}^- \\ 0 \end{bmatrix} \tag{A.13}$$

This can be seen from (Equation A.3)-(Equation A.5). *The closed form solution for $\dot{q}^+$ is given by* (Equation A.8).

REFERENCES

[1] A. LaViers, "Choreographic abstractions for style-based robotic motion," Ph.D. dissertation, Georgia Institute of Technology, 2013.

[2] D. Yeung, "Maximally smooth transition: The gluskabi raccordation," Ph.D. dissertation, Georgia Institute of Technology, 2011.

[3] A. B. Memon, "Graceful connections in dynamical systems–an approach to gait transitions in robotics," Ph.D. dissertation, Georgia Institute of Technology, 2014.

[4] E. I. Verriest and D. Yeung, "Maximally smooth transfers: Gluskabi raccordation," in *Proceedings of the 18th International Symposium on Mathematical Theory of Networks and Systems, Blacksburg, VA*, 2008.

[5] D. Yeung and E. I. Verriest, "On connecting trajectories with maximum persistence of behavior," in *Proceedings of the 48h IEEE Conference on Decision and Control (CDC) held jointly with 2009 28th Chinese Control Conference*, IEEE, 2009, pp. 5039–5044.

[6] J. C. Willems and J. W. Polderman, *Introduction to mathematical systems theory: a behavioral approach*. Springer Science & Business Media, 2013, vol. 26.

[7] A. B. Memon and E. I. Verriest, "Kernel representation approach to persistence of behavior," *IFAC Proceedings Volumes*, vol. 47, no. 3, pp. 6032–6037, 2014.

[8] ——, "Maximally persistent connections for the periodic type," *Proceedings of the 21st Internationsl Symposium of the Mathematical Theory of Networks and Systems*, 2014.

[9] V. Murali and E. I. Verriest, "Raccordation between periodic signals.," *IFAC-PapersOnLine*, vol. 50, no. 1, pp. 2211–2216, 2017.

[10] A. B. Memon, E. I. Verriest, and N.-s. P. Hyun, "Graceful gait transitions for biomimetic locomotion-the worm," in *53rd IEEE Conference on Decision and Control*, IEEE, 2014, pp. 2958–2963.

[11] D. Yeung and E. I. Verriest, "Smooth transitions via quasi-periodic paths," *IFAC Proceedings Volumes*, vol. 44, no. 1, pp. 5549–5554, 2011.

[12] ——, "On connecting periodic trajectories with quasi-periodic paths," in *49th IEEE Conference on Decision and Control (CDC)*, IEEE, 2010, pp. 4825–4830.

[13] J. Lygeros, S. Sastry, and C. Tomlin, "Hybrid systems: Foundations, advanced topics and applications," *under copyright to be published by Springer Verlag*, 2012.

[14] H. K. Khalil and J. W. Grizzle, *Nonlinear systems*. Prentice hall Upper Saddle River, NJ, 2002, vol. 3.

[15] M. H. Raibert, *Legged robots that balance*. MIT press, 1986.

[16] W. J. Schwind and D. E. Koditschek, "Control of forward velocity for a simplified planar hopping robot," in *Proceedings of 1995 IEEE International Conference on Robotics and Automation*, IEEE, vol. 1, 1995, pp. 691–696.

[17] H. Geyer, A. Seyfarth, and R. Blickhan, "Compliant leg behaviour explains basic dynamics of walking and running," *Proceedings of the Royal Society B: Biological Sciences*, vol. 273, no. 1603, pp. 2861–2867, 2006.

[18] R. J. Full and D. E. Koditschek, "Templates and anchors: Neuromechanical hypotheses of legged locomotion on land," *Journal of experimental biology*, vol. 202, no. 23, pp. 3325–3332, 1999.

[19] I. Poulakakis and J. W. Grizzle, "The spring loaded inverted pendulum as the hybrid zero dynamics of an asymmetric hopper," *IEEE Transactions on Automatic Control*, vol. 54, no. 8, pp. 1779–1793, 2009.

[20] A. Hereid, M. J. Powell, and A. D. Ames, "Embedding of slip dynamics on underactuated bipedal robots through multi-objective quadratic program based control," in *53rd IEEE Conference on Decision and Control*, IEEE, 2014, pp. 2950–2957.

[21] G. Garofalo, C. Ott, and A. Albu-Schäffer, "Walking control of fully actuated robots based on the bipedal slip model," in *2012 IEEE International Conference on Robotics and Automation*, IEEE, 2012, pp. 1456–1463.

[22] X. Xiong and A. D. Ames, "Coupling reduced order models via feedback control for 3d underactuated bipedal robotic walking," in *2018 IEEE-RAS 18th International Conference on Humanoid Robots (Humanoids)*, IEEE, 2018, pp. 1–9.

[23] R. M. Ghigliazza, R. Altendorfer, P. Holmes, and D. Koditschek, "A simply stabilized running model," *SIAM review*, vol. 47, no. 3, pp. 519–549, 2005.

[24] H. R. Vejdani, A. Wu, H. Geyer, and J. W. Hurst, "Touch-down angle control for spring-mass walking," in *2015 IEEE International Conference on Robotics and Automation (ICRA)*, IEEE, 2015, pp. 5101–5106.

[25] P. A. Bhounsule, A. Zamani, and J. Pusey, "Switching between limit cycles in a model of running using exponentially stabilizing discrete control lyapunov func-

tion," in *2018 Annual American Control Conference (ACC)*, IEEE, 2018, pp. 3714–3719.

[26] S. Kajita, F. Kanehiro, K. Kaneko, K. Fujiwara, K. Harada, K. Yokoi, and H. Hirukawa, "Biped walking pattern generation by using preview control of zero-moment point," in *2003 IEEE International Conference on Robotics and Automation (Cat. No. 03CH37422)*, IEEE, vol. 2, 2003, pp. 1620–1626.

[27] S. Kuindersma, F. Permenter, and R. Tedrake, "An efficiently solvable quadratic program for stabilizing dynamic locomotion," in *2014 IEEE International Conference on Robotics and Automation (ICRA)*, IEEE, 2014, pp. 2589–2594.

[28] H. Dai, A. Valenzuela, and R. Tedrake, "Whole-body motion planning with centroidal dynamics and full kinematics," in *2014 IEEE-RAS International Conference on Humanoid Robots*, IEEE, 2014, pp. 295–302.

[29] S. Kuindersma, R. Deits, M. Fallon, A. Valenzuela, H. Dai, F. Permenter, T. Koolen, P. Marion, and R. Tedrake, "Optimization-based locomotion planning, estimation, and control design for the atlas humanoid robot," *Autonomous Robots*, vol. 40, no. 3, pp. 429–455, 2016.

[30] Y. Zhao, B. R. Fernandez, and L. Sentis, "Robust optimal planning and control of non-periodic bipedal locomotion with a centroidal momentum model," *The International Journal of Robotics Research*, vol. 36, no. 11, pp. 1211–1242, 2017.

[31] M. Posa, S. Kuindersma, and R. Tedrake, "Optimization and stabilization of trajectories for constrained dynamical systems," in *2016 IEEE International Conference on Robotics and Automation (ICRA)*, IEEE, 2016, pp. 1366–1373.

[32] E. R. Westervelt, J. W. Grizzle, C. Chevallereau, J. H. Choi, and B. Morris, *Feedback control of dynamic bipedal robot locomotion*. CRC press, 2018.

[33] A. Hereid, E. A. Cousineau, C. M. Hubicki, and A. D. Ames, "3d dynamic walking with underactuated humanoid robots: A direct collocation framework for optimizing hybrid zero dynamics," in *2016 IEEE International Conference on Robotics and Automation (ICRA)*, IEEE, 2016, pp. 1447–1454.

[34] W.-L. Ma, A. Hereid, C. M. Hubicki, and A. D. Ames, "Efficient hzd gait generation for three-dimensional underactuated humanoid running," in *2016 IEEE/RSJ International Conference on Intelligent Robots and Systems (IROS)*, IEEE, 2016, pp. 5819–5825.

[35] R. R. Burridge, A. A. Rizzi, and D. E. Koditschek, "Sequential composition of dynamically dexterous robot behaviors," *The International Journal of Robotics Research*, vol. 18, no. 6, pp. 534–555, 1999.

[36] A. Majumdar and R. Tedrake, "Funnel libraries for real-time robust feedback motion planning," *The International Journal of Robotics Research*, vol. 36, no. 8, pp. 947–982, 2017.

[37] M. S. Motahar, S. Veer, and I. Poulakakis, "Composing limit cycles for motion planning of 3d bipedal walkers," in *2016 IEEE 55th Conference on Decision and Control (CDC)*, IEEE, 2016, pp. 6368–6374.

[38] S. Veer, M. S. Motahar, and I. Poulakakis, "Generation of and switching among limit-cycle bipedal walking gaits," in *2017 IEEE 56th Annual Conference on Decision and Control (CDC)*, IEEE, 2017, pp. 5827–5832.

[39] G. B. Folland, *Real analysis: modern techniques and their applications*. John Wiley & Sons, 1999, vol. 40.

[40] D. Liberzon, *Calculus of variations and optimal control theory: a concise introduction*. Princeton University Press, 2011.

[41] R. Bhattacharya, "Optragen: A matlab toolbox for optimal trajectory generation," in *Proceedings of the 45th IEEE Conference on Decision and Control*, IEEE, 2006, pp. 6832–6836.

[42] H. Nijmeijer and A. Van der Schaft, *Nonlinear dynamical control systems*. Springer, vol. 175.

[43] K. M. Lynch and F. C. Park, *Modern Robotics*. Cambridge University Press, 2017.

[44] D. Mellinger and V. Kumar, "Minimum snap trajectory generation and control for quadrotors," in *2011 IEEE international conference on robotics and automation*, IEEE, 2011, pp. 2520–2525.

[45] V. Murali and E. I. Verriest, "Graceful transitions between periodic orbits of parametrized nonlinear systems," in *2018 IEEE Conference on Decision and Control (CDC)*, IEEE, 2018, pp. 397–402.

[46] L. Perko, *Differential equations and dynamical systems*. Springer Science & Business Media, 2013, vol. 7.

[47] J. M. Lee, "Smooth manifolds," in *Introduction to Smooth Manifolds*, Springer, 2013, pp. 1–31.

[48] J. Hauser and C. C. Chung, "Converse lyapunov functions for exponentially stable periodic orbits," *Systems & Control Letters*, vol. 23, no. 1, pp. 27–34, 1994.

[49] E. Sel'Kov, "Self-oscillations in glycolysis," *The FEBS Journal*, vol. 4, no. 1, pp. 79–86, 1968.

[50] A. Banaszuk and J. Hauser, "Feedback linearization of transverse dynamics for periodic orbits," *Systems & control letters*, vol. 26, no. 2, pp. 95–105, 1995.

[51] A. S. Shiriaev, L. B. Freidovich, and S. V. Gusev, "Transverse linearization for controlled mechanical systems with several passive degrees of freedom," *IEEE Transactions on Automatic Control*, vol. 55, no. 4, pp. 893–906, 2010.

[52] A. S. Shiriaev and L. B. Freidovich, "Transverse linearization for impulsive mechanical systems with one passive link," *IEEE Transactions on Automatic Control*, vol. 54, no. 12, pp. 2882–2888, 2009.

[53] S. V. Gusev, A. S. Shiriaev, and L. B. Freidovich, "Lmi approach for solving periodic matrix riccati equation," *IFAC Proceedings Volumes*, vol. 40, no. 14, pp. 254–256, 2007.

[54] I. CVX Research, *CVX: Matlab software for disciplined convex programming, version 2.0*, http://cvxr.com/cvx, Aug. 2012.

[55] A. H. Chang, C. M. Hubicki, J. J. Aguilar, D. I. Goldman, A. D. Ames, and P. A. Vela, "Learning to jump in granular media: Unifying optimal control synthesis with gaussian process-based regression," in *2017 IEEE International Conference on Robotics and Automation (ICRA)*, IEEE, 2017, pp. 2154–2160.

[56] A. H. Chang, C. Hubicki, A. Ames, and P. A. Vela, "Every hop is an opportunity: Quickly classifying and adapting to terrain during targeted hopping," in *2019 International Conference on Robotics and Automation (ICRA)*, IEEE, 2019, pp. 3188–3194.

[57] E. I. Verriest, "Deterministic and stochastic multi-mode multi-dimensional systems with application to switched systems with delay," in *Proceedings of the 48h IEEE Conference on Decision and Control (CDC) held jointly with 2009 28th Chinese Control Conference*, IEEE, 2009, pp. 3958–3963.

[58] R. Tedrake, "Underactuated robotics: Algorithms for walking, running, swimming, flying, and manipulation (course notes for mit 6.832)," *Downloaded in Fall*, 2020.

[59] M. J. Coleman, A. Chatterjee, and A. Ruina, "Motions of a rimless spoked wheel: A simple three-dimensional system with impacts," *Dynamics and stability of systems*, vol. 12, no. 3, pp. 139–159, 1997.

[60] C. M. Hubicki, J. J. Aguilar, D. I. Goldman, and A. D. Ames, "Tractable terrain-aware motion planning on granular media: An impulsive jumping study," in *2016*

IEEE/RSJ International Conference on Intelligent Robots and Systems (IROS), IEEE, 2016, pp. 3887–3892.

[61] J. Aguilar and D. I. Goldman, "Robophysical study of jumping dynamics on granular media," *Nature Physics*, vol. 12, no. 3, pp. 278–283, 2016.

[62] A. Wächter and L. T. Biegler, "On the implementation of an interior-point filter line-search algorithm for large-scale nonlinear programming," *Mathematical programming*, vol. 106, no. 1, pp. 25–57, 2006.

[63] D. Laney and D. Hong, "Kinematic analysis of a novel rimless wheel with independently actuated spokes," in *29th ASME Mechanisms and Robotics Conference*, 2005.

[64] J. Yan and S. K. Agrawal, "Rimless wheel with radially expanding spokes: Dynamics, impact, and stable gait," in *Proceedings of IEEE International Conference on Robotics and Automation*, IEEE, vol. 4, 2004, pp. 3240–3244.

[65] E. I. Verriest and V. Murali, "Graceful transitions between limit cycles of a parameterized system," in *2018 Annual American Control Conference (ACC)*, IEEE, 2018, pp. 6075–6080.

[66] V. Murali, N.-S. P. Hyun, and E. I. Verriest, "Graceful transitions between periodic walking gaits of fully actuated bipedal robots," in *2020 American Control Conference (ACC)*, IEEE, 2020, pp. 1043–1048.

[67] A. D. Ames, K. Galloway, K. Sreenath, and J. W. Grizzle, "Rapidly exponentially stabilizing control lyapunov functions and hybrid zero dynamics," *IEEE Transactions on Automatic Control*, vol. 59, no. 4, pp. 876–891, 2014.

[68] A. D. Ames, "Human-inspired control of bipedal walking robots," *IEEE Transactions on Automatic Control*, vol. 59, no. 5, pp. 1115–1130, 2014.

[69] S. Collins, A. Ruina, R. Tedrake, and M. Wisse, "Efficient bipedal robots based on passive-dynamic walkers," *Science*, vol. 307, no. 5712, pp. 1082–1085, 2005.

[70] A. D. Ames, P. Tabuada, A. Jones, W.-L. Ma, M. Rungger, B. Schürmann, S. Kolathaya, and J. W. Grizzle, "First steps toward formal controller synthesis for bipedal robots with experimental implementation," *Nonlinear Analysis: Hybrid Systems*, vol. 25, pp. 155–173, 2017.